

1999

Pyrene Labeled Poly (Aryl Ether) Monodendrons: Synthesis and Photophysical Studies

Wajiha Adnan Khan
Seton Hall University

Follow this and additional works at: <https://scholarship.shu.edu/dissertations>

 Part of the [Chemistry Commons](#)

Recommended Citation

Khan, Wajiha Adnan, "Pyrene Labeled Poly (Aryl Ether) Monodendrons: Synthesis and Photophysical Studies" (1999). *Seton Hall University Dissertations and Theses (ETDs)*. 1243.
<https://scholarship.shu.edu/dissertations/1243>

**PYRENE LABELED POLY(ARYL ETHER) MONODENDRONS:
SYNTHESIS
AND
PHOTOPHYSICAL STUDIES**

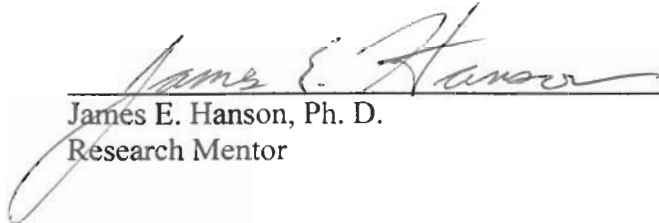
Thesis by
Wajiha Adnan Khan

In Partial Fulfilment of the Requirements
for the Degree of
Doctor of Philosophy

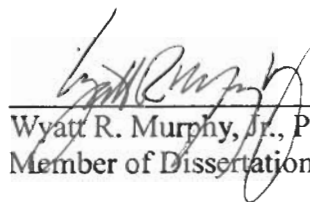
Seton Hall University
South Orange, New Jersey 07079
1999

We certify that we have read this thesis and that in our opinion it is adequate in scientific scope and quality as a dissertation for the degree of Doctor of Philosophy.

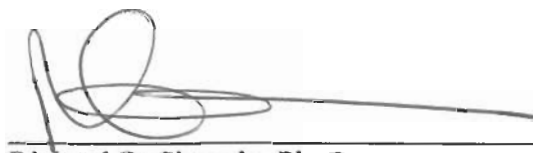
Approved



James E. Hanson, Ph. D.
Research Mentor



Wyatt R. Murphy, Jr., Ph.D.
Member of Dissertation Committee



Richard D. Sheardy, Ph. D.
Member of Dissertation Committee
Chairperson, Department of Chemistry

© 1999
Wajiha Adnan Khan
All Rights Reserved

Acknowledgements

First of all I would like to express my appreciation to my thesis advisor, Dr. James Hanson, for being an invaluable mentor during my studies at Seton Hall. Because of his enthusiasm, support and guidance throughout my research I was able to complete my doctoral work at this institution. I would like to extend my gratitude to Dr. Richard Sheardy for his friendly presence in my committee. I am grateful to Dr. Wyatt Murphy for being willing to become my committee member at the last moment and for his assistance in lifetime measurements using Laser Flash Photolysis. I would like to thank my friends Kate Jensen and Jeanne Riley who were extremely helpful when I started working in Dr. Hanson's research group. I have wonderful memories of the time that I spent with them. I owe special thanks to Margaret Galazka, Cindy Mleziva, Sohita Patel, Mahrukh Azam, Tam Nguyen, Helen Chao, Biaming Zhao, Richard Allston, Alfrado Mellace Hye-Jung Han, Sueyuan Li, and Qiuxia Zhao for their friendship and encouragement at different moments during my stay at Seton Hall. I also have the desire to thank my parents for their unending love and support. Finally I am thankful to my husband, Adnan Khan, who made a significant contributions to my successful completion of doctoral work. Because of his patience, understanding and support I was able to finish my studies with two little kids.

Abstract

For the photophysical investigations, a series of pyrene labeled poly(aryl ether) monodendrons (1-6) were synthesized. Emission spectra of pyrene and pyrene labeled monodendrons (1-6) were examined in acetonitrile, THF and cyclohexane. Lifetimes of these compounds were determined using time resolved laser flash photolysis. Pyrene shows a significant decrease in lifetime with an increase in solvent polarity from 480 ns in cyclohexane to 280 ns in acetonitrile. Pyrene labeled monodendrons (1-6) have a significantly shorter lifetime than pyrene and their lifetimes show a slight decrease with the increase in solvent polarity from 25.4 ns in cyclohexane to 20.8 ns in acetonitrile. These differences may arise from the strong coupling of the polar C-O bond with internal conversion processes.

Excimer emission was observed in concentrated solutions of pyrene and pyrene labeled monodendrons (1-5) and the Birks kinetic model was used to evaluate the kinetic rate parameters. Time resolved fluorescence studies indicate that the rate of excimer formation increases and the lifetime of the excimer decreases with the increase in size of monodendrons. The Gibbs free energy (ΔG) associated with the excimer formation at room temperature is $\cong -4.6$ kcal/mole for pyrene and -3.5 kcal/mole for pyrene labeled monodendrons (1-5). The combined steady-state and time resolved fluorescence decay experiments indicate that the formation of pyrene excimer is completely diffusion controlled and occurs only in excited state.

Quenching experiments with iodine and oxygen in dilute and concentrated solutions (containing excimer) of pyrene labeled monodendrons indicated a generally

decreasing trend in the quenching rate constant with increase in generation number and decrease in solvent polarity. The diffusion coefficient of both quenchers (I_2 and O_2) decrease and the relative viscosities increase with the increase in size of monodendrons in acetonitrile and THF. The experimentally measured diffusion coefficients for pyrene labeled monodendrons in acetonitrile and THF when combined with their quenching rate constants suggests that the higher generation monodendrons are not fully extended in solution and have some back folding. Because of this back folding the fraction of quencher accessible to the fluorophore decreases. This was also supported by molecular modeling studies using Hyperchem.

Table of Contents

List of Figures	viii
List of Schemes	xiii
List of Tables	xiv

CHAPTER 1

Introduction	1
A. Historical	2
B. Synthesis and Characterization	6
C. Fluorescenc	23
D. Quenching of Fluorescence	33

CHAPTER 2

Synthesis	39
A. Synthesis of Pyrene labeled monodendrons	40
B. Characterization	44

CHAPTER 3

Fluorescence	46
A. Introduction	47
B. Steady State Fluorescence	48
I) Monomer Fluorescence.....	48
II) Excimer Fluorescence.....	52
C. Time Resolved Fluorescence Intensity Decay	58
I) Monomer Fluorescence Decay	58
II) Excimer Fluorescence decay	62
D. Kinetics of Excimer Fluorescence	65
E. Conclusions	71

CHAPTER 4	
Quenching of Fluorescence	73
A. Introduction	74
B. Iodine Quenching	76
I) Quenching of monomer Fluorescence	76
II) Quenching of Excimer Fluorescence	94
C. Oxygen Quenching	99
I) Quenching of Monomer Fluorescence	99
II) Quenching of Excimer Fluorescence	101
D. Comparison of Iodine and Oxygen Quenching	101
E. Molecular modeling Studies	111
CHAPTER 5	
Conclusions	113
CHAPTER 6	
Experimental	117
A. General	118
B. Lifetime Measurements	119
C. Sample preparation	120
D. Synthesis	120
APPENDIX A	
Structures	125
APPENDIX B	
Geometry Optimized Structures	129
REFERENCES	
References and Notes	136

List of Figures

Chapter 1

- Figure 1-1. Intrinsic viscosity behavior of polyether dendrimers and of polystyrene.⁶
- Figure 1-2. Numbering scheme in dendritic polymers (second generation tridendron). The core molecule is 1,1,1-tris(4'-hydroxyphenyl)ethane and the branches are poly(aryl ether) monodendrons.^{8c}
- Figure 1-3. Dendritic polymer synthesized by divergent approach: (a) Poly(amine)s tetradendron²⁷ and (b) dendritic carbosilane.³²
- Figure 1-4. Oligomeric examples of three different types of architectures demonstrating the differences in branching sequences and structure: dendritic, hyperbranched and linear polyesters.³⁸
- Figure 1-5. Dendritic-linear block copolymer synthesized by Fréchet.⁴⁶
- Figure 1-6. Structural varieties involving dendrimer strategies: (a) fullerene attached to a dendron;⁷⁰ (b,c) dendrimer polymers with linear and dendritic subunits;^{44,9} (d and e) amphiphilic dendrimers.^{8a}
- Figure 1-7. Potential -energy diagram for the formation of pyrene excimer.⁹⁶

Chapter 2

- Figure 2-1. ¹H-NMR spectra of pyrene labeled poly(aryl ether) monodendrons: (a) 1-Me-O-Py (1); (b) G0-O-Py (2); (c) G0'-O-Py (3) and (d) G1-O-Py (4).

Chapter 3

- Figure 3-1. Steady-state emission spectrum of 1×10^{-7} M solution of pyrene in ACN with $\lambda_{\text{ex}} = 335$.

- Figure 3-2. Steady-state emission spectrum of 1×10^{-7} M solution of 1-methoxypyrene in ACN with $\lambda_{\text{ex}} = 335$.
- Figure 3-3. Steady-state emission spectrum of 1×10^{-7} M solution of pyrene in THF with $\lambda_{\text{ex}} = 335$.
- Figure 3-4. Steady-state emission spectrum of 1×10^{-7} M solution of 1-methoxypyrene in THF with $\lambda_{\text{ex}} = 335$.
- Figure 3-5. Steady-state emission spectrum of 1×10^{-7} M solution of pyrene in CH with $\lambda_{\text{ex}} = 335$.
- Figure 3-6. Steady-state emission spectrum of 1×10^{-7} M solution of 1-methoxypyrene in CH with $\lambda_{\text{ex}} = 335$.
- Figure 3-7. UV-Visible Absorbance spectra of 1×10^{-5} M solution of pyrene in THF.
- Figure 3-8. UV-Visible Absorbance spectra of 1×10^{-5} M solution of 1-methoxypyrene in THF.
- Figure 3-9. Steady-state emission spectrum of 1×10^{-7} M solution of G2-O-Py in THF with $\lambda_{\text{ex}} = 335$.
- Figure 3-10. Steady-state emission spectrum of pyrene in THF at different concentrations, showing the emission of excimer: (a) 1×10^{-2} M, (b) 5×10^{-3} M, (c) 1×10^{-3} M and (d) 1×10^{-5} M. The isoemissive point is at 432 nm.
- Figure 3-11. Steady-state emission spectrum of 1-methoxypyrene in THF at different concentrations, showing the emission of excimer: (a) 5×10^{-2} M, (b) 5×10^{-3} M and (c) 1×10^{-3} M. The isoemissive point is at 441 nm.
- Figure 3-12. Excimer to monomer fluorescence intensity ratio (I_D/I_M) for pyrene and pyrene labeled poly(aryl ether) monodendrons in acetonitrile, tetrahydrofuran (THF) and cyclohexane (CH).
- Figure 3-13. Fluorescence decay of 1×10^{-7} M pyrene in THF.
- Figure 3-14. Semilogarithmic form of fluorescence decay of 1×10^{-7} M pyrene in THF.
- Figure 3-15. Fluorescence decay of 1×10^{-7} M 1-methoxypyrene in THF.
- Figure 3-16. Semilogarithmic form of fluorescence decay of 1×10^{-7} M 1-methoxypyrene in THF.
- Figure 3-17. Fluorescence decay of 1×10^{-2} M pyrene in THF.
- Figure 3-18. Semilogarithmic form of fluorescence decay of 1×10^{-2} M pyrene in THF.
- Figure 3-19. Fluorescence decay of 5×10^{-2} M 1-methoxypyrene in THF.

- Figure 3-20. Semilogarithmic form of fluorescence decay of 5×10^{-2} M 1-methoxypyrene in THF.
- Figure 3-21. Variation of λ_1 (a) and λ_2 (b) with concentration for pyrene in ACN.
- Figure 3-22. Variation of λ_1 (a) and λ_2 (b) with concentration for 1-methoxypyrene in ACN.
- Figure 3-23. Variation of λ_1 (a) and λ_2 (b) with concentration for pyrene in THF.
- Figure 3-24. Variation of λ_1 (a) and λ_2 (b) with concentration for 1-methoxypyrene in THF.
- Figure 3-25. Variation of λ_1 (a) and λ_2 (b) with concentration for pyrene in CH.
- Figure 3-26. Variation of λ_1 (a) and λ_2 (b) with concentration for 1-methoxypyrene in CH.

Chapter 4

- Figure 4-1. Steady-state emission spectrum of 1×10^{-7} M pyrene in THF at different iodine concentrations: (a) 0.00 M; (b) 0.29 mM and (c) 0.73 mM.
- Figure 4-2. Steady-state emission spectrum of 1×10^{-7} M 1-methoxypyrene in THF at different iodine concentrations: (a) 0.00 M; (b) 0.29 mM and (c) 0.73 mM.
- Figure 4-3. Variation of decay constant (λ_1) of 1×10^{-7} M pyrene in THF versus iodine concentration.
- Figure 4-4. Variation of decay constant (λ_1) of 1×10^{-7} M 1-methoxypyrene in THF versus iodine concentration.
- Figure 4-5. Stern-Volmer plots for 1×10^{-7} M pyrene in ACN: (a) intensity and (b) quenching ratio by iodine.
- Figure 4-6. Stern-Volmer plots for 1×10^{-7} M pyrene in THF: (a) intensity and (b) quenching ratio by iodine.
- Figure 4-7. Stern-Volmer plots for 1×10^{-7} M pyrene in CH: (a) intensity and (b) quenching ratio by iodine.
- Figure 4-8. Stern-Volmer plots (intensity quenching ratio) for 1×10^{-7} M pyrene labeled poly(aryl ether) monodendrons in ACN for iodine quenching.

- Figure 4-9. Stern-Volmer plots (lifetime quenching ratio) for 1×10^{-7} M pyrene labeled poly(aryl ether) monodendrons in ACN for iodine quenching.
- Figure 4-10. Stern-Volmer plots (intensity quenching ratio) for 1×10^{-7} M pyrene labeled poly(aryl ether) monodendrons in THF for iodine quenching.
- Figure 4-11. Stern-Volmer plots (lifetime quenching ratio) for 1×10^{-7} M pyrene labeled poly(aryl ether) monodendrons in THF for iodine quenching.
- Figure 4-12. Stern-Volmer plots (intensity quenching ratio) for 1×10^{-7} M pyrene labeled poly(aryl ether) monodendrons in CH for iodine quenching.
- Figure 4-13. Stern-Volmer plots (lifetime quenching ratio) for 1×10^{-7} M pyrene labeled poly(aryl ether) monodendrons in CH for iodine quenching.
- Figure 4-14. Separation of the static and dynamic quenching constant of 1×10^{-7} M pyrene in THF. Static quenching constant (K_s) is obtained from the slope.
- Figure 4-15. Separation of the static and dynamic quenching constant of 1×10^{-7} M 1-methoxypyrene in THF. Static quenching constant (K_s) is obtained from the slope.
- Figure 4-16. UV-Visible absorbance spectra of 0.735 mM iodine in ACN.
- Figure 4-17. UV-Visible absorbance spectra of 0.735 mM iodine in THF.
- Figure 4-18. UV-Visible absorbance spectra of 0.735 mM iodine in CH.
- Figure 4-19. UV-Visible absorbance spectra of 1×10^{-6} M pyrene in ACN containing iodine: (a) 0.0 mM; (b) 0.735 mM; (c) 1.47 mM (d) 2.21 mM; (e) 2.94 mM and (f) 3.67 mM.
- Figure 4-20. UV-Visible absorbance spectra of 1×10^{-6} M 1-methoxypyrene in ACN containing iodine: (a) 0.0 mM and (b) 0.735 mM.
- Figure 4-21. UV-Visible absorbance spectra of 1×10^{-6} M pyrene in THF containing iodine: (a) 0 mM; (b) 1.47 mM; (c) 0.29 mM and (d) 0.735 mM.
- Figure 4-22. UV-Visible absorbance spectra of 1×10^{-6} M 1-methoxypyrene in ATHFCN containing iodine: (a) 0.0 mM, (b) 1.47 mM and (c) 0.735 mM.
- Figure 4-23. UV-Visible absorbance spectra of 1×10^{-6} M pyrene in CH containing iodine: (a) 0.0 mM; (b) 0.294 mM; (c) 0.735 mM (d) 1.47 mM; (e) 2.206 mM and (f) 2.94 mM.
- Figure 4-24. UV-Visible absorbance spectra of 1×10^{-6} M 1-methoxypyrene in CH containing iodine: (a) 0.0 mM, (b) 0.735 mM and (c) 1.47 mM.

- Figure 4-25. Emission spectra of 1×10^{-2} M pyrene in THF containing iodine: (a) 0.0 mM; (b) 0.29 mM; (c) 0.88 mM and (d) 2.20 mM.
- Figure 4-26. Emission spectra of 5×10^{-2} M 1-methoxypyrene in THF containing iodine: (a) 0.0 mM; (b) 0.29 mM; (c) 0.88 mM and (d) 2.20 mM.
- Figure 4-27. Change in the ratio of the intensity of excimer and monomer emission (I_D/I_M) with iodine concentration for pyrene (1×10^{-2} M) and pyrene labeled poly(aryl ether) monodendrons (5×10^{-2} M) in THF.
- Figure 4-28. Stern-Volmer plot for 0.01 M pyrene in THF containing iodine.
- Figure 4-29. Stern-Volmer plot for 0.05 M 1-methoxypyrene in THF containing iodine.
- Figure 4-30. Fluorescence decay of 1×10^{-7} M pyrene in THF containing quencher: (a) iodine = 1.515 mM and (b) oxygen = 1.5 mM.
- Figure 4-31. Fluorescence decay of 1×10^{-7} M 1-methoxypyrene in THF containing quencher: (a) iodine = 1.515 mM and (b) oxygen = 1.5 mM.
- Figure 4-32. Fluorescence decay of 0.01 M pyrene in THF containing quencher: (a) no quencher, (b) iodine = 1.515 mM and (c) oxygen = 1.5 mM.
- Figure 4-33. Fluorescence decay of 1×10^{-7} M 1-methoxypyrene in THF containing quencher: (a) no quencher, (b) iodine = 1.515 mM and (c) oxygen = 1.5 mM.
- Figure 4-34. The power regression fit of R_{exp} vs MW. of pyrene labeled poly(aryl ether) monodendrons (1-6) in ACN.
- Figure 4-35. The power regression fit of R_{exp} vs MW. of pyrene labeled poly(aryl ether) monodendrons (1-6) in THF.
- Figure 4-36. The power regression fit of R_{calc} vs MW. of pyrene labeled poly(aryl ether) monodendrons (1-6).
- Appendix A. Structures of pyrene and pyrene labeled poly(aryl ether) monodendrons (1-6).
- Appendix B. Geometry optimized structures of pyrene and pyrene labeled poly(aryl ether) monodendrons (1-6).

List of Schemes

Chapter 1

- Scheme 1-1. Schematical representation of the divergent dendrimer growth according to Tomalia.⁹
- Scheme 1-2. Synthesis of polyether monodendrons.³⁴
- Scheme 1-3. Synthesis of dendritic polyethers by convergent approach.³⁸
- Scheme 1-4. Formation of hyperbranched polymers using an $A_2 B$ monomer as described by Flory.³⁶
- Scheme 1-5. Formation of hyperbranched aromatic polyesters.⁷⁰
- Scheme 1-6. Synthesis of isophthalate ester functionalized dendritic-polystyrene block copolymer.⁴⁷
- Scheme 1-7. Schematic energy levels and the rate processes associated with monomer/excimer system.
- Scheme 1-8. Quenching of monomer/excimer fluorescence.

Chapter 2

- Scheme 2-1. Synthesis of 1-Me-O-Py (1).
- Scheme 2-2. Synthesis of G0-O-Py (2).
- Scheme 2-3. Synthesis of G0'-O-Py (3).
- Scheme 2-4. Synthesis of G1-O-Py (4).

List of Tables

Chapter 3

- Table 3-1. Lifetimes of pyrene and pyrene labeled poly(aryl ether) monodendrons (monomers) in ACN, THF and CH.
- Table 3-2. Lifetimes of pyrene and pyrene labeled poly(aryl ether) monodendrons (excimers) in ACN, THF and CH.
- Table 3-3. Excimer kinetics of pyrene and pyrene labeled poly(aryl ether) monodendrons in ACN.
- Table 3-4. Excimer kinetics of pyrene and pyrene labeled poly(aryl ether) monodendrons in THF.
- Table 3-5. Excimer kinetics of pyrene and pyrene labeled poly(aryl ether) monodendrons in CH.
- Table 3-6. Excited-state equilibrium constant (K) for pyrene and pyrene labeled poly(aryl ether) monodendrons in ACN, THF and CH.
- Table 3-7. Gibbs free energy (ΔG) for pyrene and pyrene labeled poly(aryl ether) monodendrons in ACN, THF and CH.

Chapter 4

- Table 4-1. Table 4-1: Dynamic quenching rate constants (K_{SV}) for 1×10^{-7} M pyrene and pyrene labeled poly(aryl ether) monodendrons (1-6) in ACN, THF and CH for iodine quenching.
- Table 4-2. Bimolecular quenching rate constants (k_{QM}) for 1×10^{-7} M pyrene and pyrene labeled poly(aryl ether) monodendrons (1-6) in ACN, THF and CH for iodine quenching.
- Table 4-3. Static quenching rate constants (K_S) for 1×10^{-7} M pyrene and pyrene labeled poly(aryl ether) monodendrons (1-6) in ACN, THF and CH for iodine quenching.

- Table 4-4. Excimer fluorescence quenching rate constant (k_{QD}) for pyrene and pyrene labeled poly(aryl ether) monodendrons (1-6) in ACN, THF and CH for iodine quenching.
- Table 4-5. Monomer fluorescence quenching rate constants (k_{QM}) for pyrene and pyrene labeled poly(aryl ether) monodendrons (1-6) in ACN, THF and CH for oxygen quenching.
- Table 4-6. Excimer fluorescence quenching rate constants (k_{QM}) for pyrene and pyrene labeled poly(aryl ether) monodendrons (1-6) solutions in ACN, THF and CH for oxygen quenching.
- Table 4-7. Diffusion coefficient (D_{Py}) of pyrene labeled monodendrons (1-6) and their radii in ACN and THF.
- Table 4-8. Diffusion coefficient of iodine (D_{I_2}) and oxygen (D_{O_2}) and relative viscosities (η_{rel}) for pyrene labeled monodendrons (1-6) in ACN.
- Table 4-9. Diffusion coefficient of iodine (D_{I_2}) and oxygen (D_{O_2}) and relative viscosities (η_{rel}) for pyrene labeled monodendrons (1-6) in THF.

CHAPTER 1
Introduction

A. Historical

Dendritic polymers are molecules with a globular structure in which well defined branches radiate from a central core, and possess large number of terminal groups with a definite geometrical growth. This is a novel class of materials with a well-defined molecular composition. Researchers are enthusiastic about using dendritic molecules as building blocks for synthesizing even more complex supermolecules and supramolecular structures.

The unique architecture of these macromolecules leads to a variety of new and unusual physical properties such as low intrinsic viscosity, high solubility, high miscibility and high reactivity (from the presence of many chain ends). Much work has been carried out in areas such as melt viscosity,¹ glass transition temperature,² rheological properties³ and even on the photoinduced electron transfer to C₆₀.⁴ The most exciting physical property of dendrimers is the variation of their intrinsic viscosities^{5,6} with molecular weight. It is found that, when the size increases beyond a certain point, the intrinsic viscosity begins to decline, contrary to the behavior of linear polymers. This effect is believed to be a consequence of the globular shapes of high generation dendrimers leaving them unable to 'tangle' with one another after the manner of linear polymers. Figure 1.1 shows the intrinsic viscosity behavior of polyether dendrimers and polystyrene.

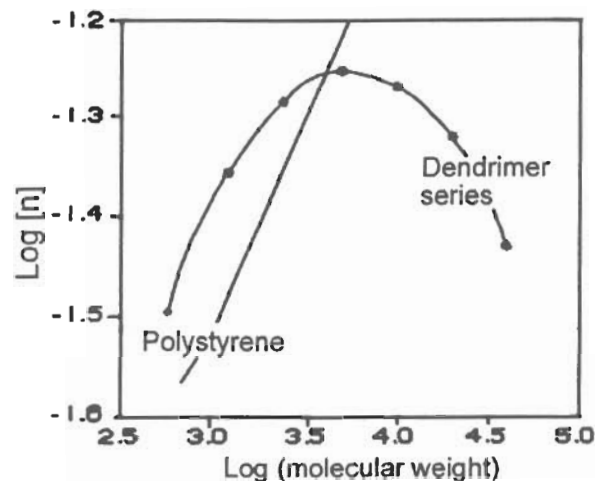


Figure 1-1. Intrinsic viscosity behavior of polyether dendrimers and of polystyrene.⁶

A large variety of dendrimers have now been synthesized up to now. Prominent examples are the polyamidoamines (PAMAM, Tomalia), polyethers (Frechet), arborols and metal containing structures (Newkome) and polyamines (Meijer). Researchers are enthusiastic about using dendritic molecules as building blocks for synthesizing even more complex supermolecules and supramolecular structure.

Current nomenclature rules do not easily accommodate these structures. It has become conventional to describe dendrimers as diverging “branches” radiating from the central “core”. Each new layer or shell of monomer surrounding the core is considered a “generation”. The outermost layer or shell of monomer surrounding the core is called “generation zero”, the next layer is “generation one” and so on. Figure 1-2 shows the branching scheme of successive generations.

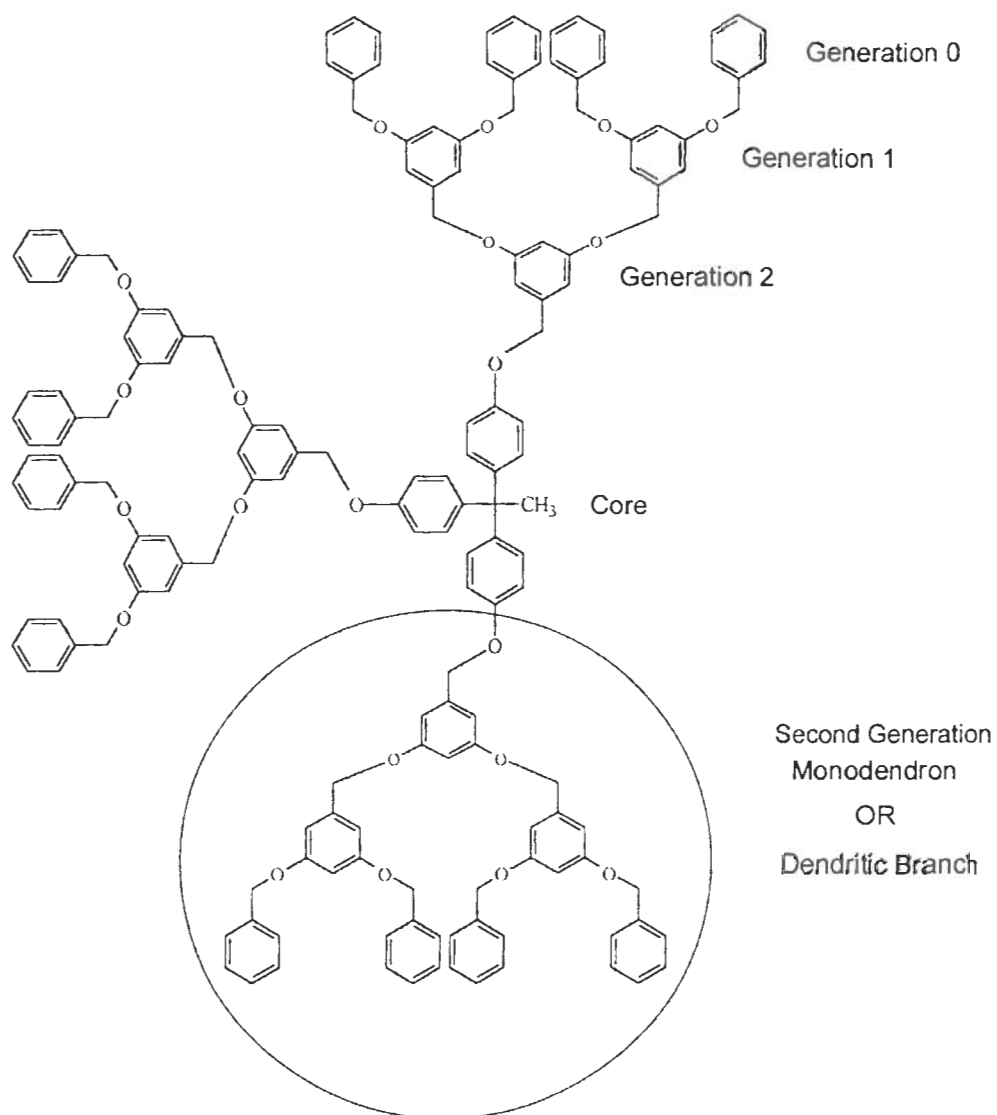


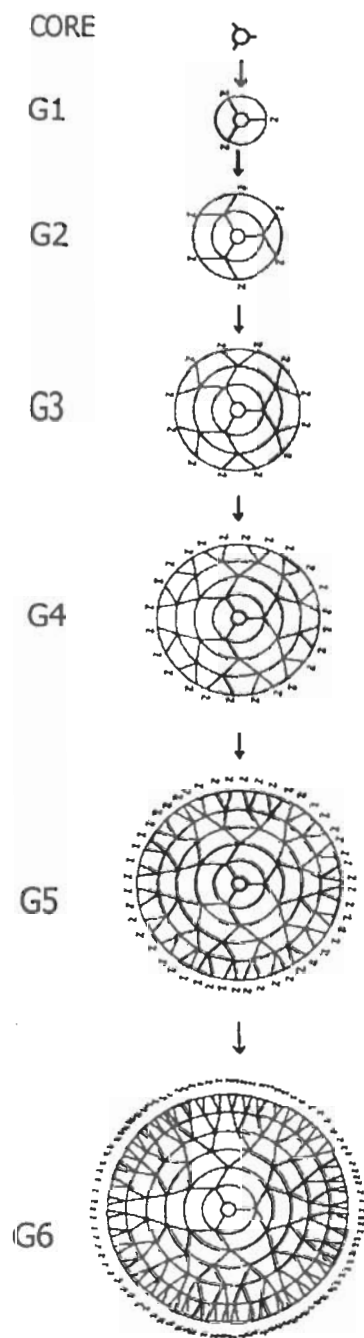
Figure 1-2. Numbering scheme in second generation tridendron (dendritic polymers). The core molecule is 1,1,1 -tris(4'-hydroxyphenyl)ethane and the branches are poly(aryl ether) monodendrons.^{8c}

Many potential applications for dendrimers have been proposed.⁷ They find use as solubilizing agents,⁸ catalysts, drug delivery agents⁹ and slow release agents for perfumes, herbicides and drugs. Research is also active in applications as diverse as polymer adhesives and coatings, additives,¹⁰ catalyst supports, thin films, laser-printing toners and MRI (magnetic resonance imaging) agents.¹¹

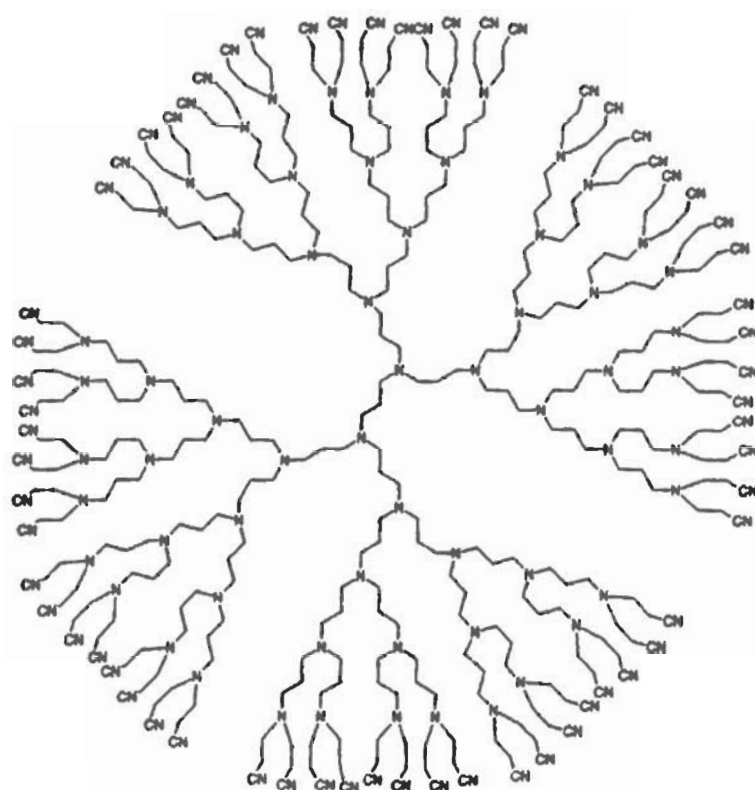
Several theoretical investigations have been performed to predict the structure and properties of dendritic polymers. Issues of special interest include density profiles in dendrimers, the localization of end groups and the limits of perfect dendrimer growth. Two theoretical models that have been reported to describe the structure of dendrimers are the “hollow sphere” model by de Gennes² and the “dense sphere” model by Muthukumar.¹² The analytical prediction of de Gennes, using a self-consistent-field (SCF) model, showed that dendrimers have all end groups at the periphery with the lowest density at the core. Also, with increasing numbers of generations, a “dense packed” state is reached when the number of chain ends expand to completely fill the surface area available. Using a kinetic approach, Muthukumar predicted greater “ingrowth” for dendrimers and the greatest density near the center with the increasing number of generations. The de Gennes model has been supported by empirical studies on the dendritic box¹³ and related structures,¹⁴ exchange interactions between radical centers,¹⁵ optical data¹³ and SANS studies on PAMAM dendrimers.^{16,17} The dense sphere model of Muthukumar has been supported by solution NMR,¹⁸ REDOR- NMR,¹⁹ SEC²⁰ SANS²¹ and viscometry studies. Both models predict the unusual properties of dendrimer although with some differences.

B. Synthesis and Characterization

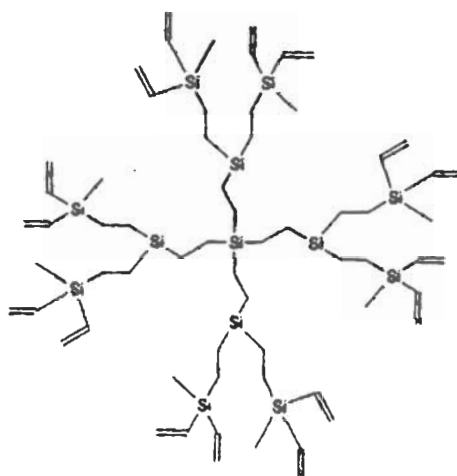
The term 'dendrimer' is now used almost universally to describe highly branched, monodisperse compounds. Most syntheses of dendrimers involve the repetitious alternation of a growth reaction and an activation reaction. Often, these reactions have to be performed at many sites on the same molecule simultaneously. These reactions must be very 'clean' and give high yield for the construction of large targets to be feasible. Many dendrimer syntheses rely upon traditional reactions, such as the Michael reaction,³ or the Williamson ether synthesis,²² whilst others involve the use of modern techniques and chemistry, such as solid-phase synthesis,^{23,24} organometallic^{25,26} chemistry, organosilicon²⁷ chemistry, organo-phosphorus¹ chemistry, or other contemporary organic methodologies.² The choice of the growth reaction dictates the way in which branching is introduced into the dendrimer. Branching may either be present in the building blocks as is more often the case or it can be created as a function of the growth reaction, as is the case with the PAMAMs and the poly(propylene imine)s. Two main methodologies exist for the synthesis of dendrimers. The synthetic methodology employed in the early dendrimer syntheses by Tomalia³ and Newkome^{28,29} came to be known as the 'divergent' approach. This name comes from the way in which the dendrimer grows outwards from the core, diverging into space. A schematic representation of divergent growth is shown in Scheme 1-1. Starting from a reactive core, a generation is grown, and then the new periphery of the molecule is activated for reaction with more monomers. The two steps can be repeated. The divergent approach is successful for the production of large quantities of dendrimers since, in each generation-adding step, the molar mass of the



Scheme 1-1. Schematical representation of the divergent dendrimer growth according to Tomalia.⁹



(a)



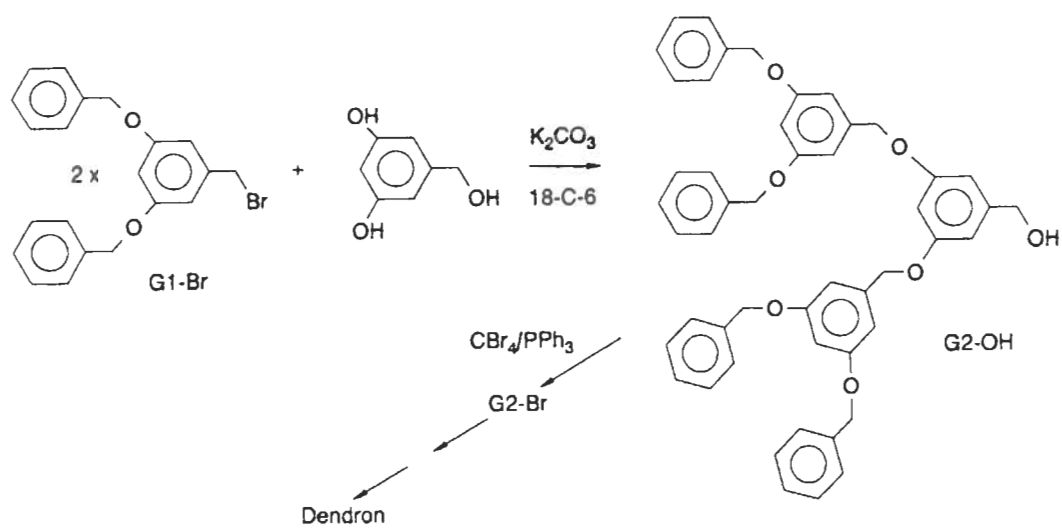
(b)

Figure 1-3. Dendritic polymers synthesized by divergent approach: (a) Poly(amine)s tetradendron²⁷ and (b) Dendritic carbosilane.³²

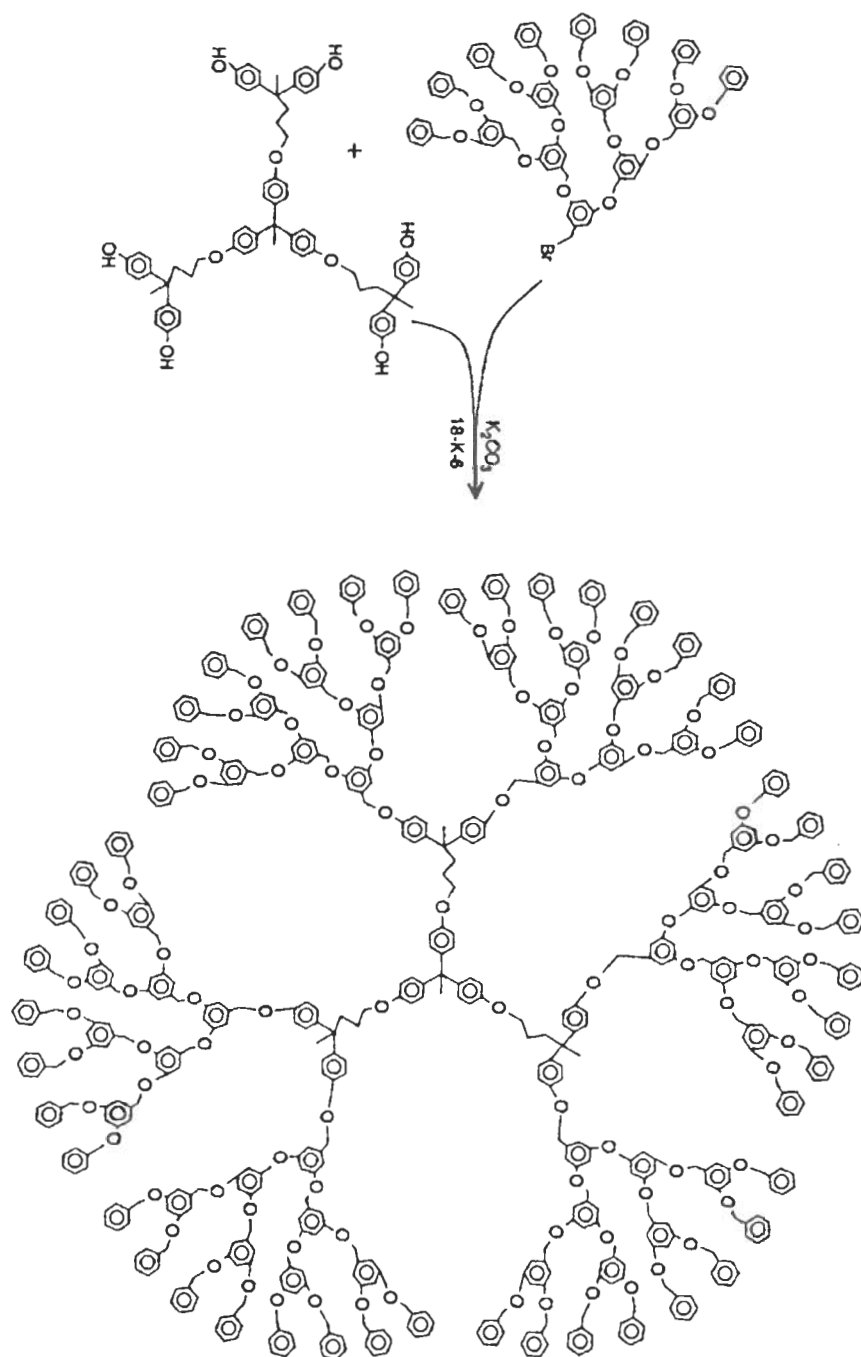
dendrimer is doubled. Figure 1-3 shows a dendritic polyamine,^{30,31} and a dendritic carbosilane³² synthesized by the divergent approach.

Very large dendrimers have been prepared in this way, but incomplete growth steps and side reactions usually lead to the isolation and characterization of slightly imperfect samples.⁴ Divergently grown dendrimers are virtually impossible to isolate pure from their side products. The 'convergent' approach was first introduced in 1989 by Frechet³³ as a response to the weaknesses of divergent syntheses. Convergent growth begins at what will end up as the surface of the dendrimer, and works inwards by gradually linking surface units together with more monomers (Scheme 1-2).³⁴ When the growing wedges are large enough, several are attached to a suitable core to give a complete dendrimer (Scheme 1-3). This method has proven to be very versatile and the aromatic polyether dendrons with their distinct functionalities at their focal point and chain ends have been widely used in the preparation of a broad array of functional dendritic structures. But the convergent methodology suffers from low yields in the synthesis of large structures. Dendritic wedges of higher generations encounter serious steric problems in the reactions of their 'focal points'.

Each of these synthetic routes has advantages and disadvantages. The divergent approach allows for the attachment on the periphery of potentially functional molecules such as saccharides or peptides. The convergent approach offers the opportunity to prepare "segregated" dendrimers and other interesting hybrid structures by employing the single reactive group at the focal point (or periphery). Convergent synthesis is



Scheme 1-2. Synthesis of polyether monodendrons.³⁴



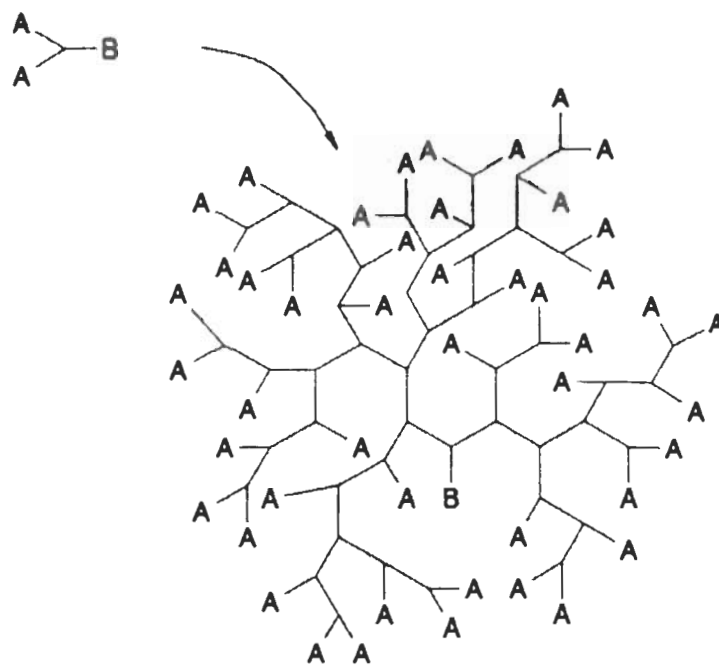
Scheme 1-3. Synthesis of dendritic polyethers by convergent approach.³⁸

preferable for studies where precisely defined structures are necessary and divergent synthesis are preferable where large amount of materials or very large size is desired.

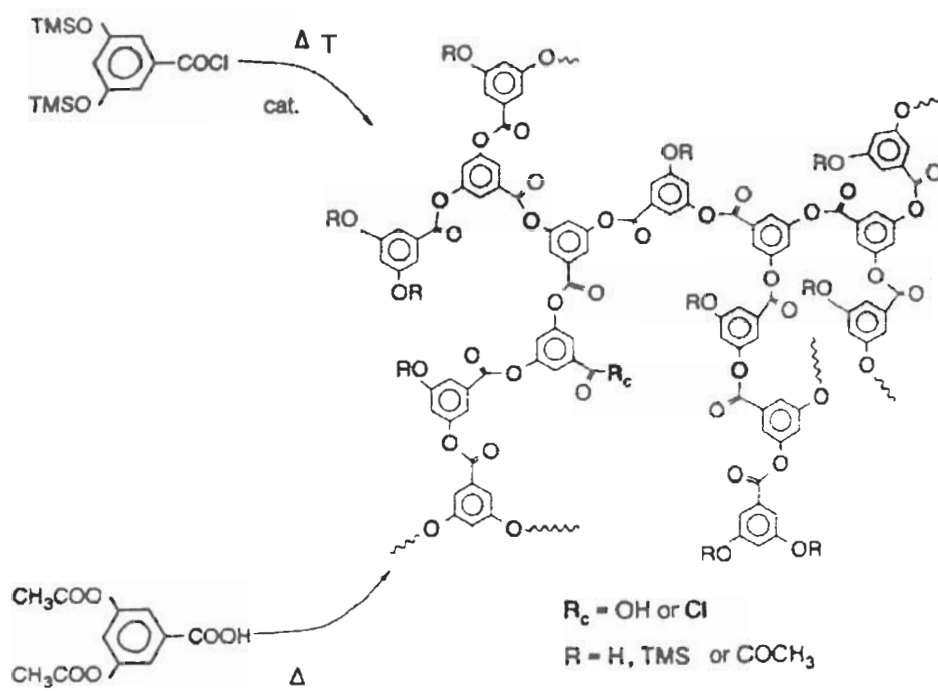
In 1998, Frechet reported the convergent synthesis of a new class of aliphatic polyether dendrons using Williamson etherification chemistry.³⁵ This dendrimer with an aliphatic polyether backbone has a great potential as a result of the combination of its inert, low absorbance building blocks, multiple reactive chain ends and uniquely functionalized focal point. By varying their surface functionalities these dendrimers might show improved biocompatibility and be rendered water-soluble or water dispersible.

Recent advances in the synthesis of low polydispersity hyperbranched polymers¹⁰ have promoted interest in their dendrimer-like properties. The formation of highly branched polymers using A_xB ($x > 1$) was first described by Flory³⁶ via polycondensation. Scheme 1-4 illustrates the manner by which hyperbranched polymers could be created using Flory's trifunctional monomer (A_2B). The characteristic features for a hyperbranched polymers derived from A_2B monomers are one unreacted B functionality, unreacted A functionalities distributed randomly throughout the polymer and a branching ideality below 100% (usually between 50 and 75%). The branching ideality of 100% for perfect dendrimers cannot be achieved by control of reaction conditions, solvent or catalyst.

The use of different monomers and different condensation reactions can yield different degrees of branching in hyperbranched structures. Scheme 1-5 shows the synthesis of hyperbranched aromatic polyesters in a one step synthesis. Both the highly

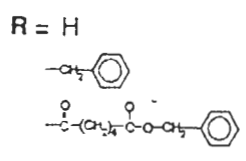
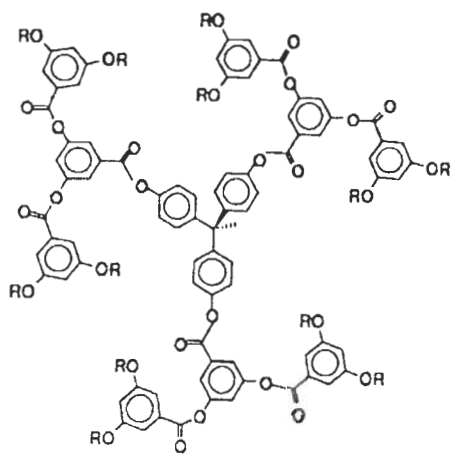


Scheme 1-4. Formation of hyperbranched polymers using an A_2B monomer as described by Flory.³⁶

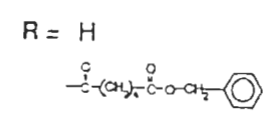
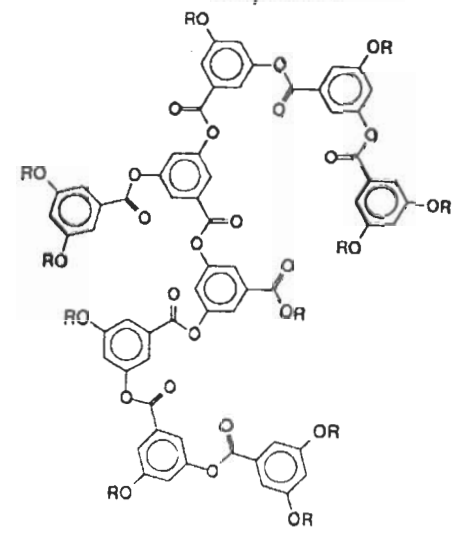


Scheme 1-5. Formation of hyperbranched aromatic polyesters.⁷⁰

Dendritic polyesters



Hyperbranched Polyesters



Linear Polyesters

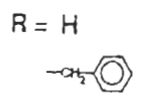
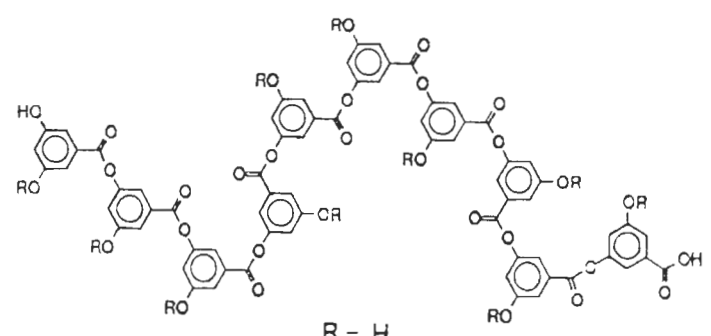


Figure 1-4. Oligomeric examples of the three types of architectures demonstrating the differences in branching sequences and structure: dendritic, hyperbranched and linear polyesters.³⁸

activated acid chloride and the acetate monomer lead to about the same degree of branching (50-60%).³⁷

It has been found that polymers with a degree of branching¹¹ (D_{br}) of over ca. 60% can display some behavior more akin to dendrimers than to their linear cousins. Although hyperbranched polymers with a D_{br} as high as 90% have been prepared by stepwise polymerization techniques, they cannot be considered true dendrimers. Hyperbranched polymers are of considerable industrial interest because of the ease of their synthesis. However, they will never attain the degree of architectural control or monodispersity which the stepwise synthesis of dendrimers offers to the synthetic chemist. Figure 1-4 shows the differences in the dendritic, hyperbranched and linear polyesters.³⁸

The polyether wedges developed by Fréchet³³ and Hawker³⁴ have found wide use as components of larger systems. Apart from the surface and core units that have been used in conjunction with these dendrons, rotaxanes⁴⁰ and even C_{60} ⁴¹ have benefited from the attachment of dendritic moieties. Meijer^{42,43} successfully synthesized dendritic-linear block copolymers by growing poly (propylene imine) dendrons from suitably monofunctionalized low molecular weight linear polystyrene. This was done by employing a divergent approach. A variety of dendritic-linear block copolymers have been synthesized by Fréchet and coworkers^{44,45} featuring both the coupling of hydrophobic and hydrophilic linear polymers to convergent polyether based monodendrons. They used the polyether dendrons possessing benzylic halides at their focal point as macromolecular initiators for the metal catalyzed “living” radical polymerization of vinylic monomers.⁴⁶ The resulting copolymer, shown in Figure 1-5,

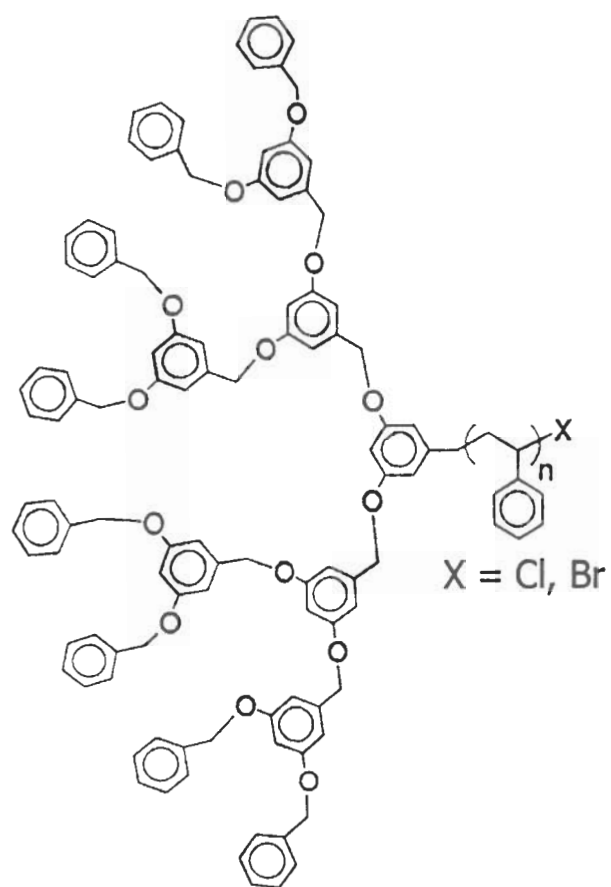
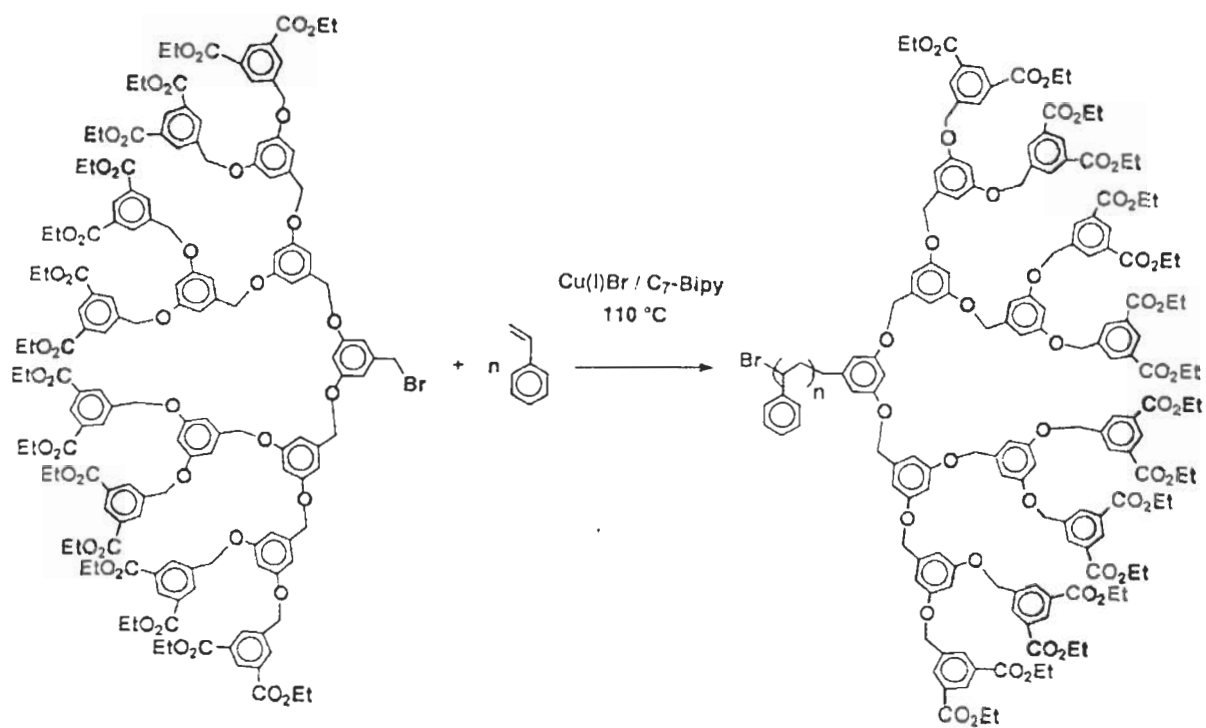


Figure 1-5. Dendritic-linear block copolymer synthesized by Fréchet.⁴⁶

was found to exhibit well-defined dendritic-linear diblock architectures, with controlled molecular weights and very low polydispersities. They successfully synthesized many other novel functionalities dendritic-linear block copolymers in which the peripheral "surface" of the dendritic block possesses diverse functionalities.⁴⁷ Scheme 1-6 shows the synthesis of isophthalate ester functionalized dendritic-polystyrene hybrids. All these dendritic-linear block copolymers have been shown to exhibit interesting solution, solid-state and interfacial properties.⁴⁸

Perhaps the most striking example of the post-synthesis modification of a dendrimer is the demonstration of the 'dendritic box' by Meijer.⁴⁹ It was found that a 'shell' could be formed on the surface of a poly(propylene imine) dendrimer by reacting the terminal amines with bulky amino acids. This shell was used for the size-specific entrapment of guest molecules within the dendritic structure, and could later be removed to release the guest. This particular dendritic box is not suitable for drug delivery. However, this group is now trying to design boxes that could be opened enzymatically and photochemically.

If one is to have ultimate control over the construction of dendrimers, then a more versatile principle for the synthesis of involved architectures is needed. In order to synthesize structures, methodology must allow the selective incorporation of functionality within the dendritic structure. Since the stepwise synthesis of dendrimers involves the repetitious alternation of a growth reaction and an activation reaction, it is possible to create structures as shown in Figure 1-6. Fréchet has shown in a series of publications, how the convergent approach can be utilized to control the surface¹⁰ and internal¹¹ functionality of dendrimers. By the reaction of a wedge with large excess of



Scheme 1-6. Synthesis of isophthalate ester functionalized dendritic-polystyrene block copolymer.⁴⁷

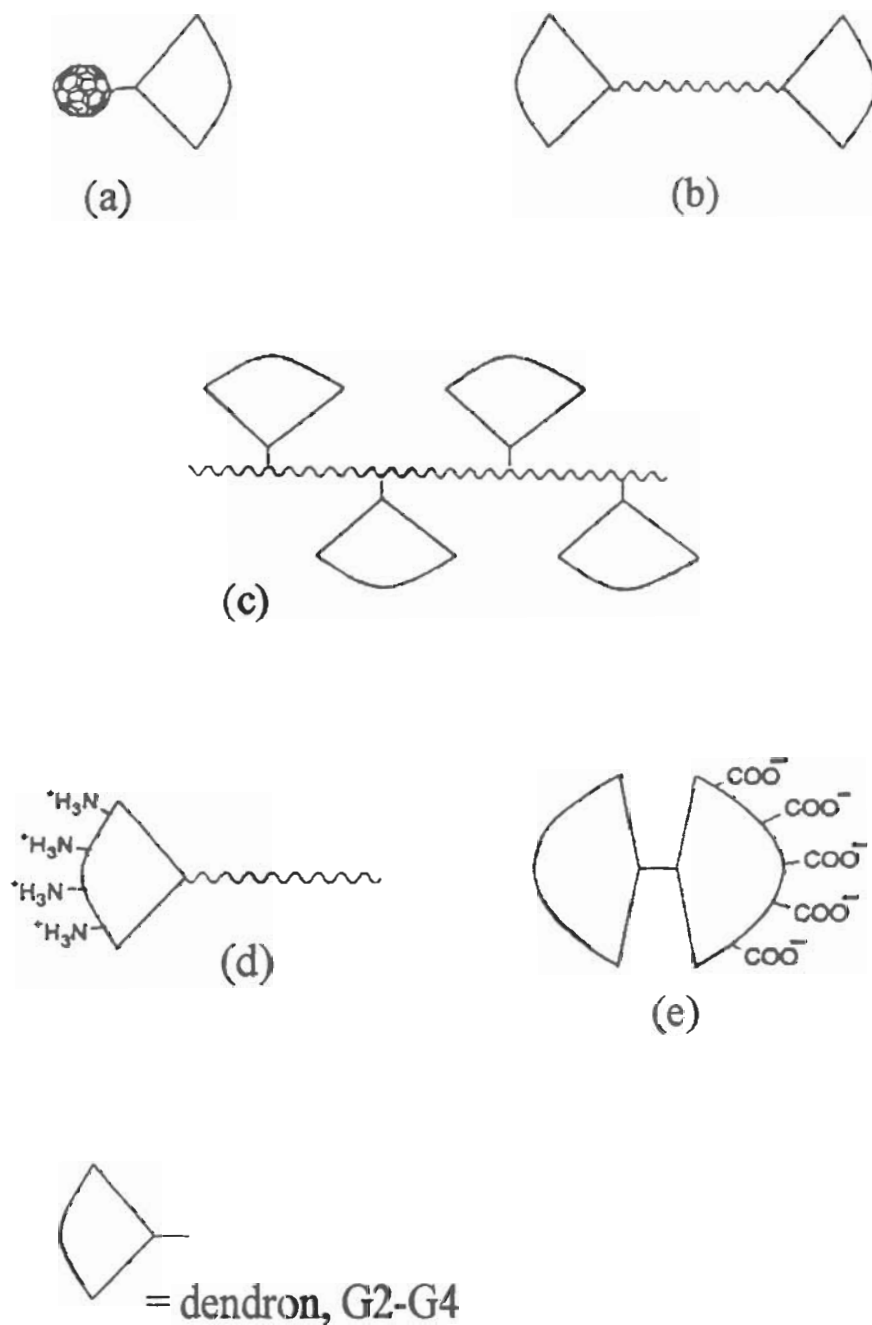


Figure 1-6. Structural varieties involving dendrimer strategies: (a) fullerene attached to a dendron;⁷⁰ (b, c) hybrid polymers with linear and **dendritic subunits**;^{44,9} (d,e) amphiphilic dendrimers.^{8a}

monomer or with a monoprotected monomer, a half-reacted branching unit can be generated. Another wedge can be attached to the other branch in a further step, giving a branching unit with different functionality on each branch. This technique has been used successfully in the synthesis of mono-surface functionalized and internally functionalized dendrimers

Functional groups can also be built in as surface groups at the beginning of a convergent synthesis or at the end of a divergent scheme. The size, shape, surface chemistry, flexibility, and topology can be precisely defined and controlled, and this allows for nanoscopic tailoring. The great density of surface groups may be functionally tailored for superstrong adhesives, chemical/biological molecule detection, catalysis of toxic molecules, and as interaction sites with linear polymers to modify bulk/solution properties. The interior of dendritic polymers can also be functionally tailored for a variety of uses including catalysis of toxic molecules and molecular recognition, which have been demonstrated at sites covalently bonded to the interior architecture (molecular imprinting).

From a pharmaceutical and a medical point of view, these polymeric systems are particularly promising because they can serve as micro- or nanoparticulate carriers for drug delivery systems development. In addition, because of the very large number of free arms they can be used for immobilization of drugs, cells, enzymes or antibodies, whereby a very high density of biological agent is attained in a very small volume. These have significant potential to serve as models for the investigation of supramolecular biological interactions, as well as for the study of highly ionic polymeric systems. Of particular

importance in biomedical and pharmaceutical research is their ability to act as supports for immobilization of bioactive agents.

The design of dendritic monomers with the applications of the final structures in mind has been the inspiration for a wide variety of building blocks, ranging from simple chiral units⁵⁰ to liquid crystalline moieties. They are constructed from branching units and a core. In the design of an application-based dendrimer,^{24,25} certain moieties are required within the structure. There are many examples of dendrimers whose constitutions have been designed with a purpose in mind. Porphyrin cores have been introduced into dendrimers by both convergent and divergent routes.^{51,27} These structures have been used to examine the effect of the dendritic microenvironment on the selectivity of catalysis by the porphyrins and on the electrochemical behavior of the porphyrin. Functional cores have also been used to study the effect of microenvironment on chirality⁵¹ and solvatochromic effects.²

Balzani⁴¹ demonstrated the synthesis of dendritic polynuclear metal complexes with ruthenium atoms acting as branching points. The luminescence and redox properties of the dendrimers were studied in an investigation of the dendrimer as a potential light harvesting or directional energy transfer unit.⁵² Chemically interesting groups such as tetrathiafulvalene²⁸ (TTF), cholesterol,⁵³ tryptophan and various saccharides^{54,55} have been successfully incorporated onto the surface of dendrimers, as have complexes of ruthenium⁵⁶ and nickel.⁷

Nuclear Magnetic Resonance (NMR) spectroscopy has been found to be an invaluable technique in the characterization of dendrimers. Indeed, ¹H and ¹³C NMR

spectra of dendrimers are surprisingly simple and contain a great deal of information about defects and impurities in their structures. Other methods, familiar to polymer chemists, have been used extensively in the characterization of dendrimers. Electron microscopy has been of great use in the visualization of dendrimers⁵¹ and their aggregates^{28,42} and Gel Permeation Chromatography (GPC) has been used for the calculation of radii of gyration, hydrodynamic radii²⁷ and polydispersities. Low Angle Laser Light Scattering (LALLS), Small Angle Neutron (SANS) and X-ray (SAXS).³⁶ Scattering techniques have met with limited use. Many results have been obtained by the use of Matrix Assisted Laser Desorption / Ionisation - Time of Flight (MALDI-TOF)^{24,57} and ElectroSpray (ES)^{58,25} mass spectrometric methods. There are a few examples of crystalline⁵⁹ dendrimers, powder, and single crystal⁶⁰ X-ray studies of dendrimers, but these are confined to low generations and rigid, hindered molecules.

C. Fluorescence

Fluorescence has proven to be a versatile tool for a myriad of applications. It is a powerful technique for studying molecular interactions in analytical chemistry, biochemistry, cell biology and physiology, photochemistry and environmental science. For polymers, fluorescence techniques have been applied in the study of a wide range of processes such as end-to-end cyclization, micellization, diffusion within latex particles, phase separation in polymer blends and polymerization kinetics.^{61,62} It has also been extensively used to study the microenvironment of micelles⁶³ liposomes and proteins.^{64,65}

These investigations were accomplished by either addition of a small molecule fluorescent **probe**⁶⁶ to a polymer system or by covalent attachment or incorporation of fluorescent labels into the polymer chains.

Fluorescence measurements have been used in studying dendrimer structure in number of ways. They provided useful information on the morphology of condensation-type dendritic polymers.⁶⁷ The microenvironment inside a dendrimer has been studied by the use of fluorescence intensity (I) and fluorescence lifetime (τ) measurements.^{68,69}

Fluorescence spectroscopy has been used to characterize the structure of starburst dendrimers possessing an external anionic surface. Pyrene was used as a photoluminescence probe to sense various hydrophobic sites in the microheterogeneous architecture offered by poly(amidoamine) starburst dendrimers possessing sodium carboxylate surfaces.⁶⁷ Many investigators have made use of different functional probes in order to study dendritic microenvironments. These probes can either be attached covalently to the dendritic structure, like the photochemical,⁴¹ chiral,¹³ and solvatochromic⁷⁰ moieties or they can be introduced as guest species. Probes are typically discrete compounds, such as pyrene, naphthalene, anthracene and numerous other compounds and derivatives and have photophysical responses dependent upon medium polarity, rigidity or other properties. Use of a non-covalent probe involves equilibration as a guest molecule within the system of study, followed by evaluation of the photophysical response. Fluorescent probe techniques have evolved rapidly in the last two decades from the study of microheterogeneous assemblies such as micelles, membranes and vesicles. These have also applied to the characterization of thermal and mechanical properties of polymers⁷¹ and for the detection of hydrophobic microdomains

in aqueous solutions of amphiphilic polymers.⁷² The sensitivity of molecular probes to the characteristics of their environment is the basis for the use of these chromophores and fluorophores in the analysis of complex molecular assemblies. The optical properties that generally reflect environmental conditions include excitation and emission wavelength, molar absorptivity, and fluorescence quantum yield.

Spectroscopic methods have also produced information about dendritic microenvironments. PAMAM dendrimers have been shown⁷³ to decrease ¹³C relaxation times for internal generations, suggesting that these moieties are less mobile than the surface groups. Rotational-Echo Double Resonance (REDOR) solid-state NMR spectroscopy has been used²⁸ to examine the shape of the Fréchet polyethers, and Electron Spin Resonance (ESR)²⁸ spectroscopy of complexed PAMAMs has been examined. Computer modeling⁵⁵ of dendrimers has been used extensively for the purposes of visualization and dynamics experiments.

Photophysical measurements, particularly excimer fluorescence and quenching of fluorescence, have often been used to study polymers in solution. Excimer formation⁷⁴ is a much-studied subject, particularly for pyrene⁷⁵ and for pyrene as a probe for various processes in micelles,⁷⁶ bilayers⁷⁷ and polymers.⁷⁸ It has been shown⁷⁹ that when a molecule like pyrene is attached to some other species, the excimer kinetics reflect features of the dynamics of the species to which the pyrenes are attached.

Forster and Kasper⁸⁰ first observed the emission of excimers in concentrated solutions of pyrene in 1954. They are now known to be common to most aromatic hydrocarbons and their derivatives.⁸¹ Excimers are excited state complexes which consists of two identical species, one of which is in the excited state before the

complexation. The difference between the equilibrium geometry of the excited state relative to the ground state produces a broad structureless band in the emission spectrum at longer wavelength (lower energy) than the structured monomer. In 1955, Forster and Kasper⁸² first proposed a mechanism for excimer formation. This mechanism did not consider reversibility. In later work by Williams,⁸³ it was found necessary to include reversibility and the mechanism was modified accordingly.^{84,85} The monomer /excimer kinetics can be explained by the kinetic scheme shown in Scheme 1-7.

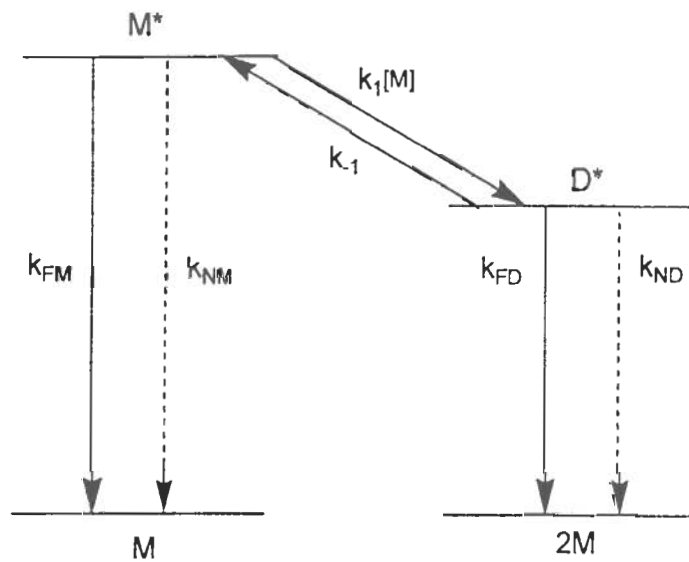
It is not possible to separate the effect of k_{FM} from k_{NM} or the effect of k_{FD} from k_{ND} , so it is useful to define

$$k_M = k_{FM} + k_{NM} \quad (1-1)$$

$$k_D = k_{FD} + k_{ND} \quad (1-2)$$

After excitation of a ground state monomer, M, in concentrated solutions, the formation of a new excited species, D*, occurs by the second order excited monomer to excimer reaction and is characterized by $k_1[M]$, where [M] is the monomer concentration in moles / liter. The excimer can dissociate back to regenerate monomer by a first order reaction with rate constant k_{-1} . Both excited monomer and excimer have first order intrinsic relaxation processes, the sum of whose rate constants is represented by k_M and k_D respectively.

In concentrated solutions, excimer (D*) is formed by interaction between an excited monomer, M*, and the ground state species, M. Formation of D* competes effectively with M* fluorescence and the observed luminescence is dominated by the radiative decay of D*. The fluorescence of D* at longer wavelength is a measure of the stabilization energy of the excimer relative to the separate M, M* pair. In a dilute



Scheme 1-7. Schematic energy levels and the rate processes associated with monomer/excimer system.

Where

M = ground state monomer

M^* = excited monomer

D^* = excimer molecules

k_1 = the rate coefficient for the formation of excimer

k_{-1} = the rate of dissociation of excimer

k_{FM} = fluorescence decay of M^* to M

k_{NM} are the first order non-radiative relaxation (internal quenching) of M^* to M

k_{FD} = the fluorescence decay of D^* to D

k_{ND} = non-radiative decay of D^* to D

solution, M^* does not encounter M during its radiative lifetime and only monomer emission is observed.

Monomer-Excimer kinetics are generally studied in terms of the Birks model⁸⁵ in which the time dependence of the rate of excimer formation is not considered.^{86,87} Rate coefficients for diffusion controlled processes are always time dependent.^{90,91} Martinho^{90,91} introduced a time dependent rate coefficient term in pyrene excimer formation kinetics and presented a new method of analyses of time-dependent phenomenon in excimer formation. The appearance of a transient term complicates the data analysis, normally making it very difficult to obtain an analytical solution for decay functions.^{92,93} For this reason, when the contribution of the transient term to the global decay constant is small, neglecting it does not introduce large errors into the calculations of steady-state rate coefficients from experimental data. Other scientists^{94,95} have also reported the dynamics of pyrene monomer and excimer fluorescence using Birks model. The experimental data fit the Birks kinetic model very well when the monomer and excimer fluorescence decays profiles are analyzed separately.⁹⁰

The kinetic equations for the mechanism shown in Scheme 1-7 were solved by Birks.⁸⁵ The kinetic scheme predicts that after excitation of a pyrene solution by a delta-pulse, the monomer intensity decays as a sum of two exponential terms and is given by

$$I_M(t) \propto \exp(-\lambda_1 t) + A \exp(-\lambda_2 t) \quad (1-3)$$

$$\text{Where } A = (k_M + k_I[M] - \lambda_1) / (\lambda_2 - k_M + k_I) \quad (1-4)$$

$$\text{Or } I_M(t) = a_1 \exp(-\lambda_1 t) + a_2 \exp(-\lambda_2 t) \quad (1-5)$$

While the excimer intensity initially increases and then decreases as a difference of two exponential terms as

$$I_D(t) \propto \exp(-\lambda_1 t) - \exp(-\lambda_2 t) \quad (1-6)$$

$$I_D(t) = a_3[\exp(-\lambda_1 t) - \exp(-\lambda_2 t)] \quad (1-7)$$

After a delta-pulse of excitation, the concentration of monomer and excimer at time $t = 0$ is $[M^*]_0$ and $[D^*]_0$ respectively and at subsequent time t is given by $[M^*]$ and $[D^*]$ respectively. The rates of change of $[M^*]$ and $[D^*]$ are given by

$$d[M^*]/dt = -(k_M + k_1[M])[M^*] + k_{-1}[D^*] \quad (1-8)$$

$$d[D^*]/dt = -(k_D + k_{-1})[D^*] + k_1[M][M^*] \quad (1-9)$$

Solving (3) and (4) and applying the initial conditions at $t = 0$, we obtain

$$[M^*] = \{[M^*]_0/(\lambda_2 - \lambda_1)\} \{(\lambda_2 - (k_M + k_1[M]))\exp(-\lambda_1 t) + ((k_M + k_1[M]) - \lambda_1)\exp(-\lambda_2 t)\} \quad (1-10)$$

$$[D^*] = \{[M^*]_0 k_1[M]/(\lambda_2 - \lambda_1)\} \{\exp(-\lambda_1 t) - \exp(-\lambda_2 t)\} \quad (1-11)$$

$$\lambda_{2,1} = \frac{1}{2}[(k_M + k_1[M]) + (k_D + k_{-1})] \pm \sqrt{\{(k_D + k_{-1}) - (k_M + k_1[M])\}^2 + 4 k_{-1} k_1 [M]} \quad (1-12)$$

The decay parameters λ_1 and λ_2 can be determined from observations of the fluorescence response functions, $I_M(t)$ and $I_D(t)$. The two emissions are observed separately through appropriate filters. Such measurements can be made using a pulse

fluorometer or phase and modulation fluorometer.⁸⁶ The time delay (t_L) between the maxima of $f_D(t)$ and of the exciting light pulse ' $p(t)$ ' is given by the following equation

$$t_L = [\ln (\lambda_2 / \lambda_1)] / [(\lambda_2 - \lambda_1)] \quad (1-13)$$

λ_1 can be calculated from a semilog plot of the excimer fluorescence response with time. λ_2 can be evaluated using equation (1-13). The rate parameter k_M , k_D , k_1 and k_{-1} at a given temperature can be evaluated from the data on λ_1 and λ_2 as a function of concentration (c). The following limiting properties are useful for this purpose.

(i) As $c \rightarrow 0$:

$$\lambda_1 = k_M \quad (1-14a)$$

$$\lambda_2 = k_D + k_{-1} \quad (1-14b)$$

(ii) As $c \rightarrow \infty$:

$$\lambda_1 = k_D \quad (1-15a)$$

$$\lambda_2 = k_D + k_{-1} + k_1 c \quad (1-15b)$$

$$(\partial \lambda_1 / \partial c) \rightarrow 0 \quad (1-15c)$$

$$(\partial \lambda_2 / \partial c) \rightarrow k_1 \quad (1-15d)$$

(iii) At all values of c :

$$\lambda_1 + \lambda_2 = k_M + k_D + k_{-1} + k_1 c \quad (1-16)$$

The lifetimes τ_M and τ_D of the M^* and D^* fluorescence are defined at infinite dilution and at infinite concentration respectively, as

$$\tau_M = 1 / k_M \text{ (where } k_M = \lambda_1 \text{ at } c=0) \quad (1-17)$$

$$\tau_D = 1 / k_D \text{ (where } k_D = \lambda_1 \text{ as } c \rightarrow \infty) \quad (1-18)$$

Figure 1-7 shows the potential energy diagram of the pyrene excimer.⁹⁶ The energy of a ground-state pyrene pair (PyPy) remains constant when they are at a distance greater than approximately 10 Å. The energy rises as they come close together and at a distance of about 4Å, (which is the equilibrium separation of excimer) the energy rises rapidly due to occupied π orbital repulsions. The absorption spectra of pyrene do not show an absorption corresponding to $\text{PyPy} \rightarrow \text{PyPy}^*$, and PyPy^* emits as a broad structureless band. This is because the “molecule” dissociates before it can complete a vibrational cycle and too few PyPy molecules are in a collision complex at a close enough distance for a significant amount of Franck-Condon excitation to the excimer to occur. From the spectroscopic analysis of pyrene excimer emission, it has been concluded that the “face to face” pyrene singlet excimer is favored.⁹⁶ (The Gibbs free energy associated with the excimer formation at ambient temperature is $\Delta G \cong -4$ kcal/mole.)

Birks et. al⁸⁵ in 1963 performed the steady-state and lifetime studies of the pyrene monomer and excimer fluorescence in cyclohexane at temperatures from 293 to 340 K. Others^{94,97} have also reported the dynamics of pyrene monomer and excimer fluorescence using Birks model. The formation of excimer requires diffusion of the pyrene labeled

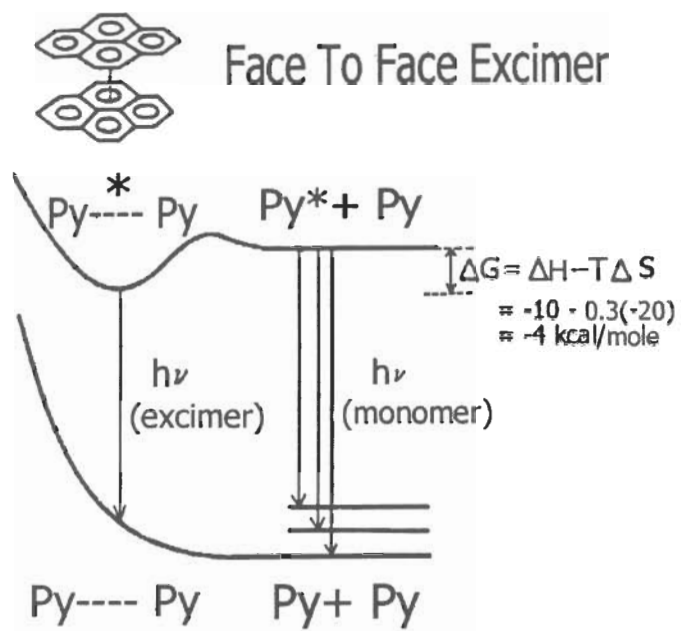


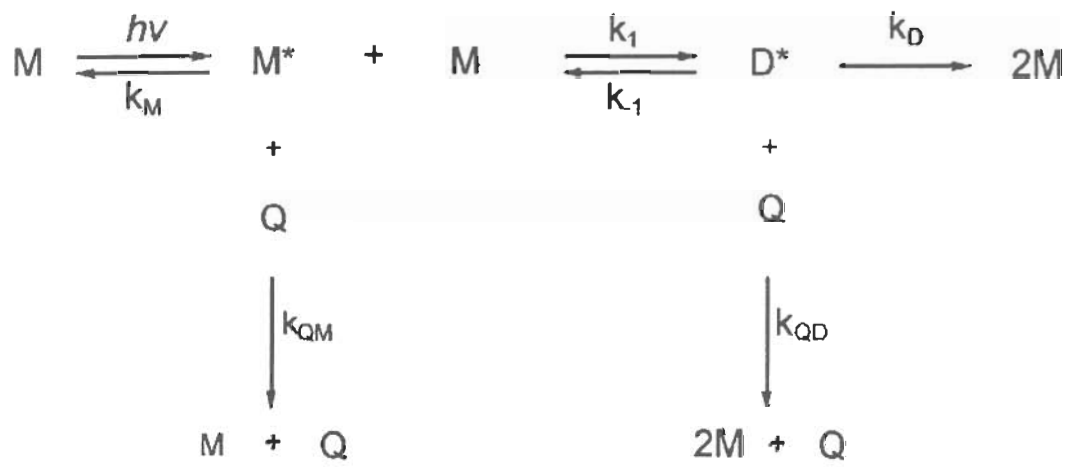
Figure 1-7. Potential energy diagram for the formation of pyrene excimer.⁹⁶

poly(aryl ether) monodendrons branches. The excimer formation rate coefficient carries information about the effect of size of the branches on their diffusion.

D. Quenching of Fluorescence

Fluorescence quenching refers to any process that reduces the lifetime of the excited state. Quenching can be investigated by either steady state or time resolved methods. In steady state the change in the property of probe (typically emission intensity) is observed as a function of quencher concentration. In time resolved measurements, changes in the emission lifetime (τ) are observed with quencher concentration. The excited probe can typically be deactivated by a number of substances that act as quencher.

A variety of processes can result in quenching. They include excited state reaction, energy transfer, static quenching (complex formation) and collisional quenching. The importance of each type of mechanism depends not only on the fluorophore and quencher but also on the properties of the medium. Collision and static quenching require contact between the fluorophore and quencher. These methods are useful to measure the rate of diffusion and exposure of fluorescent species to the quencher. Scheme 1-8 was used to analyze the steady state and time resolved fluorescence measurements of pyrene solutions in the presence of quencher⁹⁸.



Scheme 1-8. Quenching of monomer/excimer fluorescence.

Where

Q = quencher

k_{QM} = excited monomer quenching rate constant

k_{QD} = excimer quenching rate constant

Dynamic quenching is a process that competes with emission for depopulation of the excited state and the fluorescence lifetime decreases in proportion to the yield. It results in the equivalent decrease in fluorescence intensity and lifetime and can be described by the following equations developed by Stern-Volmer:⁹⁹

$$I_0/I = 1 + K_{SV} [Q] \quad (1-19)$$

$$\tau_0/\tau = 1 + K_{SV} [Q] \quad (1-20)$$

$$K_{SV} = k_q \tau_0 \quad (1-21)$$

Here $[Q]$ is the quencher concentration, I_0 and I are the fluorescence intensities in the absence and presence of quencher, respectively, and τ_0 and τ are the lifetime of the fluorophore in the absence and presence of quencher respectively. K_{SV} and k_q are the Stern-Volmer and bimolecular quenching constants.

The rate constant for dynamic quenching is also given by

$$k_q = \gamma k_0 \quad (1-22)$$

Where γ is the quenching efficiency (for oxygen and iodine, the two quenchers used in this study, $\gamma \cong 1$)¹⁰⁰ and k_0 is the bimolecular collision rate constant. The bimolecular collision rate constant can be estimated from the diffusion constants of both fluorophore and quencher using the Smoluchowski equation

$$k_0 = 4 \pi N' (R_f + R_q) (D_f + D_q) \quad (1-23)$$

Where N' is Avogadro's number per millimole, R_f and R_q are the radii of the fluorophore and quencher and D_f and D_q are the diffusion coefficients of fluorophore and quencher.

Diffusion coefficients may be obtained from the Stokes-Einstein relation

$$D = kT / (6\pi\eta R) \quad (1-24)$$

Where k is the Boltzmann constant, η is the solvent viscosity D is the diffusion coefficient and R is the collision radius.

The dynamic component of quenching is apparent when I_0 / I (1-19) and τ_0 / τ (1-21) are equal. This was first pointed out by Perrin¹⁰¹ and Wawilov¹⁰² and experimentally shown by Szymanowsky.¹⁰³ The existence of two modes of quenching for the same fluorophore (dynamic and static) is revealed by positive curvature in the Stern-Volmer plot^{104,105} where the ratio of intensities I_0 / I is greater than the lifetime ratio τ_0 / τ .^{106,100} This type of deviation from the expected linear plot can be explained by the fact that only a certain fraction of excited states is actually quenched by the collision mechanism as described by Stern-Volmer. Some of the excited states are deactivated essentially instantaneously after formation because a quencher molecule happens to be positioned in their proximity at the time they are excited. The two most common models^{100,104} that can be employed to describe this instantaneous, or static, quenching process are the formation of a ground state complex between the fluorophore and the quencher and the sphere of action quenching model.

Ground state complex model: Static quenching due to the formation of nonfluorescent ground state complex between the fluorophore and the quencher reduces only the yield since the lifetime of the uncomplexed fluorophore remains constant. A modified form of the Stern-Volmer equation is used when the fluorophore can be quenched by collision (dynamic quenching) and complex formation (static quenching) with the same quencher.¹⁰⁰ Hence,

$$I_0/I = (1 + K_{SV}[Q])(1 + K_S[Q]) \quad (1-25)$$

Where K_S is a static quenching constant.⁶⁴

When $(I_0/I) > (\tau_0/\tau)$, the static component of the quenching can also be determined from the ratio of equations (1-19) and (1-21) as.¹⁰⁰

$$I_0/I / (\tau_0/\tau) = 1 + K_S[Q] \quad (1-26)$$

The quantity K_S is seen to reflect only the static component of the quenching. Dynamic component of quenching is determined from the slope of the Stern-Volmer equation (1-19).

Sphere of action static quenching model: This type of quenching occurs when the quencher molecule is adjacent to the fluorophore at the moment of excitation. The percentage of such complexed fluorophores increases as the mole fraction of quencher

increases in the solution. This phenomenon is frequently interpreted as a “sphere of action” in which the probability of quenching is unity. The modified form of Stern-Volmer equation that describes the situation is given by the following modified form of Stern-Volmer equation:¹⁰⁴

$$(I_0 / I) = (1 + K_{SV}[Q]) \exp(Q_v N / 1000) \quad (1-27)$$

where v is the volume of the sphere.

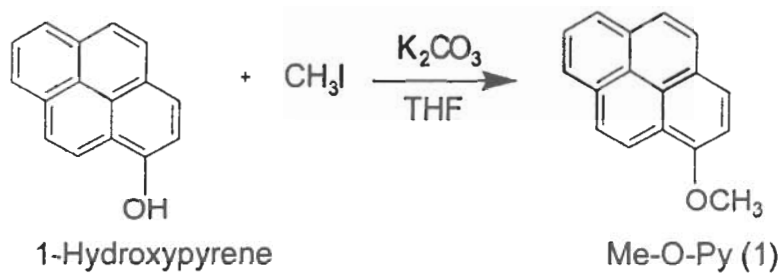
This quenching is usually significant when positive deviation in Stern-Volmer is observed without ground state complex formation or when the extent of static quenching constant is small.¹⁰⁰

Quenching studies provide a means to obtain information about the structure of pyrene labeled monodendrons. The quenching of the fluorescent probe (pyrene) by iodine and molecular oxygen has been used in the characterization of monodendrons to obtain more detailed information on the microscopic structure and dynamics of pyrene labeled poly(aryl ether) monodendrons.

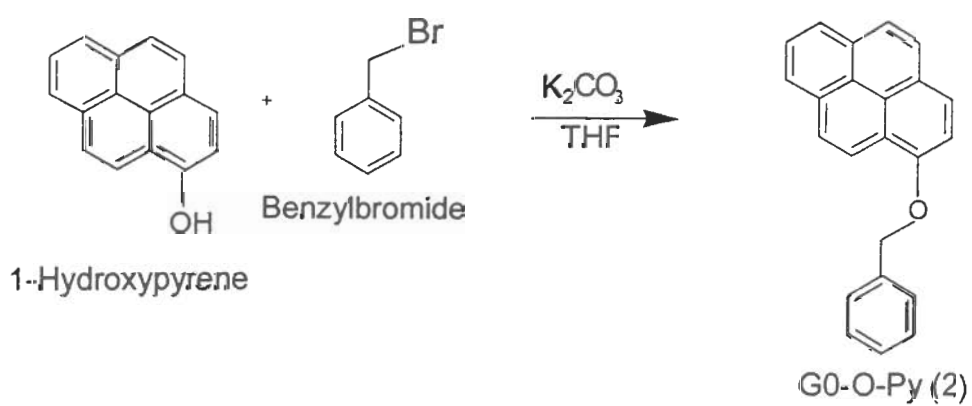
CHAPTER 2
Synthesis

A. Synthesis

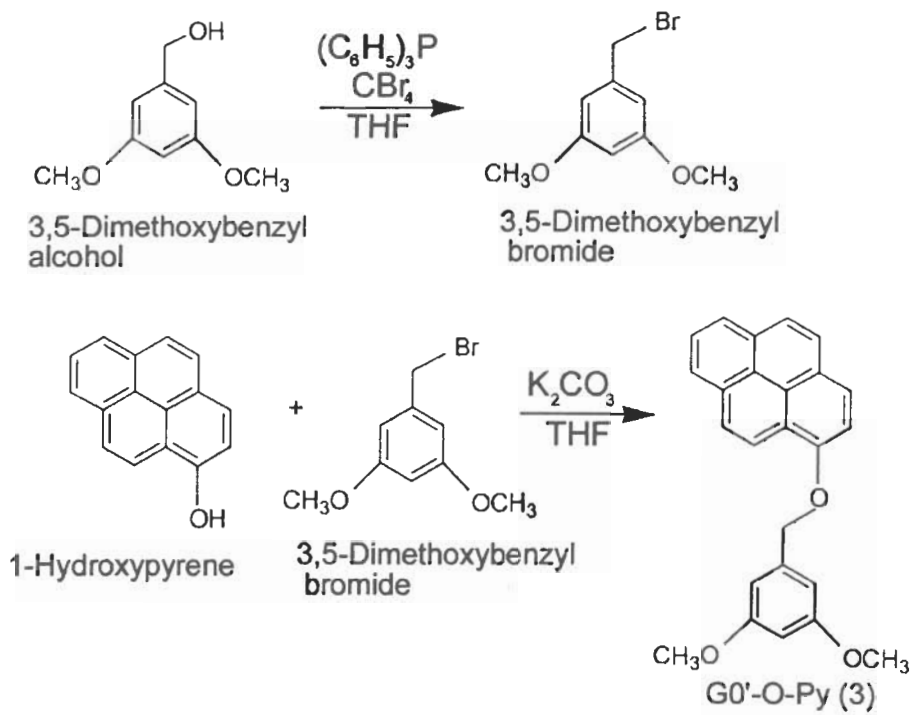
For the photophysical studies a series of pyrene labeled poly(aryl ether) monodendrons (1-6), with successive increase in size and molecular weight, were synthesized by a modification of a literature procedure.¹⁰⁷ These compounds were 1-Me-O-Py (1), G0-O-Py (2), G0'-O-Py (3) and G1-O-Py (4). 1-Me-O-Py was prepared by refluxing commercially available 1-hydroxypyrene and methyl iodide in THF in the presence of the base potassium carbonate in dry THF as shown in Scheme 2-1. Scheme 2-2 shows the synthetic approach for synthesizing G0-O-Py. This compound was prepared by refluxing 1-hydroxypyrene with commercially available benzyl bromide and potassium carbonate in dry acetone. Synthesis of G0'-O-Py and G1-O-Py were completed in two steps each as shown in Schemes 2-3 and 2-4 respectively. The first step in Scheme 2-3(a) shows the bromination of commercially available 3,5 dimethoxybenzyl alcohol with carbon tetrabromide and triphenylphosphine in dry THF to give 3,5-dimethoxybenzyl bromide. The second step involves the coupling of 3,5-dimethoxybenzyl bromide with 1-hydroxypyrene to give G0'-O-Py. Synthesis of G1-O-Py first requires the bromination of 1-(3',5'-dibenzyloxy)benzyl alcohol with carbon tetrabromide and triphenylphosphine in dry THF to form 1-(3',5'-dibenzyloxy)benzyl bromide and then coupling of 1-(3',5'-dibenzyloxy)benzyl bromide with 1-hydroxypyrene to give G1-O-Py (Scheme 2-4). The details of the reactions to give the pyrene labeled poly(aryl ether) monodendrons are provided in the experimental section.



Scheme 2-1. Synthesis of 1-Me-O-Py (1).



Scheme 2-2. Synthesis of G0-O-Py (2).



Scheme 2-3. Synthesis of G0'-O-Py (3).

Pyrene labeled poly(aryl ether) monodendrons, G2-O-Py (5) and G3-O-Py (6), used in the study were synthesized by Riley¹⁰⁷ using methyl 3,5-dihydroxybenzoate as the monomer in a modification of Frechet's synthesis based on 3,5-dihydroxybenzyl alcohol.^{8b} The structures of all the compounds used in the study are shown in Appendix A.

B. Characterization

All compounds were characterized using ¹H-NMR spectroscopy. All ¹H-NMR spectra were obtained in CDCl₃. Figure 2-1 shows the ¹H-NMR spectra of pyrene labeled monodendrons. Aromatic protons of pyrene were observed in the region of 7.50-8.53 ppm. The exterior phenyl protons were found to resonate in the region of 7.26-7.48 ppm and the interior protons in the region of 6.46-6.85 ppm. The resonance of the benzyl protons specific to the ether linkage was observed at 5.10 ppm for interior groups and in the region of 5.35-5.43 for exterior groups. The protons of the methoxy group were easily distinguished at 4.15 for 1-Me-O-Py (1) and 3.80 ppm for G0'-O-Py (2). Details of the ¹H-NMR spectra of the pyrene labeled monodendrons are provided in the experimental section.

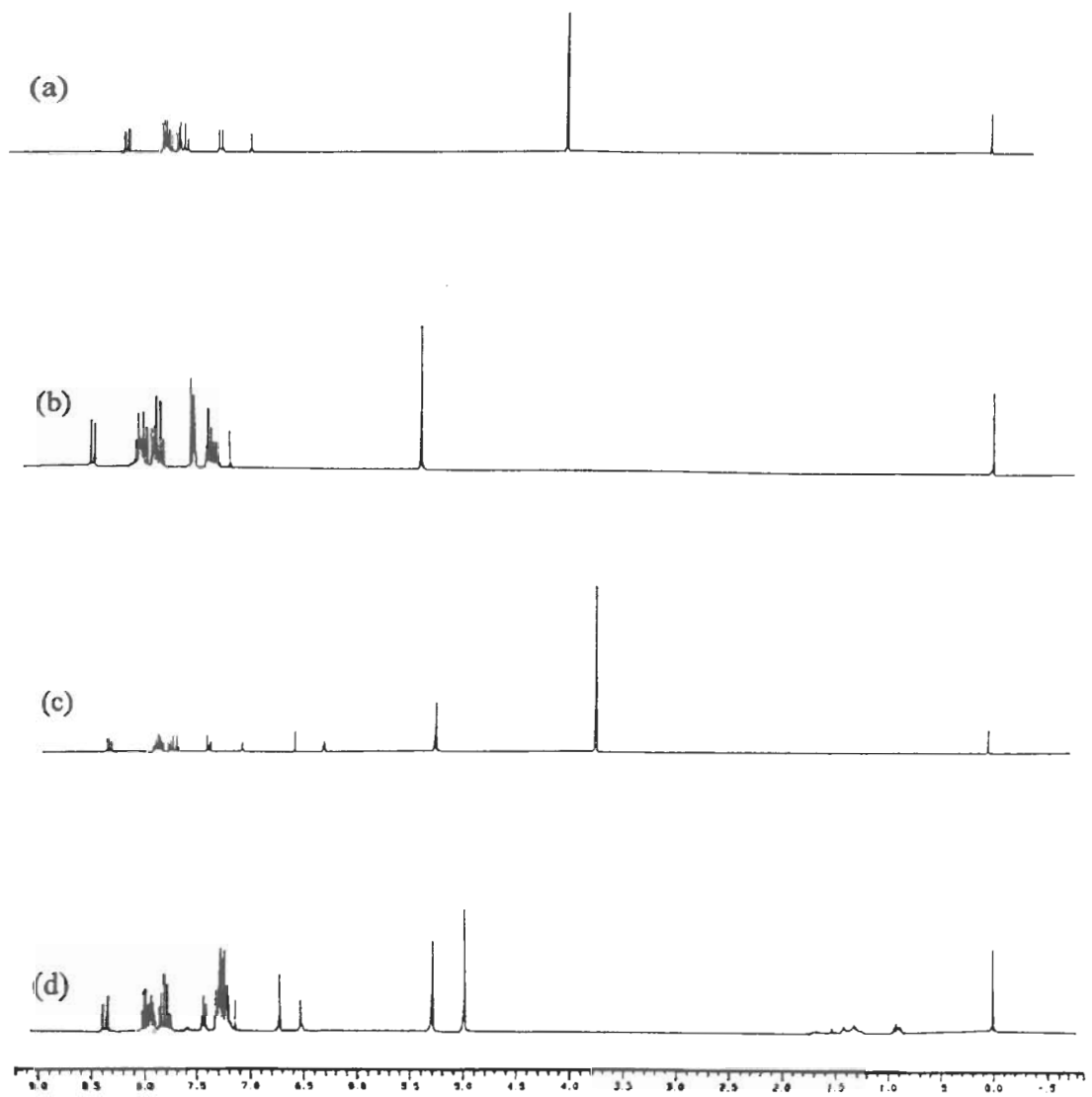


Figure 2-1. ^1H -NMR spectra of pyrene labeled **poly(aryl ether)** monodendrons: (a) 1-Me-O-Py (**1**); (b) G0-O-Py (**2**); (c) G0'-O-Py (**3**) and (d) G1-O-Py (**4**).

CHAPTER 3
Fluorescence Studies

A. Introduction

Fluorescence measurements have been used to study dendrimer structure in a number of ways. The microenvironment inside the dendrimer has been studied^{108,68} by the use of fluorescence intensity (I) and fluorescence lifetime (τ) measurements. These measurements are done either by addition of a small molecule fluorescent probe to a polymer system or by covalent attachment of fluorescent labels to the polymer chain. Fluorescence label techniques provide a particularly useful tool for studies of the microscopic dynamics and conformation of polymers,^{109,110} and pyrene is a widely used label for such studies.^{111,112} When a molecule such as pyrene is covalently attached to a polymer, the excimer kinetics reflect the dynamics of the polymer to which the pyrene is attached. Excimer fluorescence is a characteristic of many polycyclic hydrocarbons and their derivatives.^{113,114} Birks⁸⁵ reported monomer and excimer fluorescence of deoxygenated solutions of pyrene in cyclohexane at temperature from 293 to 340 K. Martinho¹¹⁵ analyzed the rate parameters of pyrene solutions in benzene using Birks kinetic scheme. In 1992, Zagrobelny et al.⁹⁷ reported detailed studies on the formation of pyrene excimer in supercritical carbon dioxide. They investigated the photophysics of pyrene as a function of temperature and fluid density using steady state and time resolved fluorescence decay kinetics. Recently Yusa¹² have reported the phase behavior of a cholesterol bearing polymethacrylate in solution by use of pyrene as fluorescence label. Molecular dynamic simulations also provide information about dendrimer properties.

Murat et al.¹³ reported the molecular dynamic study of dendrimer molecules in solvents of varying quality.

For the photophysical studies of monodendrons, pyrene was chosen as a probe (or energy donor in quenching) since it is an excimer-forming molecule and its properties are well known. Using steady state fluorescence spectroscopy, excimer and monomer fluorescence of pyrene labeled monodendrons (1-6) were examined in solvents of different polarity and viscosity. The lifetime of excimer and monomer were determined using time resolved laser flash photolysis. All results are compared with pyrene studied under the similar conditions. The formation of excimer requires diffusion of the pyrene labeled monodendrons. Measurement of the rate of excimer formation provides information about the effect of size of the branches on diffusion. The Birks kinetic model, used to evaluate the kinetic rate parameters, has been discussed in detail in Chapter 1. Both steady state and time resolved fluorescence provides useful information about excimer kinetics.

B. Steady State Fluorescence

1) Monomer Fluorescence: Steady state fluorescence of pyrene and pyrene labeled poly(aryl ether) monodendrons (1-6) were determined in acetonitrile (ACN), tetrahydrofuran (THF) and cyclohexane (CH). Monomer emission was observed at right angle (90°) using very dilute solutions (1×10^{-7} M) to minimize the contribution of excimer. The details of sample preparation are described in Chapter 5. Figures 3-1 to 3-6 show the steady state emission spectra of pyrene and 1-methoxypyrene in acetonitrile,

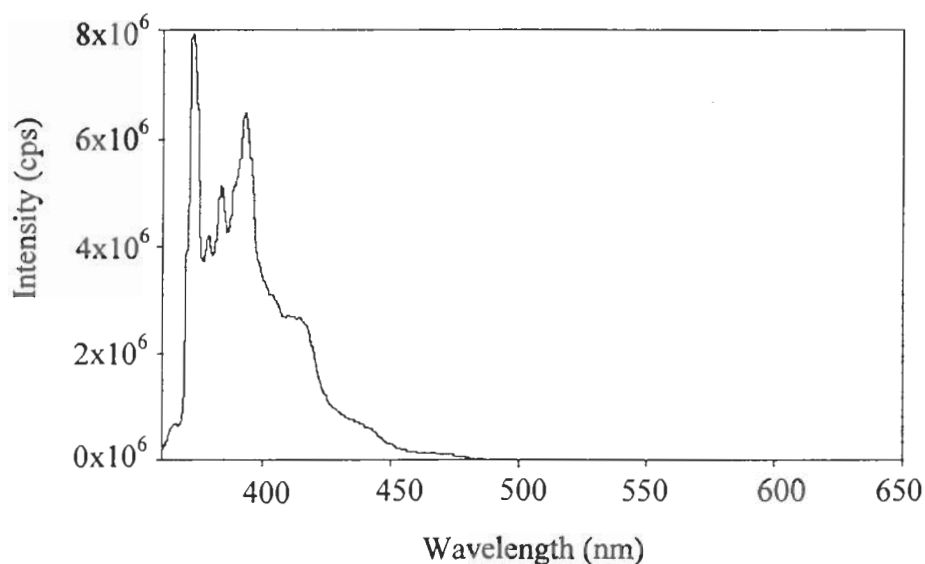


Figure 3-1. Steady-state emission spectrum of 1×10^{-7} M solution of pyrene in ACN with $\lambda_{\text{ex}} = 335$.

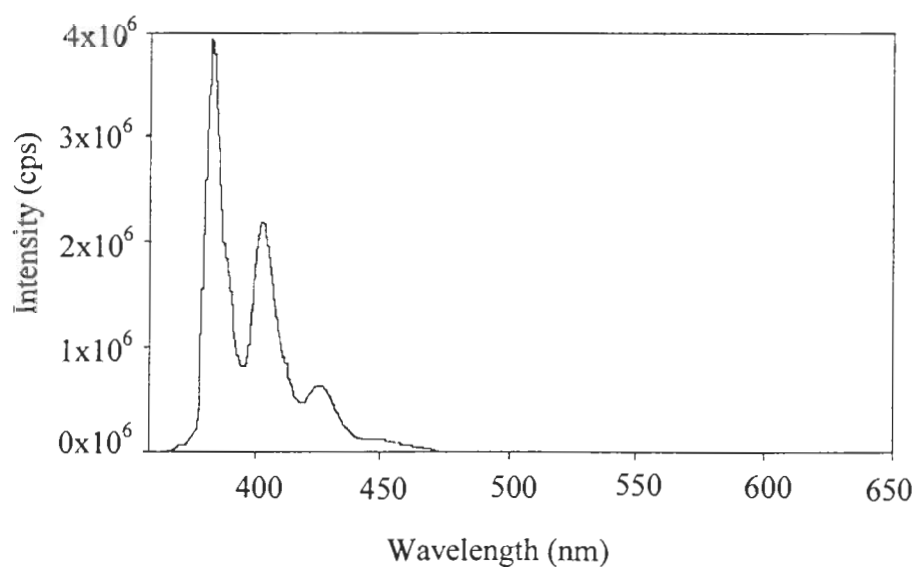


Figure 3-2. Steady-state emission spectrum of 1×10^{-7} M solution of 1-methoxypyrene in ACN with $\lambda_{\text{ex}} = 335$. The 1-methoxypyrene is a representative of all of the pyrene labeled poly(aryl ether) monodendrons.

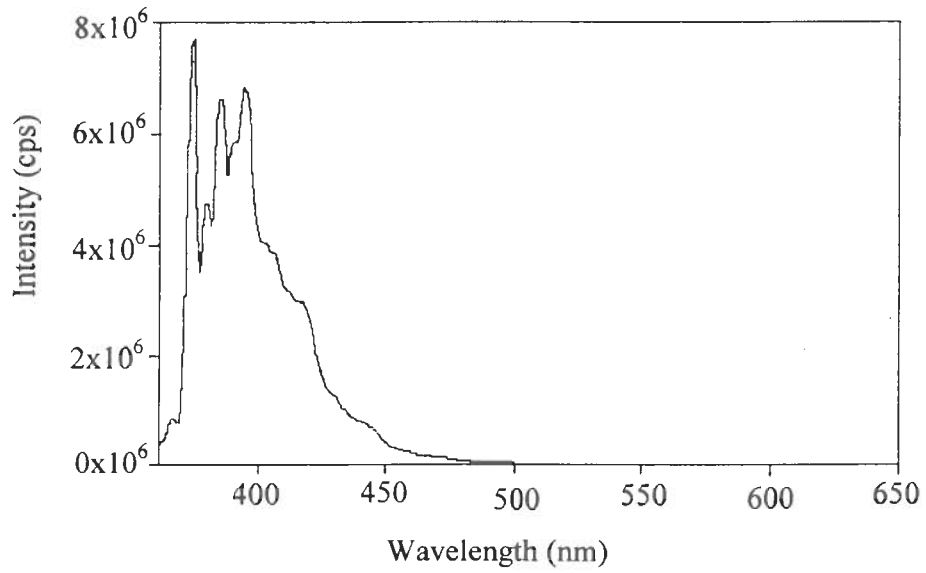


Figure 3-3. Steady-state emission spectrum of 1×10^{-7} M solution of pyrene in THF with $\lambda_{\text{ex}} = 335$.

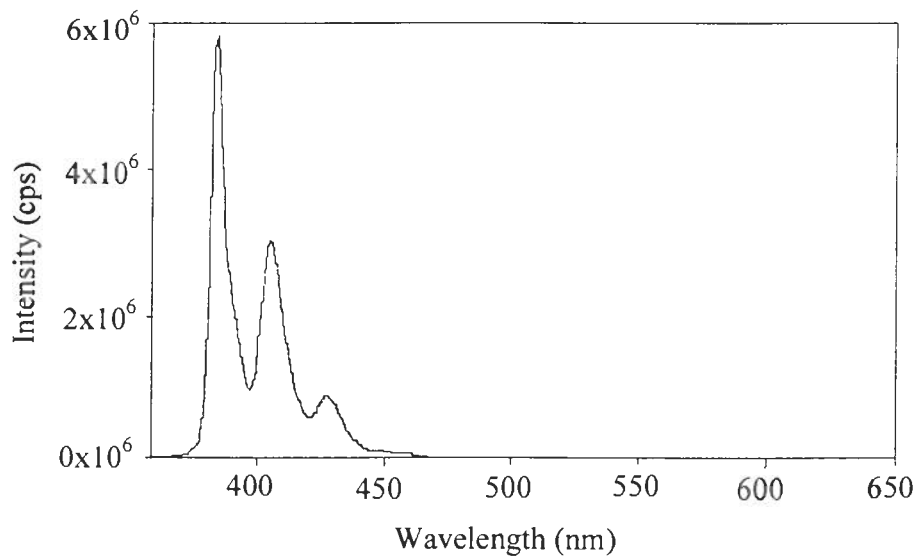


Figure 3-4. Steady-state emission spectrum of 1×10^{-7} M solution of 1-methoxypyrene in THF with $\lambda_{\text{ex}} = 335$.

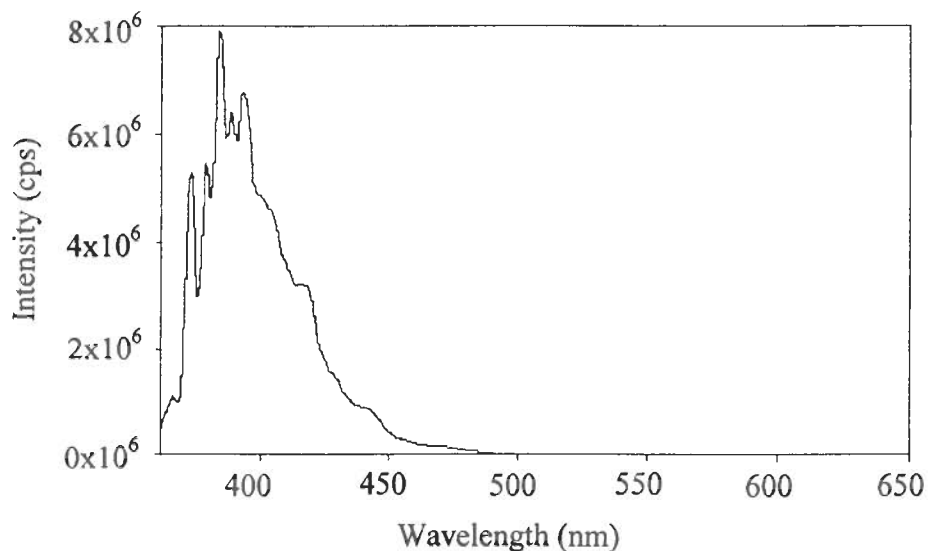


Figure 3-5. Steady-state emission spectrum of 1×10^{-7} M solution of pyrene in CH with $\lambda_{\text{ex}} = 335$.

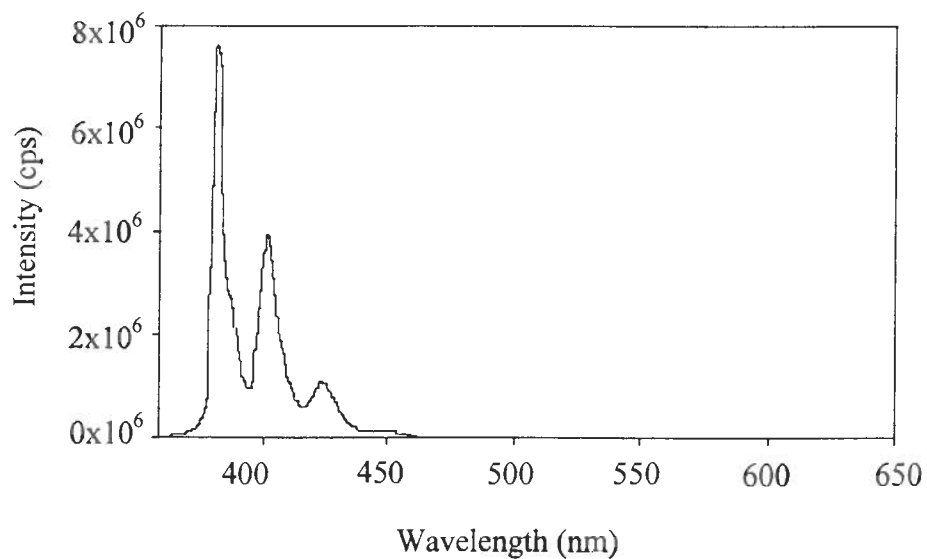


Figure 3-6. Steady-state emission spectrum of 1×10^{-7} M solution of 1-methoxypyrene in CH with $\lambda_{\text{ex}} = 335$.

THF and cyclohexane. The emission wavelength was scanned from 350 to 600 nm with excitation at 335 nm. The emission spectrum of pyrene shows five sharp major vibronic bands with λ_{max} at 373 nm and is reported to be greatly effected by solvent polarity.¹² 1-Methoxypyrene differs in some respects from pyrene. It has three relatively broad vibronic bands with λ_{max} at 385 nm and is much less sensitive to the solvent polarity. Absorbance spectra of pyrene and 1-methoxypyrene in THF are shown in Figure 3-7 and Figure 3-8 respectively. The average vibrational spacing in the absorbance and emission spectra of 1-methoxypyrene are 1194 and 1400 cm^{-1} respectively. The emission spectrum of anisole and phenol have been reported with two broad vibronic bands and benzene with four sharp major vibronic bands.^{12b} The average vibrational spacing in the absorbance and emission spectra of anisole are 1025 and 1100 cm^{-1} respectively. Also in phenol the average vibrational spacing in the absorbance and emission spectra are 1050 and 1100 cm^{-1} respectively. All these suggests that the differences between pyrene and methoxypyrene may arise from the strong coupling of the vibrations of the polar C-O bond with internal conversion processes. The emission spectra of the other pyrene labeled poly(aryl ether) monodendrons (2-6) are not significantly different from that of 1-methoxypyrene (1). Figure 3-9 shows the emission spectrum of G2-O-Py (2) in THF.

II) Excimer Fluorescence: Excimer fluorescence was observed at front face using concentrated solutions. The solutions were excited at 335 nm and scanned from 360 to 600nm. The excimer emission was observed at longer wavelength as a broad structureless band after monomer emission. Figure 3-10 shows the emission spectra of

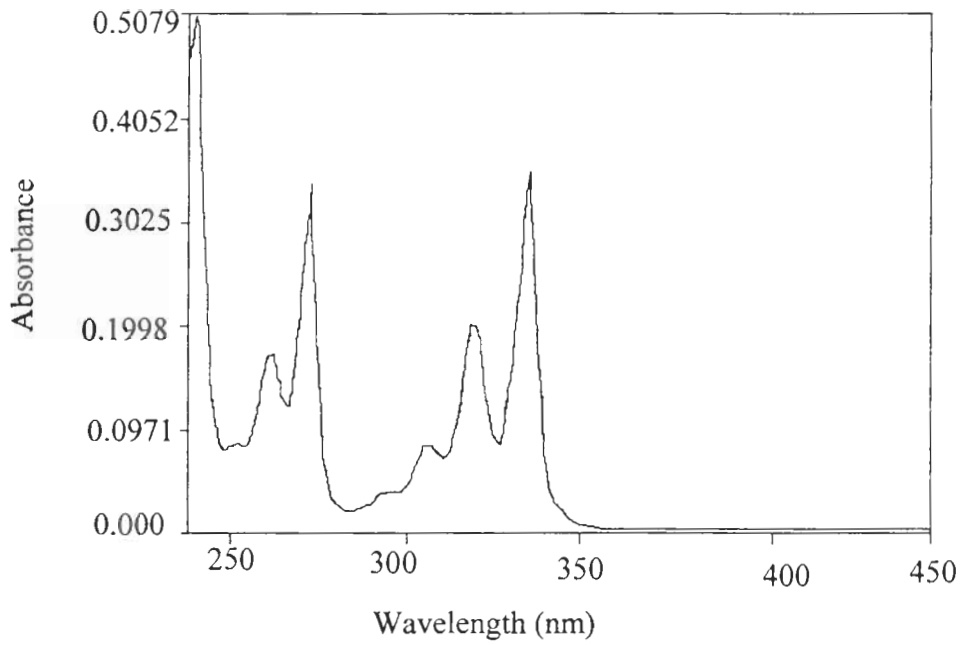


Figure 3-7. UV-Visible Absorbance spectra of 1×10^{-5} M solution of pyrene in THF.

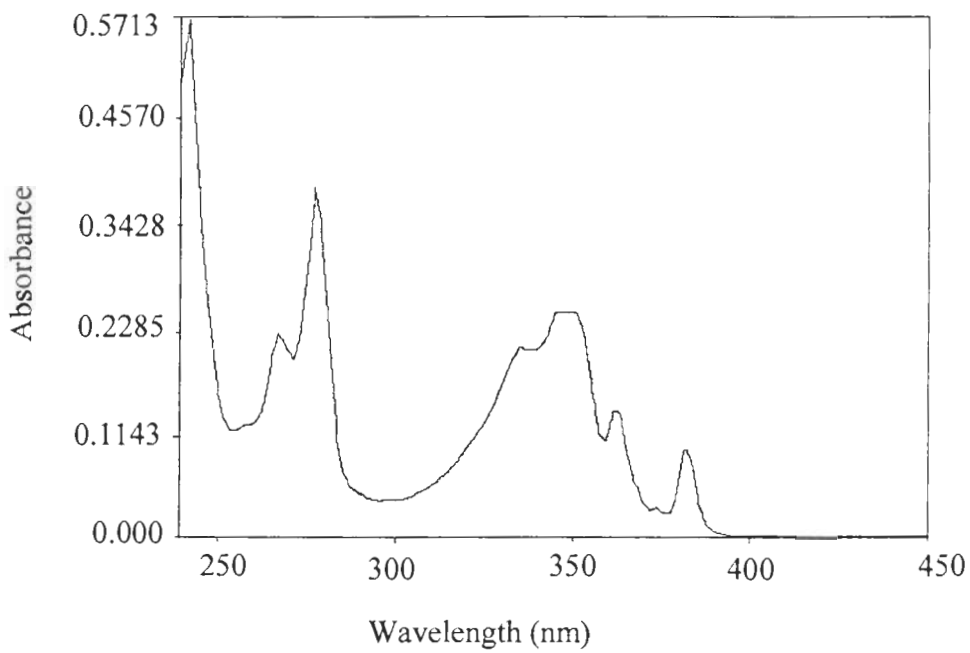


Figure 3-8. UV-Visible Absorbance spectra of 1.05×10^{-5} M solution of 1-methoxypyrene in THF.

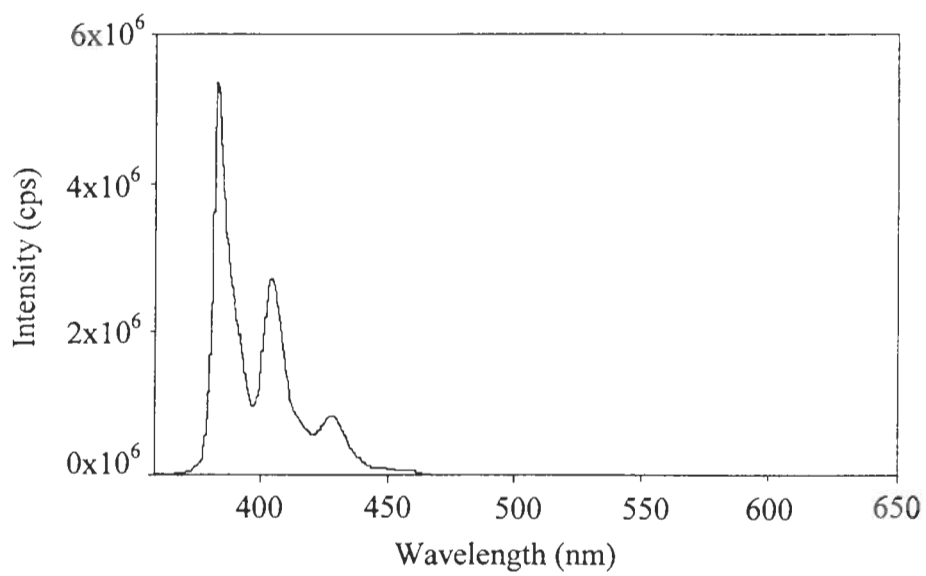


Figure 3-9. Steady-state emission spectrum of 1×10^{-7} M solution of G2-O-Py in THF with $\lambda_{\text{ex}} = 335$.

pyrene in THF at different concentrations. The monomer emission is observed at $\lambda_{\text{max}} = 373$ nm and excimer at 478 nm. At concentrations of 1×10^{-6} M or less the fluorescence is concentration independent and is composed of pure monomer fluorescence. As the concentration increases a decrease in the intensity of monomer and an increase in the intensity of excimer is observed. The isoemissive point of excimer to monomer emission for pyrene was observed at 432 nm. Figure 3-11 shows the emission spectra of 1-methoxypyrene (1) in THF at different concentrations. Monomer fluorescence is observed at 385 nm and excimer at 494 nm with an isoemissive point at 441 nm. Other pyrene labeled monodendrons (2-5) also exhibited the monomer and excimer fluorescence along with the isoemissive point at 441 nm. In all pyrene labeled monodendrons (1-5) excimer is observed at higher wavelengths (lower energy) than pyrene. The G3-O-Py (6) was not soluble in appreciable amount to study excimer emission. The solubility of all pyrene labeled poly(aryl ether) monodendrons (1-5) decreases with the increase in generation. THF ($\eta_{\text{D}} = 0.575$, $\epsilon = 7.58$) is found to be a better solvent for all generations than acetonitrile ($\eta_{\text{D}} = 0.345$, $\epsilon = 35.94$) and cyclohexane ($\eta_{\text{D}} = 0.975$, $\epsilon = 2.023$). Absorption spectra of dilute (containing monomer only) and concentrated solutions (containing both monomer and excimer) of pyrene and pyrene labeled poly(aryl ether) monodendrons are identical in all solvents. This indicates that ground state dimers are not present in concentrated solutions. Excimer fluorescence is observed in all solvents. Pyrene labeled monodendrons (1-5) require higher concentrations than pyrene for significant excimer formation. The emission spectra are essentially the same in all three solvents, except the fluorescence intensities are slightly

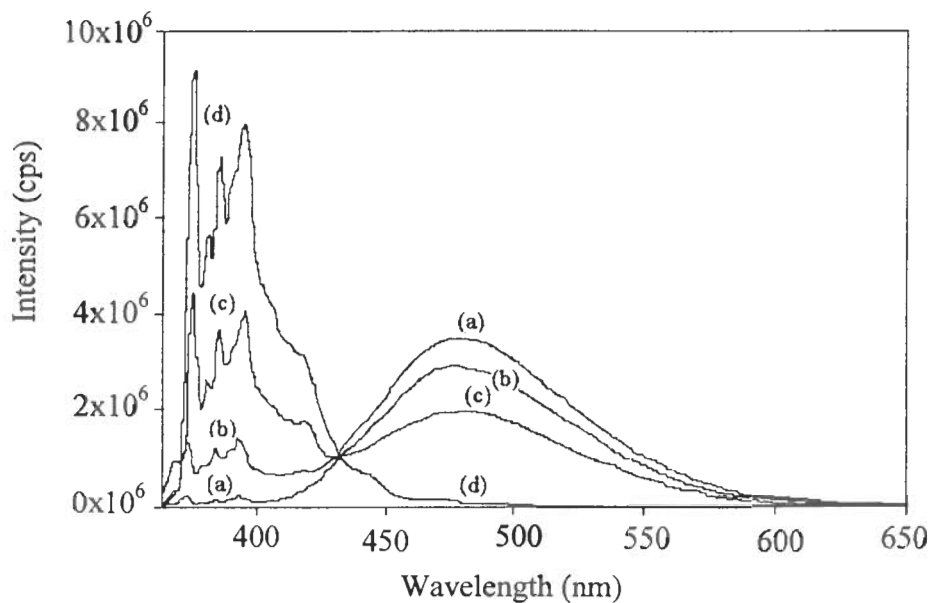


Figure 3-10. Steady-state emission spectra of pyrene in THF at different concentrations, showing the emission of excimer: (a) 5×10^{-2} M, (b) 5×10^{-3} M, (c) 1×10^{-3} M and (d) 1×10^{-5} M. The isoemissive point is at 432 nm.

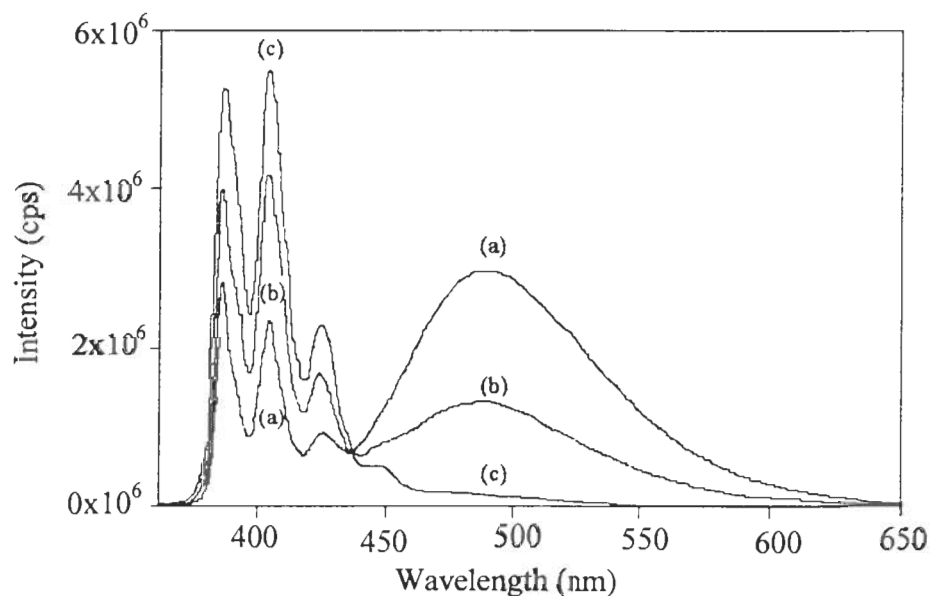


Figure 3-11. Steady-state emission spectra of 1-methoxypyrene in THF at different concentrations, showing the emission of excimer: (a) 5×10^{-2} M, (b) 1×10^{-2} M and (c) 1×10^{-3} M. The isoemissive point is at 441 nm.

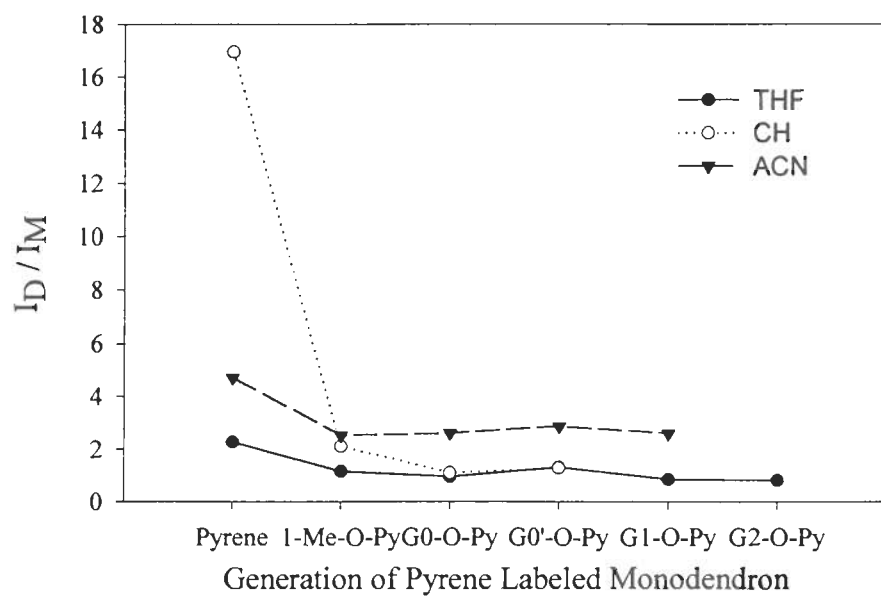


Figure 3-12. Excimer to monomer fluorescence intensity ratio (I_D / I_M) for pyrene and pyrene labeled poly(aryl ether) monodendrons in tetrahydrofuran (THF), cyclohexane (CH) and acetonitrile (ACN).

higher in cyclohexane and acetonitrile than THF. The intensities of excimer emission relative to monomer emission (I_D / I_M) for pyrene labeled monodendrons were examined in acetonitrile, THF and cyclohexane. (Figure 3-12). Excimer formation appears greater in poor solvents than in good solvents. It is in the order ACN > CH > THF for all pyrene labeled poly(aryl ether) monodendrons (1-5). This may be due to more compact structures in poor solvents, or by increased steric demands by the monodendrons in good solvents. The amount of dendron overlap decreases with increases in solvent quality. In all solvents the excimer formation of pyrene labeled poly(aryl ether) monodendrons is markedly lower compared with pyrene. A difference is observed in the I_D / I_M ratio with the increase in size of monodendrons, possibly due to restricted interaction between pyrene groups with the increase in size of monodendrons.

C. Time resolved Fluorescence Intensity Decay

I) Monomer Fluorescence Decay: Time resolved fluorescence decay curves were measured for pyrene and pyrene labeled poly(aryl ether) monodendrons (1-6) in acetonitrile, THF and cyclohexane. Monomer decay curves were observed using dilute solutions where only monomer fluorescence is observed at a wavelength of 373 nm for pyrene and 385 nm for pyrene labeled poly(aryl ether) monodendrons (1-6). Representative decays for pyrene and 1-methoxypyrene in acetonitrile, THF and cyclohexane in both intensity format and semi logarithmic format are shown in Figure 3-13 through Figure 3-16. The decay constant ($\lambda = k_M$) was recovered from the slope of a linear fit of the decay curve in semilogarithmic format. The lifetimes ($\tau = 1/\lambda$) were

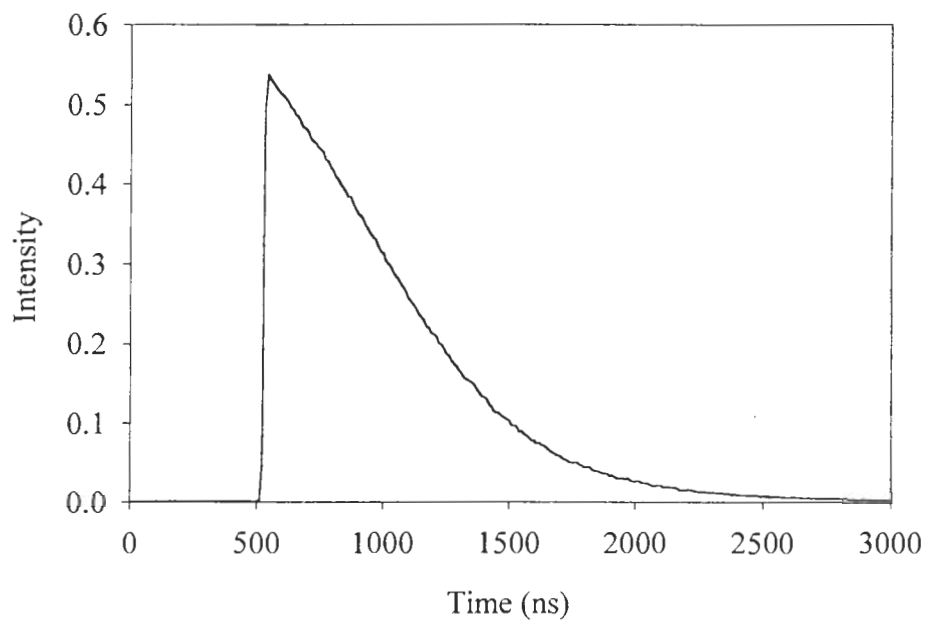


Figure 3-13. Fluorescence decay of 1×10^{-7} M pyrene monomer in THF.

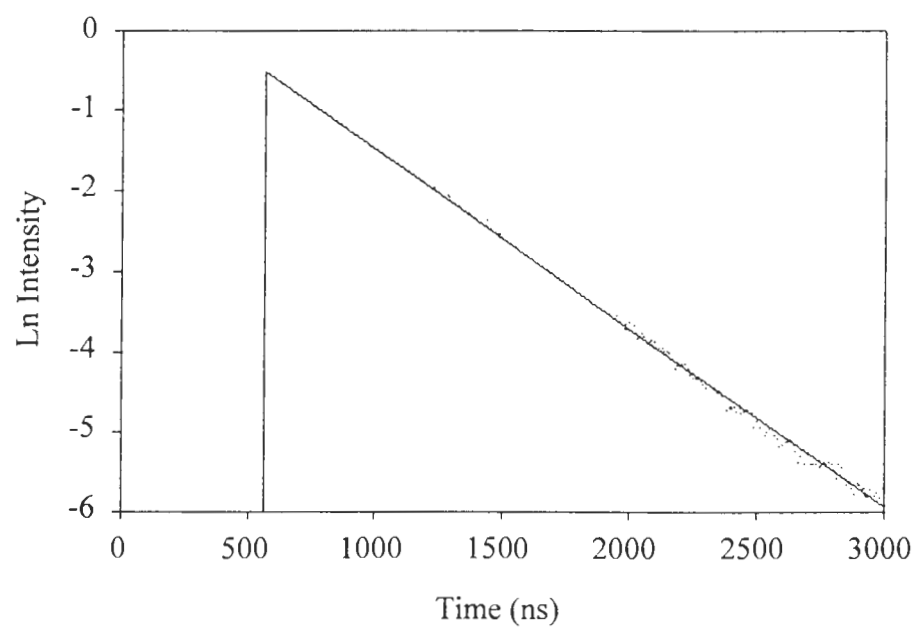


Figure 3-14. Semilogarithmic form of fluorescence decay of 1×10^{-7} M pyrene monomer in THF.

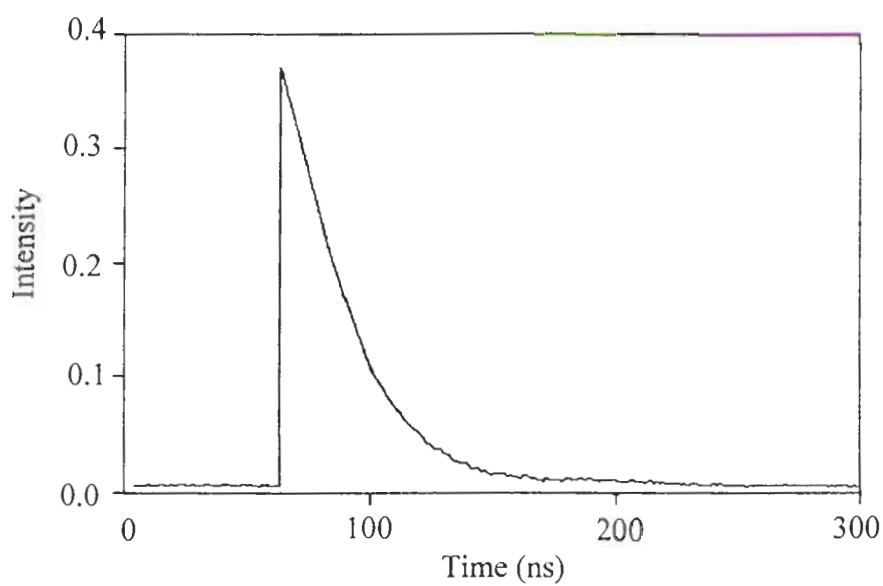


Figure 3-15. Fluorescence decay of 1×10^{-7} M 1-methoxypyrene in THF.

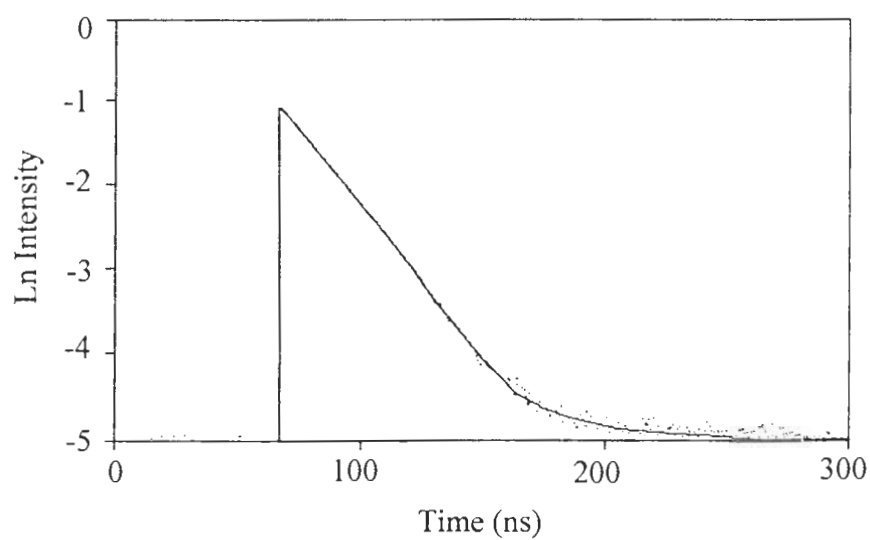


Figure 3-16. Semilogarithmic form of fluorescence decay of 1×10^{-7} M 1-methoxypyrene in THF.

Table 3-1. Lifetimes of pyrene and pyrene labeled poly(aryl ether) monodendrons (monomer) in ACN, THF and CH.

Compound	ACN	THF	CH
	τ (ns)	τ (ns)	τ (ns)
Pyrene	281.69	377.64	481.46
1-Me-O-Py (1)	20.69	22.76	25.08
G0-O-Py (2)	20.72	22.80	25.12
G0'-O-Py (3)	20.73	22.85	25.30
G1-O-Py (4)	20.81	22.94	25.51
G2-O-Py (5)	20.95	23.15	25.65
G3-O-Py (6)	21.49	23.02	25.72

Table 3-2. Lifetimes of pyrene and pyrene labeled poly(aryl ether) monodendrons (excimer) in ACN, THF and CH.

Compound	ACN	THF	CH
	τ (ns)	τ (ns)	τ (ns)
Pyrene	57.14	63.07	73.8
1-Me-O-Py (1)	38.46	46.62	48.28
G0-O-Py (2)	41.21	48.6	49.75
G0'-O-Py (3)	44.67	52.18	52.57
G1-O-Py (4)	47.84	52.89	--- ^a
G2-O-Py (5)	--- ^a	53.4	--- ^a

a. Compound was not soluble enough to obtain the excimer lifetime.

obtained by taking the inverse of the decay constant. The lifetime of pyrene and pyrene labeled poly(aryl ether) monodendrons (1-6) in acetonitrile, THF and cyclohexane are reported in Table 3-1. The pyrene labeled poly(aryl ether) monodendrons (1-6) have a significantly shorter lifetime than pyrene and their lifetimes do not change significantly with increase in the size of monodendrons. Their lifetimes show a slight decrease with increase in solvent polarity, from 25.4 ns in cyclohexane to 20.8 nsec in acetonitrile. Pyrene monomer shows a significant decrease in lifetime with increase in solvent polarity the lifetime decreases from 480 ns in cyclohexane to 280 ns in acetonitrile.

II) Excimer Fluorescence Decay: Time resolved fluorescence decay of excimer was measured using concentrated solutions of pyrene and pyrene labeled monodendrons (1-5). These measurements were done in acetonitrile, THF and cyclohexane. The G3-O-Py (6) was not soluble enough to study excimer fluorescence decay. Excimer fluorescence decay was observed at 540 nm for pyrene and at 550 nm for pyrene labeled poly(aryl ether) monodendrons (1-5). These wavelengths were selected to observe the decay of excimer fluorescence while excluding monomer fluorescence decay. The decay curves of pyrene and 1-methoxypyrene (1) in THF, in intensity and semi logarithmic format are shown in Figures 3-17 through 3-20. The excimer decay curves show a rise time before decay. The rise time is characteristic of excimer and is not observed in monomer decay. The decay constant of excimer ($\lambda = k_D$) was obtained from the slope of the linear fit of the decay curve in logarithmic format. Table 3-2 shows the

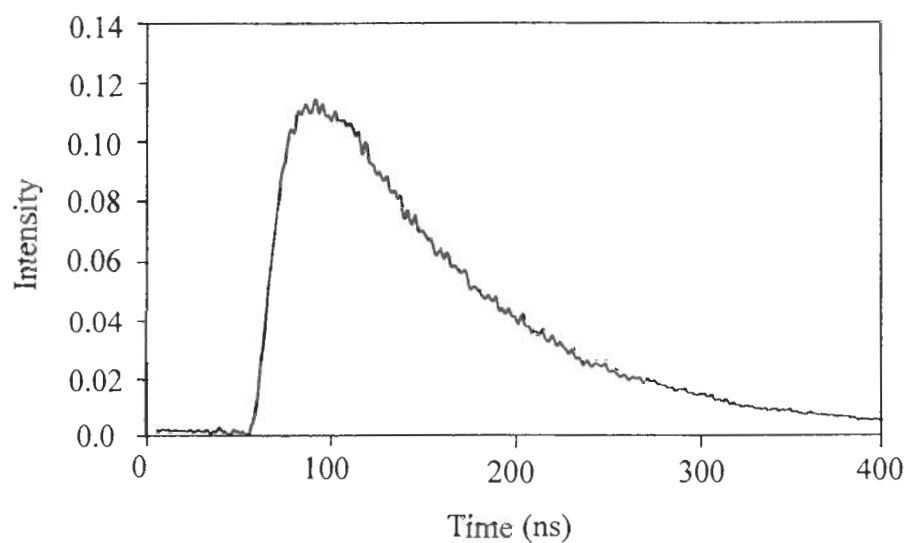


Figure 3-17. Fluorescence decay of 1×10^{-2} M pyrene in THF.

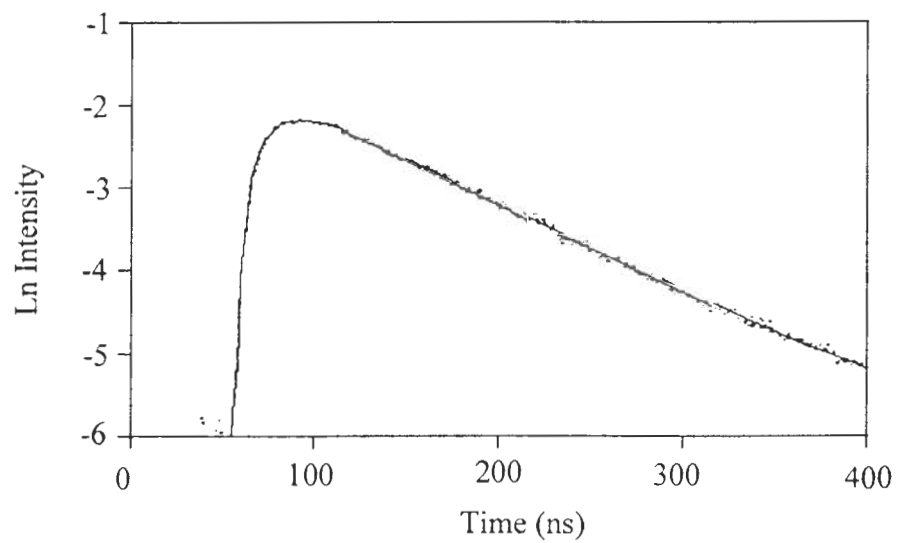


Figure 3-18. Semilogarithmic form of fluorescence decay of 1×10^{-2} M pyrene in THF.

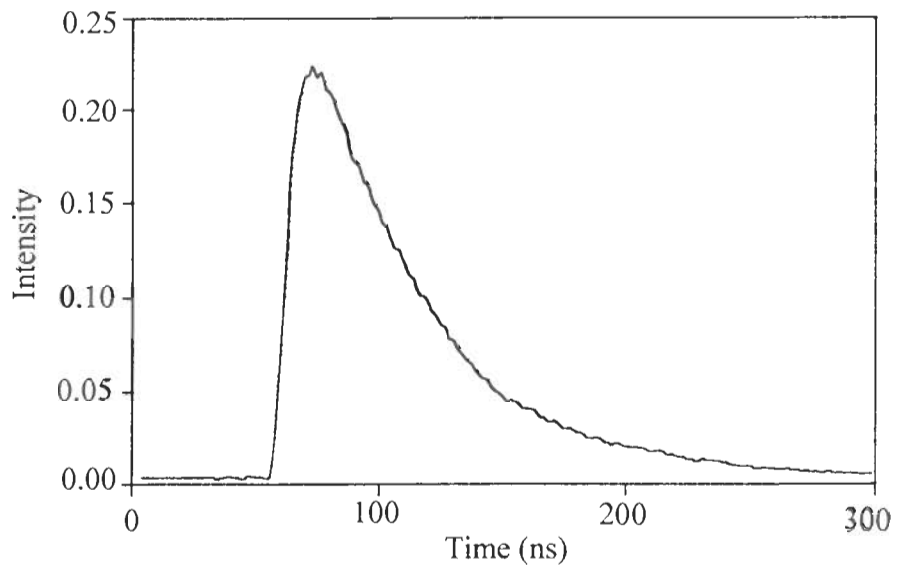


Figure 3-19. Fluorescence decay of 5×10^{-2} M 1-methoxypyrene in THF.

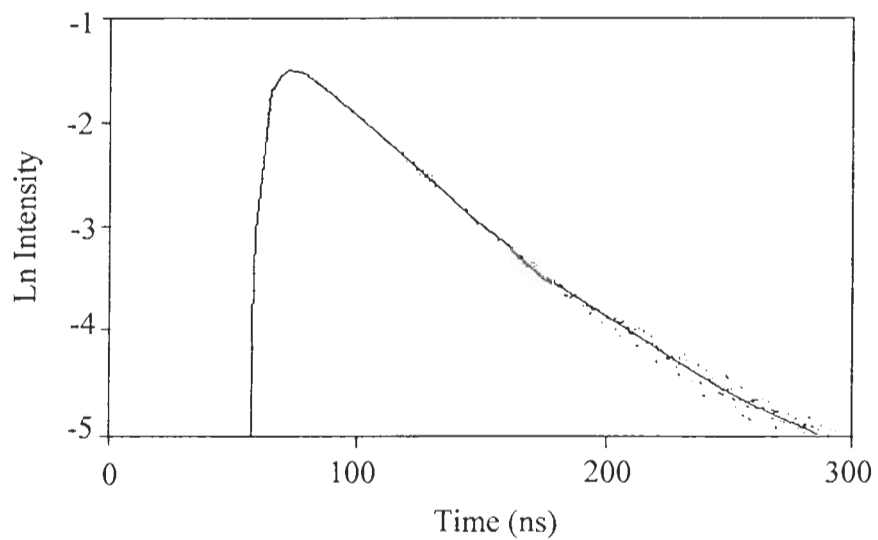


Figure 3-20. Semilogarithmic form of fluorescence decay of 5×10^{-2} M 1-methoxypyrene in THF.

lifetime ($\tau = 1/\lambda$) of pyrene and pyrene labeled poly(aryl ether) monodendrons (1-5) excimers in different solvents. It is observed that pyrene labeled monodendron (1-5) excimers have a significantly longer lifetime than their monomer while pyrene excimer has a significantly shorter lifetime than the monomer.

D. Kinetics of Excimer Fluorescence

Excimer kinetics were determined using the method of Birks's as described earlier in Chapter 1. Rate parameters were determined for pyrene and pyrene labeled poly(aryl ether) monodendrons (1-5) in acetonitrile THF and cyclohexane. To measure the rate parameters, time resolved fluorescence decay curves were measured for pyrene and pyrene labeled monodendrons (1-5) with a successive decrease in concentration from 5×10^{-2} to 1×10^{-8} M. The decay curves of monomer and excimer fluorescence were analyzed as described earlier to give the Birks parameters λ_1 and λ_2 . The decay constant λ_1 was determined from the slope of the decay curve in logarithmic format while λ_2 was calculated using equation 1-13 (Chapter 1). The variations of decay constant λ_1 and λ_2 versus concentration [c] for pyrene and 1-methoxypyrene in acetonitrile, THF and cyclohexane are shown in Figures 3- 21 through 3-26. The rate parameters k_M , k_D , k_I and k_{-I} were calculated from the data on λ_1 and λ_2 as a function of concentration and using the limiting properties of λ_1 and λ_2 as mentioned previously in Chapter 1. These rate constants in acetonitrile, THF and cyclohexane are reported in Tables 3-3, 3-4 and 3-5 respectively. For pyrene and pyrene labeled poly (aryl ether) monodendrons the rates

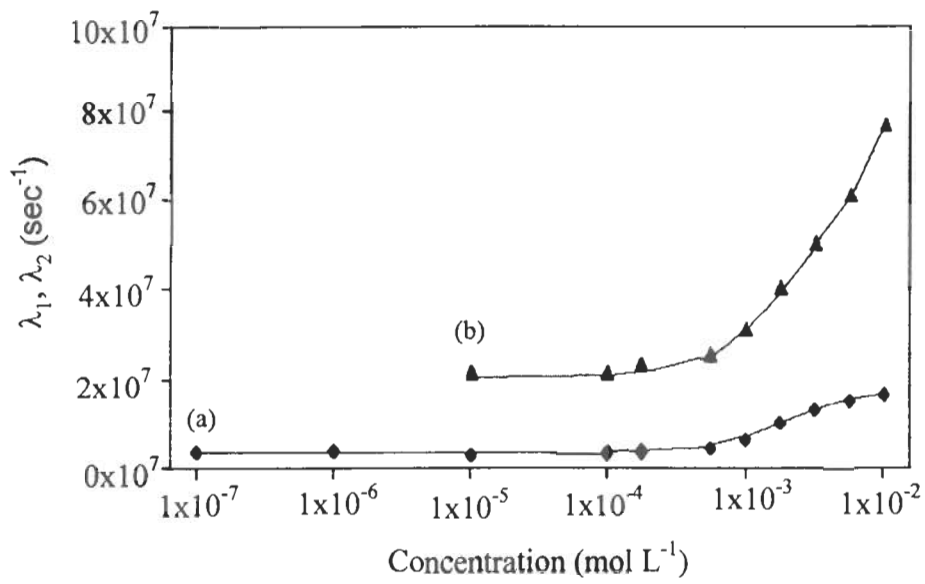


Figure 3-21. Variation of λ_1 (a) and λ_2 (b) with concentration for pyrene in ACN.

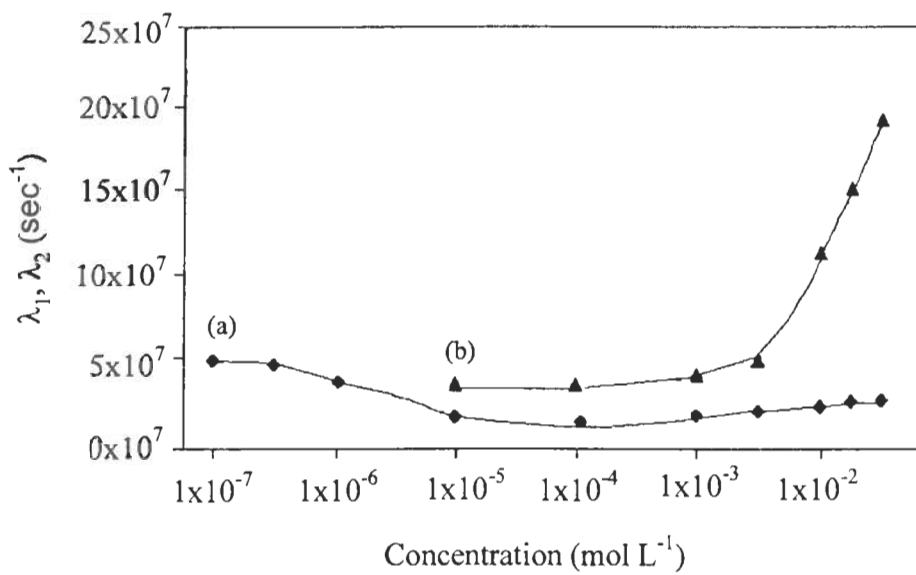


Figure 3-22. Variation of λ_1 (a) and λ_2 (b) with concentration for 1-methoxypyrene in ACN.

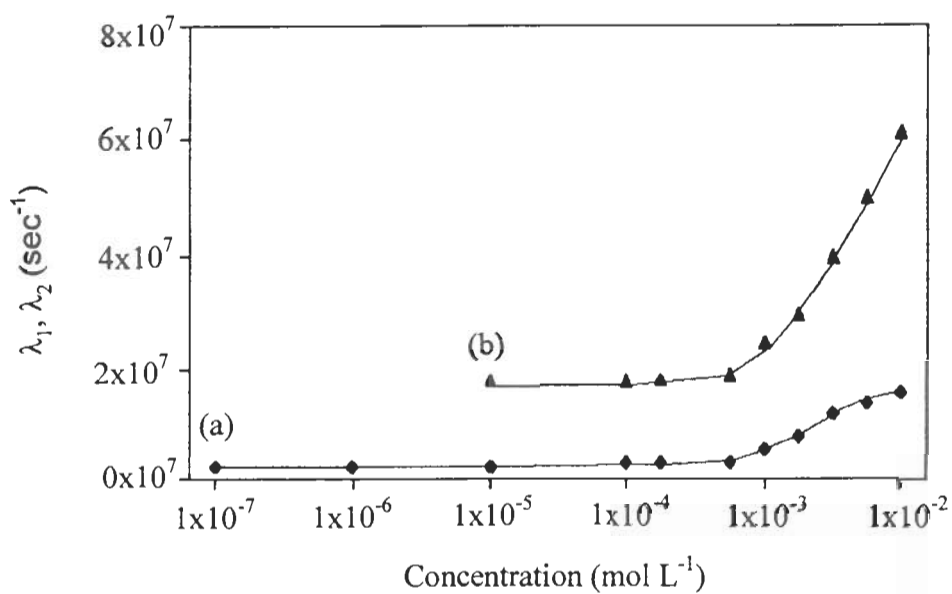


Figure 3-23. Variation of λ_1 (a) and λ_2 (b) with concentration for pyrene in THF.

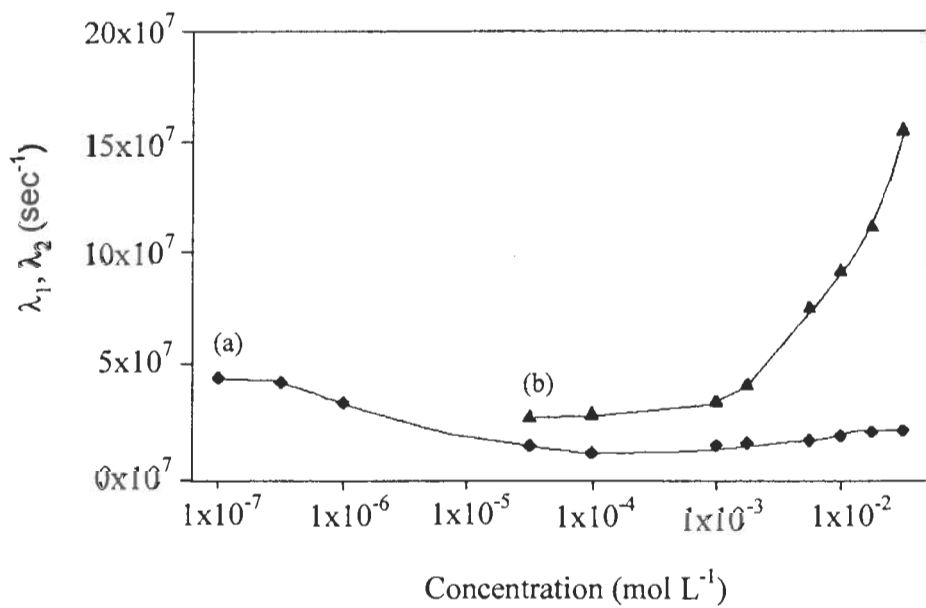


Figure 3-24. Variation of λ_1 (a) and λ_2 (b) with concentration for 1-methoxypyrene in THF.

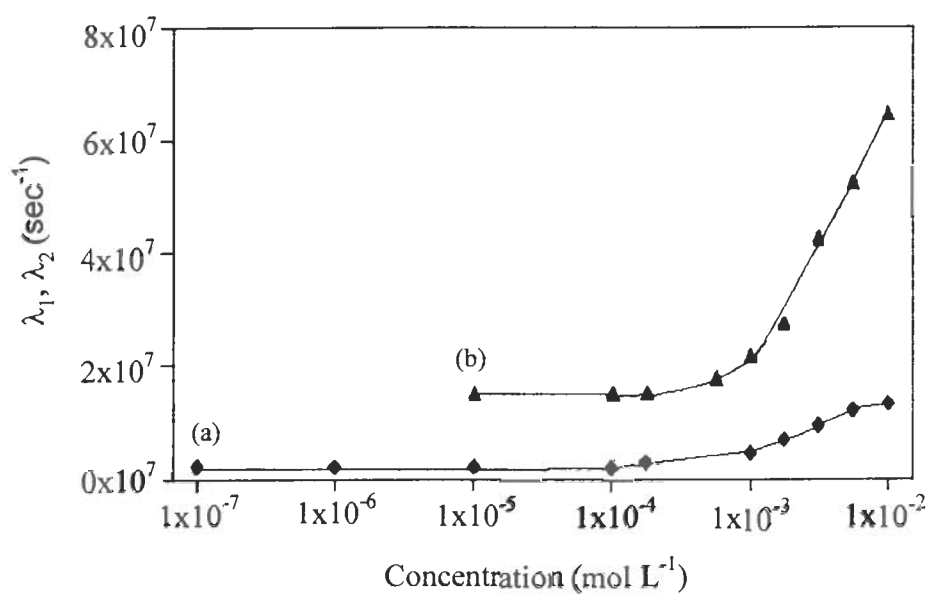


Figure 3-25. Variation of λ_1 (a) and λ_2 (b) with concentration for pyrene in CH.

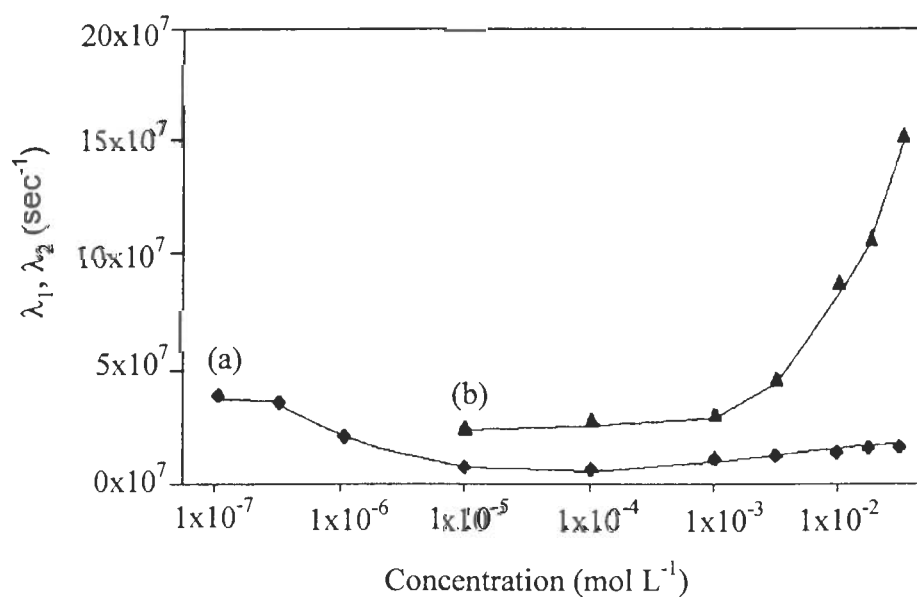


Figure 3-26. Variation of λ_1 (a) and λ_2 (b) with concentration for 1-methoxy pyrene in CH.

Table 3-3. Excimer kinetics of pyrene and pyrene labeled poly(aryl ether)monodendrons in ACN.

Compound	ACN			
	k_M (s^{-1})	k_D (s^{-1})	k_I ($M^{-1}s^{-1}$)	k_{-I} (s^{-1})
Pyrene	0.35×10^7	1.75×10^7	6.99×10^9	4.51×10^6
1-Me-O-Py (1)	4.83×10^7	2.60×10^7	2.73×10^9	8.1×10^6
G0-O-Py (2)	4.826×10^7	2.43×10^7	2.85×10^9	8.8×10^6
G0'-O-Py (3)	4.82×10^7	2.24×10^7	2.76×10^9	8.6×10^6
G1-O-Py (4)	4.80×10^7	2.09×10^7	2.72×10^9	8.1×10^6
G2-O-Py (5)	4.77×10^7	--- ^a	--- ^a	--- ^a
G3-O-Py (6)	4.65×10^7	--- ^a	--- ^a	--- ^a

Table 3-4. Excimer kinetics of pyrene and pyrene labeled poly(aryl ether)monodendrons in THF.

Compound	THF			
	k_M (s^{-1})	k_D (s^{-1})	k_I ($M^{-1}s^{-1}$)	k_{-I} (s^{-1})
Pyrene	0.26×10^7	1.58×10^7	5.56×10^9	2.53×10^6
1-Me-O-Py (1)	4.39×10^7	2.14×10^7	2.12×10^9	5.88×10^6
G0-O-Py (2)	4.38×10^7	2.06×10^7	2.10×10^9	6.24×10^6
G0'-O-Py (3)	4.37×10^7	1.92×10^7	1.95×10^9	5.84×10^6
G1-O-Py (4)	4.36×10^7	1.89×10^7	1.99×10^9	5.59×10^6
G2-O-Py (5)	4.32×10^7	1.87×10^7	1.85×10^9	5.57×10^6
G3-O-Py (6)	4.34×10^7	--- ^a	--- ^a	--- ^a

Table 3-5. Excimer kinetics of pyrene and pyrene labeled poly(aryl ether)monodendrons in CH.

Compound	CH			
	k_M (s^{-1})	k_D (s^{-1})	k_I ($M^{-1}s^{-1}$)	k_{-I} (s^{-1})
Pyrene	0.21×10^7	1.35×10^7	6.12×10^9	1.7×10^6
1-Me-O-Py (1)	3.99×10^7	2.07×10^7	2.18×10^9	6.3×10^6
G0-O-Py (2)	3.98×10^7	2.01×10^7	2.20×10^9	5.9×10^6
G0'-O-Py (3)	3.95×10^7	1.90×10^7	2.10×10^9	5.6×10^6
G1-O-Py (4)	3.92×10^7	--- ^a	--- ^a	--- ^a
G2-O-Py (5)	3.90×10^7	--- ^a	--- ^a	--- ^a
G3-O-Py (6)	3.89×10^7	--- ^a	--- ^a	--- ^a

a. Compound was not soluble enough to obtain the data.

Table 3-6. Excited-state equilibrium constant (K) for pyrene and pyrene labeled poly(aryl ether) monodendrons in ACN, THF and CH.

Compound	ACN K (M ⁻¹)	THF K (M ⁻¹)	CH K (M ⁻¹)
Pyrene	1.55x10 ³	2.20 x10 ³	3.60 x10 ³
1-Me-O-Py (1)	3.37x10 ²	3.60 x10 ²	3.64x10 ²
G0-O-Py (2)	3.24 x10 ²	3.36 x10 ²	3.73x10 ²
G0'-O-Py (3)	3.20 x10 ²	3.33 x10 ²	3.75x10 ²
G1-O-Py (4)	3.20 x10 ²	3.34 x10 ²	--- ^a
G2-O-Py (5)	--- ^a	3.32 x10 ²	--- ^a

a. Compound was not soluble enough to get the data.

Table 3-7. Gibbs free energy (ΔG) for pyrene and pyrene labeled poly(aryl ether) monodendrons in acetonitrile, THF and cyclohexane.

Compound	ACN ΔG (kcal/mole)	THF ΔG (kcal/mole)	CH ΔG (kcal/mole)
Pyrene	-4.35 x10 ³	-4.56 x10 ³	-4.85 x10 ³
1-Me-O-Py (1)	-3.45 x10 ³	-3.48 x10 ³	-3.49 x10 ³
G0-O-Py (2)	-3.42 x10 ³	-3.44 x10 ³	-3.51 x10 ³
G0'-O-Py (3)	-3.41 x10 ³	-3.44 x10 ³	-3.51 x10 ³
G1-O-Py (4)	-3.41 x10 ³	-3.44 x10 ³	--- ^a
G2-O-Py (5)	--- ^a	-3.41 x10 ³	--- ^a

a. Compound was not soluble enough to get the data.

of excimer formation (k_1) and dissociation (k_{-1}) are significantly higher in acetonitrile than cyclohexane and THF due to lower viscosity of the latter solvent. The excited state equilibrium constant ($K = k_1/k_{-1}$) was also calculated and is given in Table 3-6. Pyrene and pyrene labeled poly(aryl ether) monodendrons show a slight decrease in K in the order CH > THF > ACN. This change is more significant in pyrene than poly(aryl ether) monodendrons. The Gibbs free energies (ΔG) associated with the excimer formation were calculated for pyrene and pyrene labeled monodendrons (1-5) in acetonitrile, THF and cyclohexane at room temperature and are reported in Table 3-7. The results suggests that the formation of excimer is favorable at room temperature and $\Delta G \cong -4.6$ kcal/mole for pyrene and -3.5 kcal/mole for pyrene labeled monodendrons (1-5).

E. Conclusion

Excimer formation was observed in all solvents. No evidence was observed for the formation of ground-state pyrene dimers in any solvent. The results of this work provide detailed insight into the kinetics of excimer formation in acetonitrile, THF and cyclohexane. No transient effects were observed in the fluorescence decay of pyrene or pyrene labeled monodendrons (1-6). First-order rate constants are obtained in the time resolved fluorescence decay curve analysis. The combined steady-state and time resolved fluorescence decay experiments indicate that the formation of pyrene excimer is completely diffusion controlled and occurs only in excited state. Steady-state results show that the excimer to monomer emission decreases with increase in size of monodendrons. This is expected with the decrease in diffusion and by the significant

decrease in the frequency of encounters such that the overall excimer formation tends to decrease. This is supported by the decrease in the value of k_1 with the increase in size of monodendrons (1-6). Time resolved fluorescence studies indicate that the rate of excimer formation increases and the lifetime decreases with the increase in solvent polarity. The excited state equilibrium constants ($K = k_1/k_{-1}$) slightly decrease with the increase in size of poly(aryl ether) monodendrons. The ΔG values do not change significantly with the increase in size of monodendrons suggesting that the energetics (ΔG) of excimer formation are unaffected by the size of dendrimer.

CHAPTER 4
Quenching of Fluorescence

A. Introduction

Fluorescence quenching is widely studied both as a fundamental phenomenon and in the application of fluorescence to chemical and biochemical problems. It provides valuable information about the structure and dynamics of proteins and receptors.^{119,120} It is widely used for characterization of the behavior of chain molecules in solution. Frank et al.¹²¹ investigated the chain segmental density and diffusion properties of arborescent polystyrenes by labeling the polymers with pyrene and observing their quenching behavior using nitrobenzene as a quencher. Their results indicated that the segmental density of arborescent polystyrene was significantly higher than for linear polystyrene. The apparent diffusion coefficient of nitrobenzene was significantly lower in solution of the arborescent polystyrene than for the linear polystyrene, indicating restricted mobility of the quencher in the arborescent samples. Gopidas⁶⁹ reported the electron transfer quenching of photoexcited $\text{Ru}(\text{Phen})_3^{2+}$ by methyl viologen and ferrocyanide ion as quencher. They monitored the luminescence decay of excited complex in solution containing various anionic micelles and anionic starburst dendrimers. Their analysis of the kinetics of luminescence quenching revealed similarities between starburst dendrimer and anionic micelles.

Fluorescence quenching involves deactivation of the excited state with a quencher molecule. A variety of substances can act as quenchers of fluorescence. One of the best known efficient collisional quenchers is molecular oxygen.¹²² It is known to quench most of the aromatic hydrocarbons.¹²³ The data indicate that quenching by oxygen is a

diffusion controlled process in which virtually every collision with the excited fluorophore is effective in quenching. (The quenching efficiency approaches ~ 1.00)

The fluorescence quenching of organic fluorophores by heavy atoms is another topic that has gained much attention.^{124,125} Heavy atoms may be attached to the fluorescent molecule (internal heavy atom effect) or added to the fluorescent molecule (external heavy atom effect). Martinho⁹⁸ reported the quenching of pyrene monomer and excimer fluorescence using iodine, iodoform and iodomethane as quenchers. The studies were done in different solvents and quenching rate constants were determined. The quenching rates were found to be higher than the values predicted by the theory of totally diffusion controlled reactions. This indicated that quenching occurred at larger distances than the encounter radius.

The heavy atom quenching process is known to be primarily collisional by the formation of a non-fluorescent complex and is explained by Stern-Volmer relationship. A positive deviation from linearity is sometimes observed in the Stern-Volmer plot due to the presence of a static component in the quenching. Details of the Stern-Volmer analysis are reported in Chapter 1.

Fluorescence studies by intensity and lifetime measurements have proven useful in gaining insight into the structure of dendrimers in solution. Quenching studies can be used as a tool to understand more about the structure and dynamics of pyrene labeled poly(aryl ether) monodendrons. The quenching of dilute and concentrated solutions of pyrene and pyrene labeled poly(aryl ether) monodendrons fluorescence were observed in different solvents by measurement of emission spectra and fluorescence lifetimes in the presence of iodine and oxygen as quenchers. UV-visible absorption spectra of these

compounds in the presence of quencher were also examined. Results of both iodine and oxygen quenching experiments will help explain the structure of monodendrons in solution. Comparison of fluorescence and quenching of fluorescence of pyrene labeled poly(aryl ether) monodendrons with pyrene was carried out in order to determine the effect of size of monodendrons with increase in generation, so their structural differences with the increase in size of monodendrons and permeability in solution can be explained.

B. Iodine Quenching

I) Quenching of Monomer Fluorescence: Quenching of pyrene monomer fluorescence by iodine was observed in 1×10^{-7} M solutions of pyrene and pyrene labeled poly(aryl ether) monodendrons (**1-6**) in acetonitrile, THF and cyclohexane by steady state (intensity) and dynamic (fluorescence lifetime) measurements. Steady-state measurements were performed by monitoring the change in the intensities of the emission spectra of pyrene and pyrene labeled monodendrons with the addition of quencher. The emission spectra containing a quencher maintain their shape but show a decrease in intensity of monomer emission with the increase in quencher concentration. Figures 4-1 and 4-2 show the emission spectra of dilute solutions of pyrene and 1-methoxypyrene in THF at different quencher concentrations. The quenching behavior of the pyrene compounds was further investigated by measuring the fluorescence intensity decay at different iodine concentrations. Single exponential decays were observed with the addition of iodine and the fluorescence lifetimes decreased with iodine addition for pyrene and pyrene labeled monodendrons (**1-6**). Figures 4-3 and 4-4 show the variation of the decay constants of pyrene and 1-methoxypyrene in THF with increase in iodine

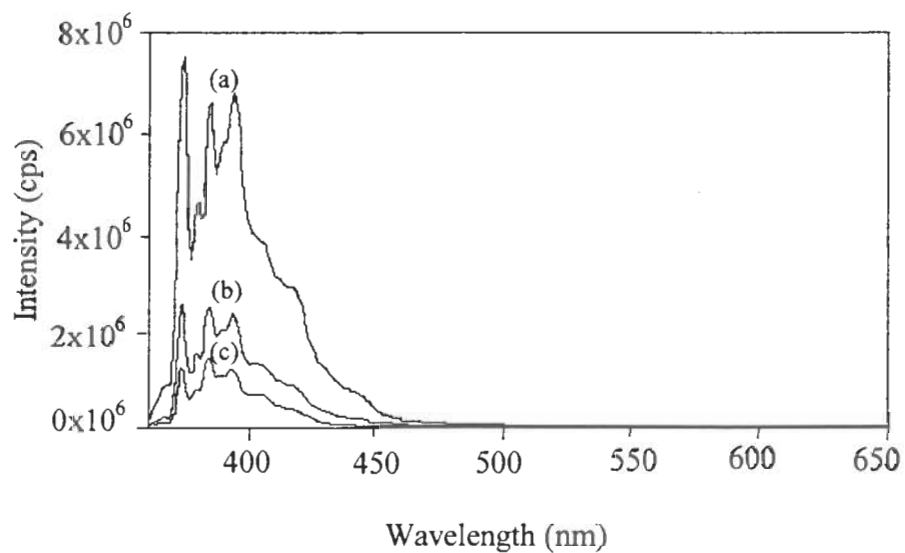


Figure 4-1. **Steady-state** emission spectrum of 1×10^{-7} M pyrene in THF at different iodine concentrations: (a) 0.00 mM; (b) 0.29 mM and (c) 0.73 mM.

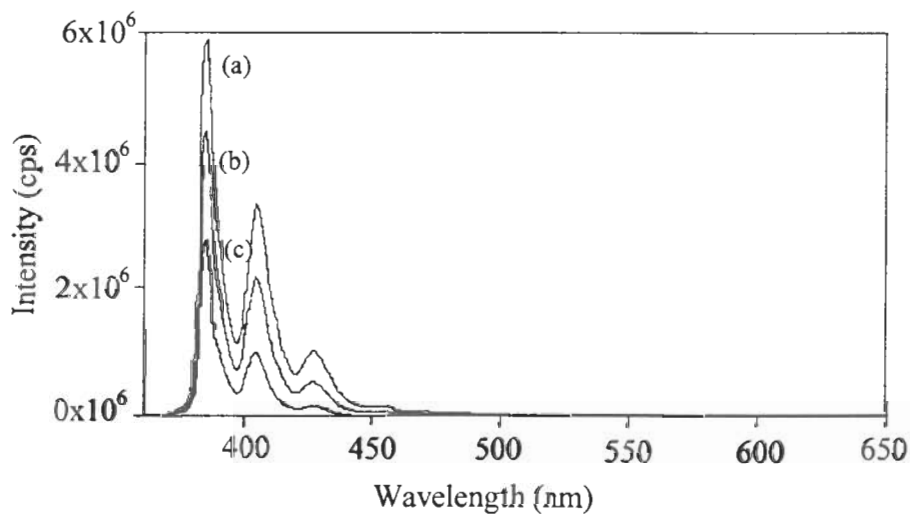


Figure 4-2. **Steady-state** emission spectrum of 1×10^{-7} M 1-methoxypyrene in THF at different iodine concentrations: (a) 0.00 mM; (b) 0.29 mM and (c) 0.73 mM.

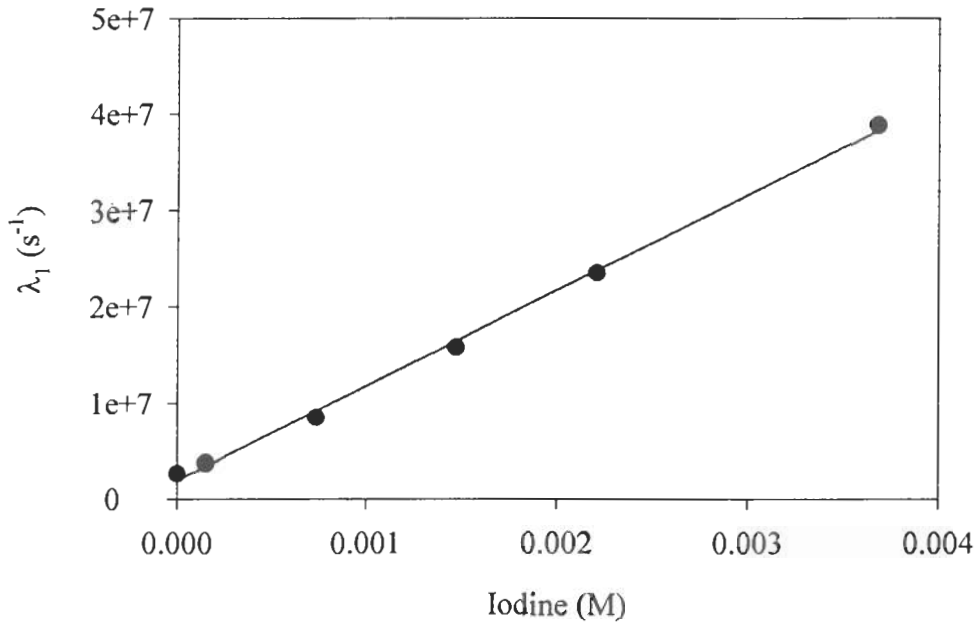


Figure 4-3. Variation of decay constant (λ_1) of 1×10^{-7} M pyrene in THF versus iodine concentration.

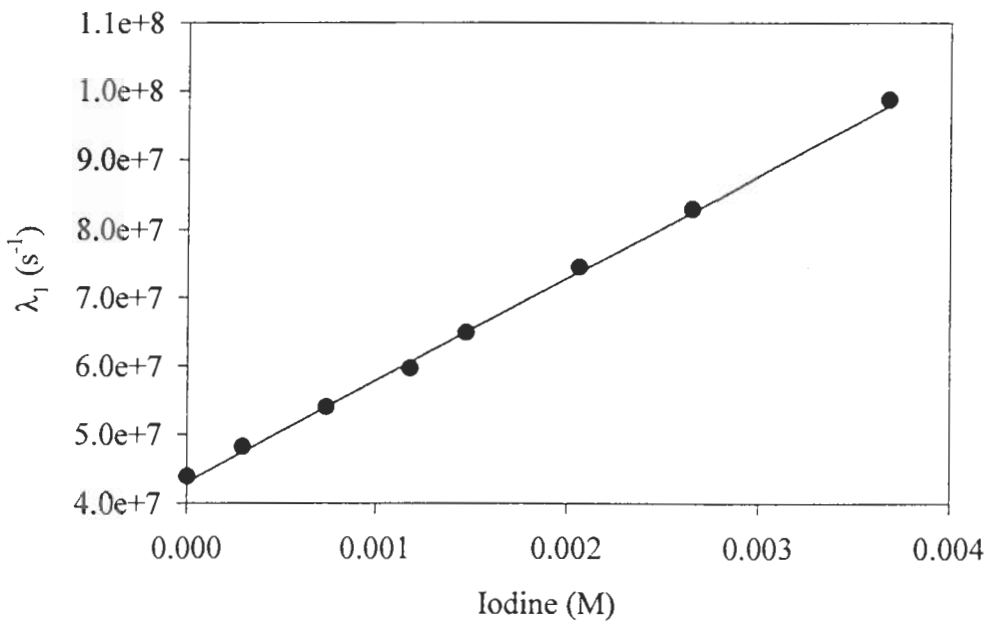


Figure 4-4. Variation of decay constant (λ_1) of 1×10^{-7} M 1-methoxypyrene in THF versus iodine concentration.

concentration. The effect of iodine concentration on the fluorescence intensity and lifetime of the monodendrons in different solvents was analyzed by the Stern-Volmer method.⁹⁹ Figure 4-5 through 4-7 show the Stern-Volmer plots (in intensity and lifetime measurement) for pyrene in acetonitrile, THF and cyclohexane. The linear dependence of τ_0 / τ and quadratic dependence of I_0 / I on iodine concentration indicated the presence of both dynamic and static quenching in acetonitrile and THF.^{104,105} In cyclohexane, only a slight deviation from linearity was observed in the Stern-Volmer plot by intensity measurements. This suggested that, in cyclohexane, the contribution of static quenching is negligible and only dynamic quenching occurred from iodine. Figures 4-8 through 4-13 show the Stern-Volmer plots by intensity measurements and lifetime measurements for pyrene labeled poly(aryl ether) monodendrons (1-6) in acetonitrile, THF and cyclohexane respectively. As with pyrene, a positive deviations in the Stern-Volmer intensity plots were observed for pyrene labeled monodendrons (1-6). In cyclohexane, a linear Stern-Volmer plot was observed for all pyrene labeled monodendrons. This indicated that in CH, the fluorophores (pyrene labeled monodendrons) obey the Stern-Volmer equation and quenching by iodine is essentially dynamic. A linear Stern-Volmer plot is generally indicative of a single class of fluorophores, all equally accessible to quencher. The proportional decrease in fluorescence lifetime with quencher indicates that the observed quenching is due to a diffusional process. Static quenching results from ground-state association between the fluorophore and the quencher such that the associated fluorophores no longer fluoresce. The lifetime measurements are not affected by the formation of ground-state associations because the fluorophores that are not associated with quencher emit normally with the same lifetime as in the absence of

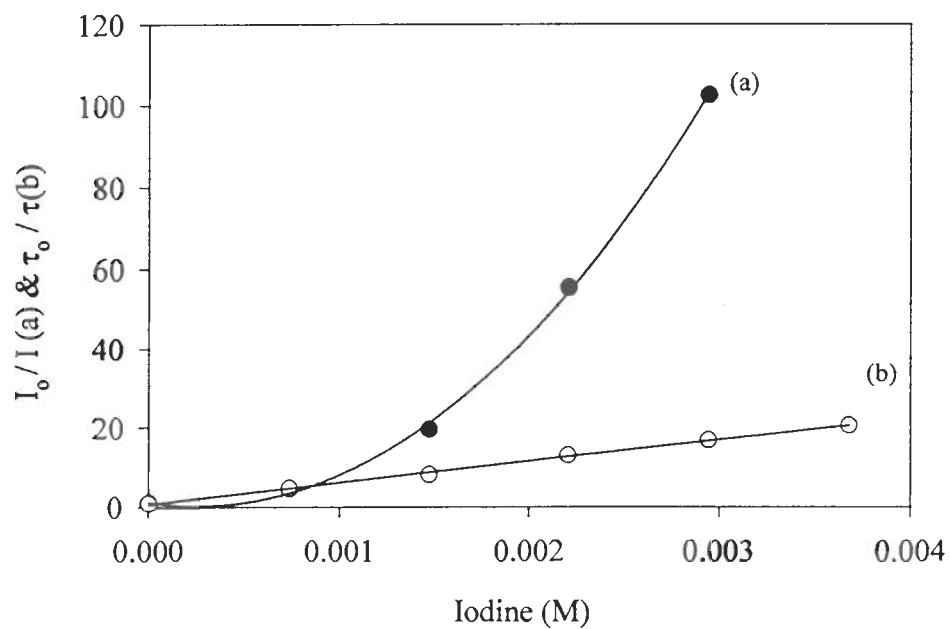


Figure 4-5. Stern-Volmer plots for 1×10^{-7} M pyrene in ACN: (a) Intensity and (b) lifetime quenching ratio by iodine.

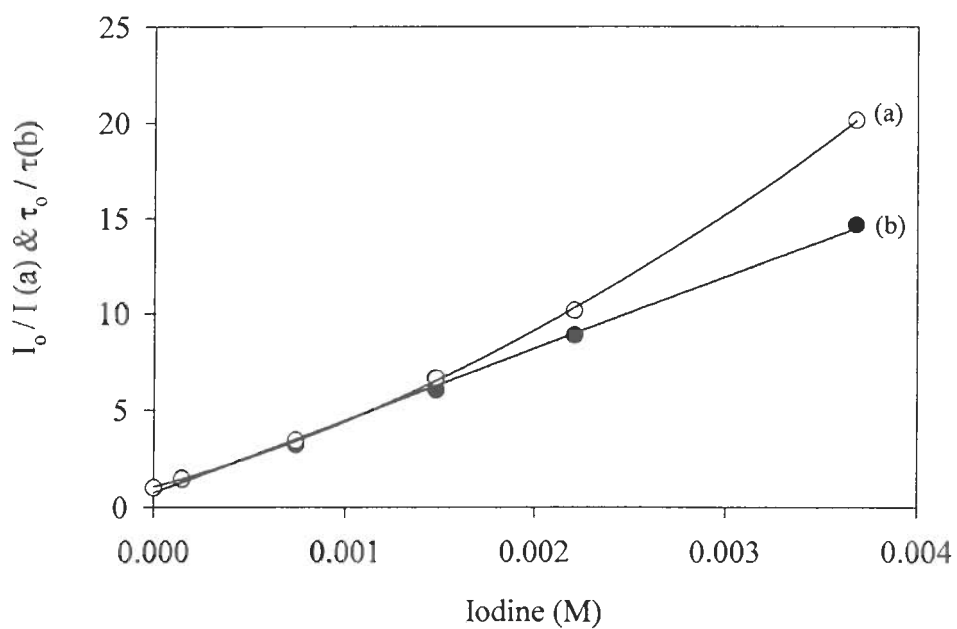


Figure 4-6. Stern-Volmer plots for 1×10^{-7} M pyrene in THF: (a) Intensity and (b) lifetime quenching ratio by iodine.

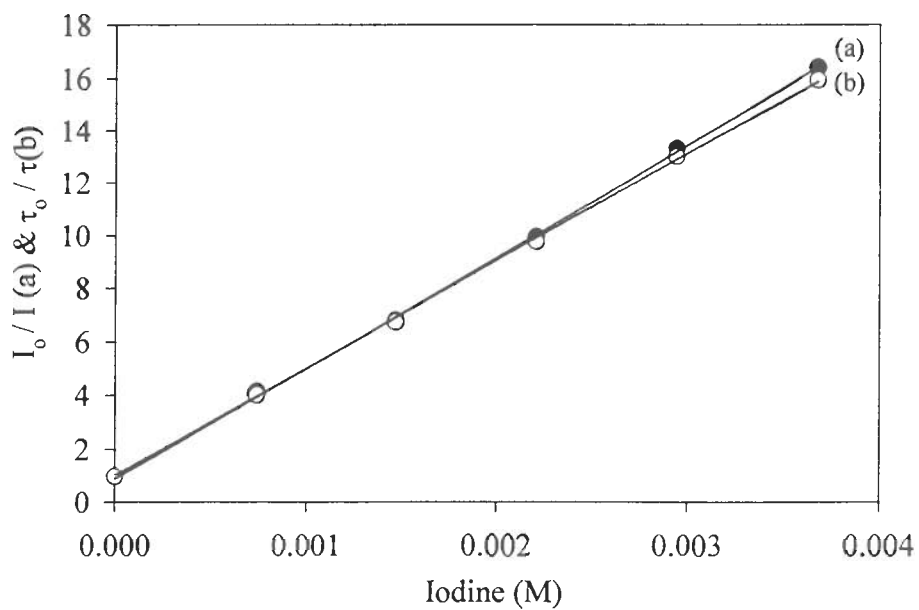


Figure 4-7. Stern-Volmer plots for 1×10^{-7} M pyrene in CH: (a) Intensity and (b) lifetime quenching ratio by iodine.

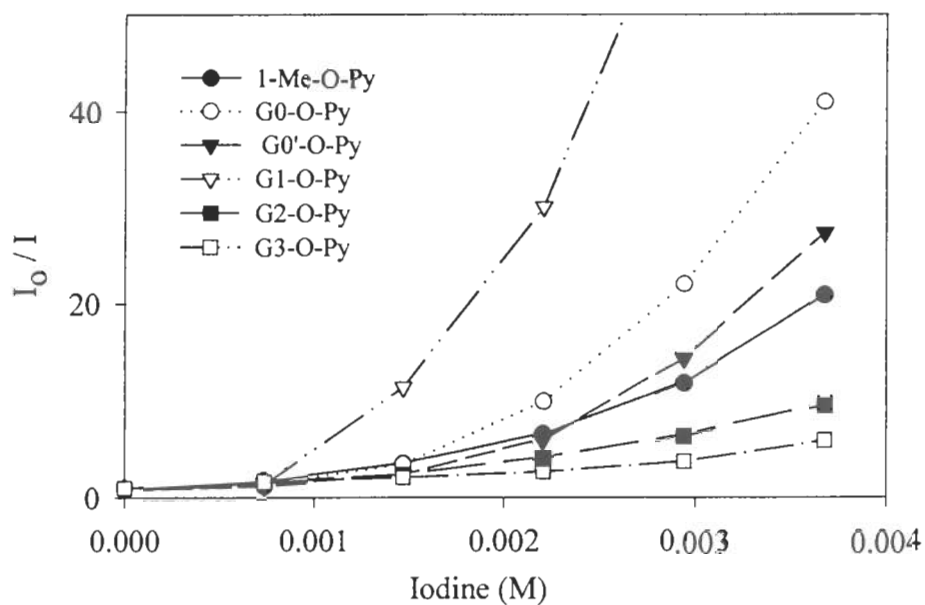


Figure 4-8. Stern-Volmer plots (intensity quenching ratio) for 1×10^{-7} M pyrene labeled poly(aryl ether) monodendrons in ACN for iodine quenching.

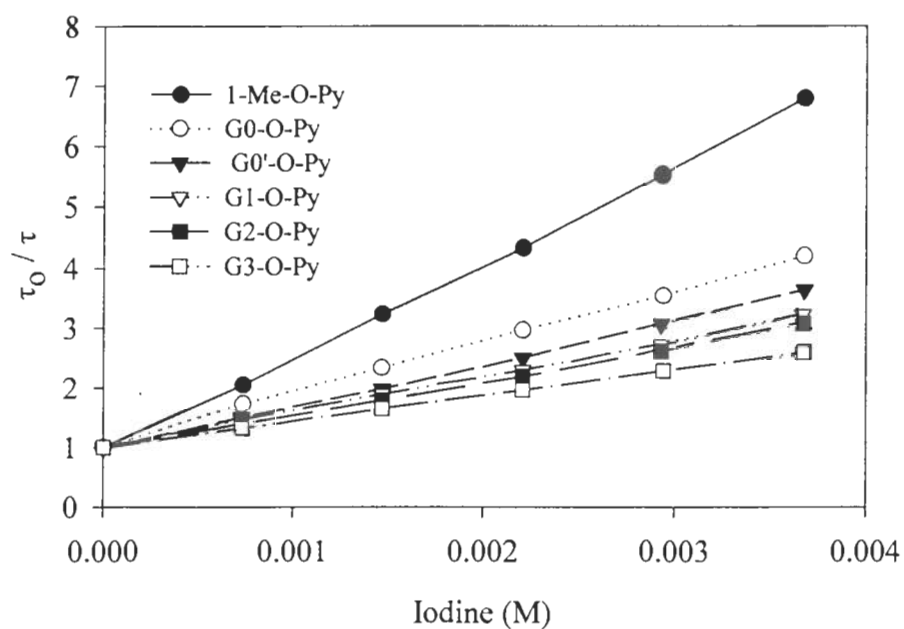


Figure 4-9. Stern-Volmer plots (lifetime quenching ratio) for 1×10^{-7} M pyrene labeled poly(aryl ether) monodendrons in ACN for iodine quenching.

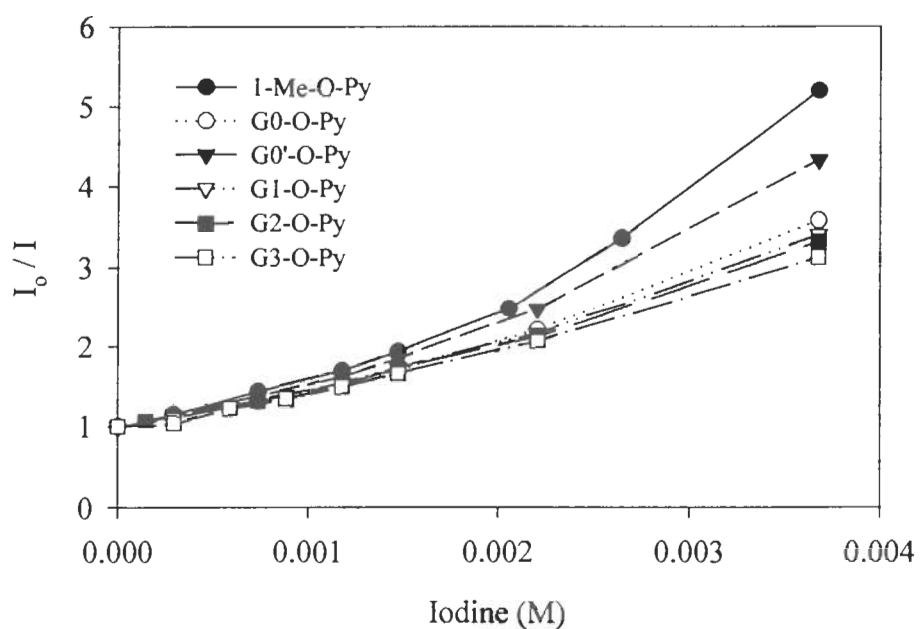


Figure 4-10. Stern-Volmer plots (intensity quenching ratio) for 1×10^{-7} M pyrene labeled poly(aryl ether) monodendrons in THF for iodine quenching.

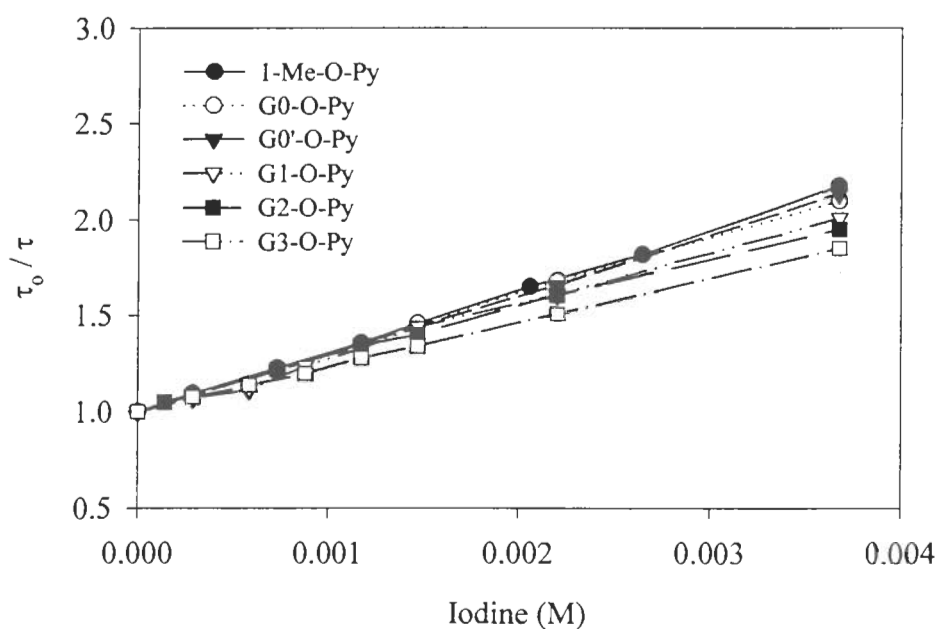


Figure 4-11. Stern-Volmer plots (lifetime quenching ratio) for 1×10^{-7} M pyrene labeled poly(aryl ether) monodendrons in THF for iodine quenching.

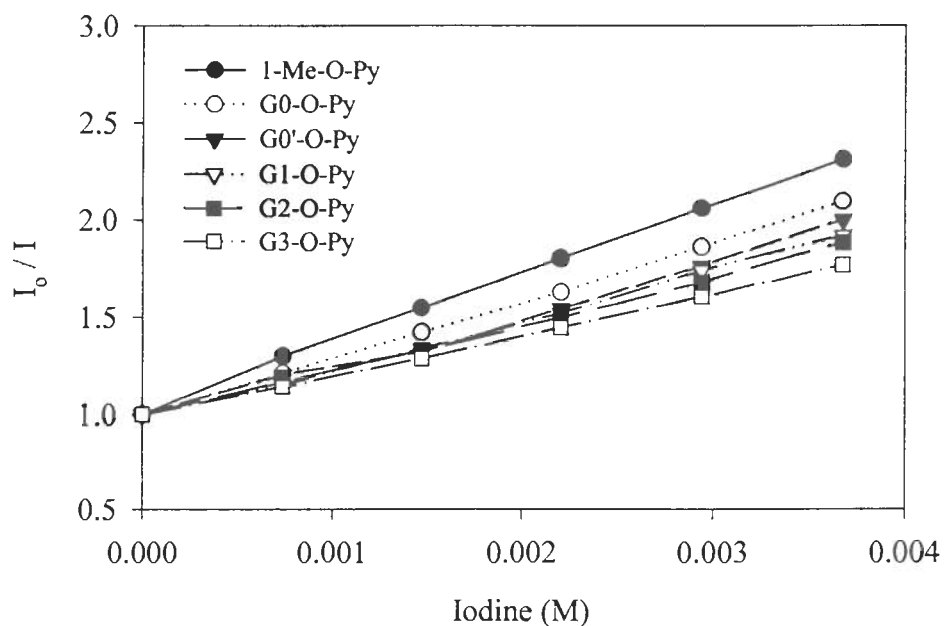


Figure 4-12. Stern-Volmer plots (intensity quenching ratio) for 1×10^{-7} M pyrene labeled poly(aryl ether) monodendrons in CH for iodine quenching.

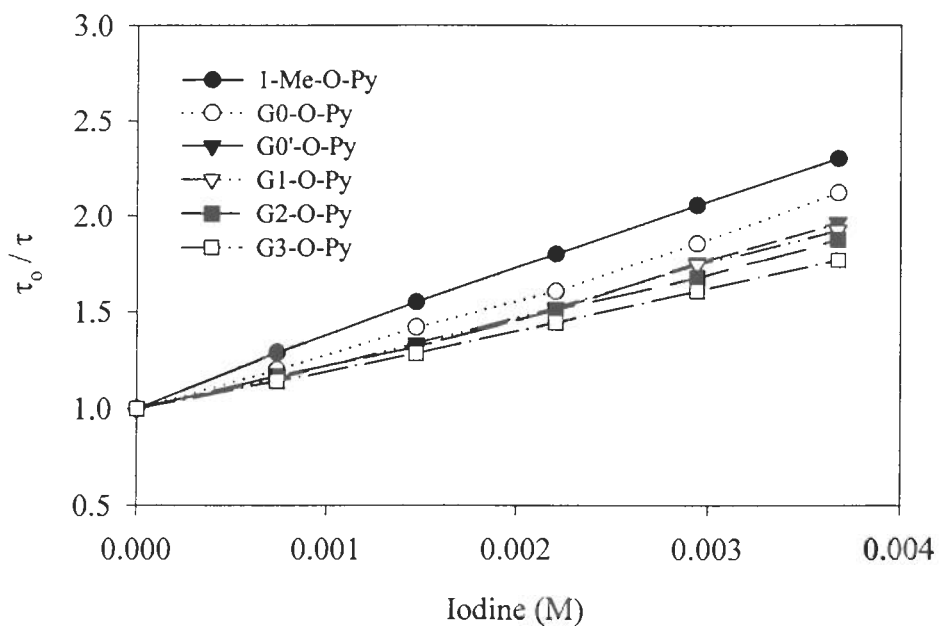


Figure 4-13. Stern-Volmer plots (lifetime quenching ratio) for 1×10^{-7} M pyrene labeled poly(aryl ether) monodendrons in CH for iodine quenching.

quencher. Dynamic quenching constants (K_{SV}) for pyrene labeled monodendrons in different solvents were determined from the slope of the Stern-Volmer plot of τ_0 / τ against quencher concentration and are reported in Table 4-1.

By knowing the lifetime of pyrene and pyrene labeled monodendrons in the absence of quencher (Table 3-1) the bimolecular quenching (k_{QM}) constants for pyrene and pyrene labeled monodendrons monomer were determined in different solvents and are reported in Table 4-2.

If both intensity (I_0 / I) and lifetime (τ_0 / τ) data are available for the same quencher then the static quenching constant (K_S) can be calculated from the slope of the plot of $(I_0 / I) / (\tau_0 / \tau)$ versus quencher concentration. (This procedure is discussed in Chapter 1) Figures 4-14 and 4-15 show separation of the static and dynamic quenching constants of pyrene and 1-methoxypyrene by iodine in THF. The static quenching rate constants obtained for pyrene and pyrene labeled monodendrons in different solvents are reported in Table 4-3.

Iodine is both a static and dynamic quencher in polar solvents like acetonitrile and THF, while in non-polar cyclohexane it is a dynamic quencher. The strong dependence of static quenching component on solvent polarity suggests that static quenching occurs by charge-transfer interaction. This interaction may be the formation of a charge transfer complex with the pyrene compounds or by a sphere of action mechanism. Iodine is known to form a charge transfer complex with solvents which can donate π -electrons effectively. In resonance terms the complex can be described as $S \cdots I_2 \leftrightarrow S^+ I_2^-$ with

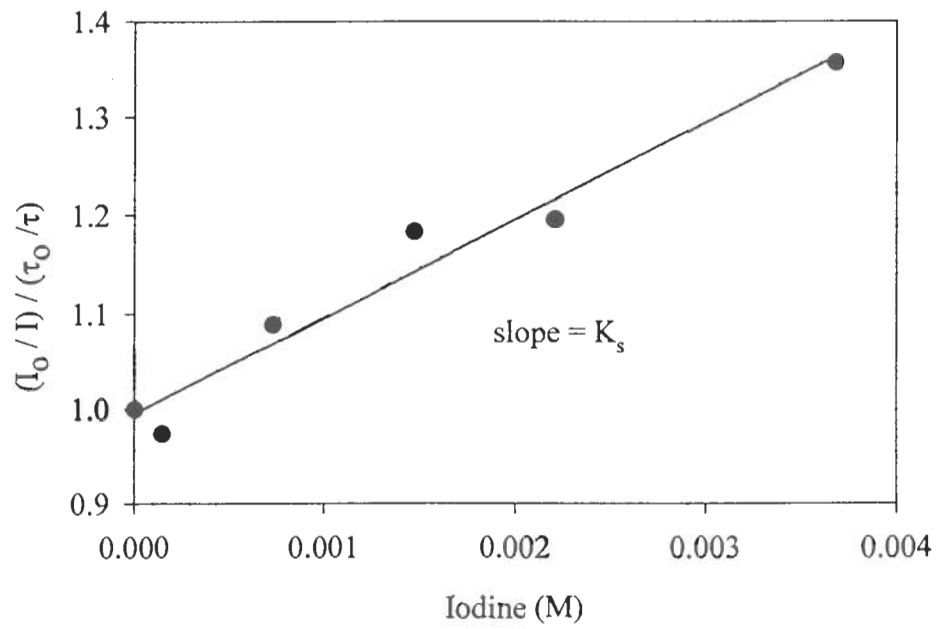


Figure 4-14. Separation of the static and dynamic quenching constant of 1×10^{-7} M pyrene in THF. Static quenching constant (K_s) is obtained from the slope.

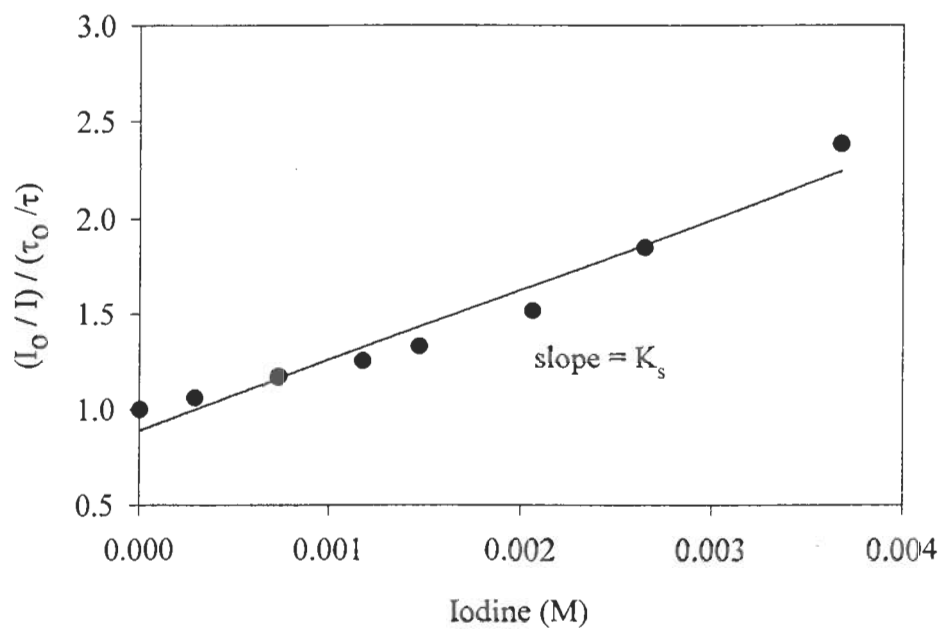


Figure 4-15. Separation of the static and dynamic quenching constant of 1×10^{-7} M 1-methoxypyrene in THF. Static quenching constant (K_s) is obtained from the slope.

Table 4-1. Dynamic quenching rate constants (K_{SV}) for 1×10^{-7} M pyrene and pyrene labeled poly (aryl ether) monodendrons (1-6) in ACN, THF and CH for iodine quenching.

Compound	ACN $K_{SV} (M^{-1})$	THF $K_{SV} (M^{-1})$	CH $K_{SV} (M^{-1})$
Pyrene	5.38×10^3	3.75×10^3	4.07×10^3
1-Me-O-P (1)	1.59×10^3	3.95×10^2	3.47×10^2
G0-O-P (2)	8.58×10^2	3.14×10^2	3.01×10^2
G0'-O-P (3)	7.19×10^2	2.98×10^2	2.62×10^2
G1-O-P (4)	6.02×10^2	3.24×10^2	2.54×10^2
G2-O-P (5)	5.71×10^2	2.97×10^2	2.38×10^2
G3-O-P (6)	4.35×10^2	2.51×10^2	2.09×10^2

Table 4-2. Bimolecular quenching rate constants (k_{QM}) for 1×10^{-7} M pyrene and pyrene labeled poly(aryl ether) monodendrons (1-6) in ACN, THF and CH for iodine quenching.

Compound	ACN $k_{QM} (M^{-1} s^{-1})$	THF $k_{QM} (M^{-1} s^{-1})$	CH $k_{QM} (M^{-1} s^{-1})$
Pyrene	1.91×10^{10}	9.89×10^9	8.45×10^9
1-Me-O-P (1)	7.68×10^{10}	1.73×10^{10}	1.38×10^{10}
G0-O-P (2)	4.14×10^{10}	1.45×10^{10}	1.20×10^{10}
G0'-O-P (3)	3.46×10^{10}	1.30×10^{10}	1.03×10^{10}
G1-O-P (4)	2.89×10^{10}	1.39×10^{10}	9.89×10^9
G2-O-P (5)	2.74×10^{10}	1.28×10^{10}	9.27×10^9
G3-O-P (6)	2.02×10^{10}	1.09×10^{10}	8.14×10^9

Table 4-3. Static quenching rate constants (K_S) for 1×10^{-7} M pyrene and pyrene labeled poly(aryl ether) monodendrons (1-6) in ACN, THF and CH for iodine quenching.

Compound	ACN $K_S (M^{-1})$	THF $K_S (M^{-1})$	CH $K_S (M^{-1})$
Pyrene	1.91×10^3	2.71×10^2	18.47
1-Me-O-P (1)	5.67×10^2	3.68×10^2	1.05
G0-O-P (2)	2.97×10^3	1.77×10^2	1.00
G0'-O-P (3)	1.86×10^3	2.84×10^2	1.00
G1-O-P (4)	3.94×10^4	1.50×10^2	1.00
G2-O-P (5)	5.15×10^2	1.51×10^2	1.00
G3-O-P (6)	3.02×10^2	1.42×10^2	1.00

a. Concentration of iodine present in solution.

the non-polar form predominating. In the presence of solvents that are strong electron donors, the following real reaction occurs:¹²⁶



In solvents which are poor electron pair donors the S-I₂ interaction is extremely weak and scarcely perturbs the I₂ molecule.^{126,127} Evidence for complex formation was obtained from the changes in the absorption spectra of pyrene and pyrene labeled monodendrons in polar solvents. Figures 4-16 through 4-18 show the UV spectra of iodine in acetonitrile and cyclohexane. In acetonitrile, three absorption bands were observed. Absorption at 458nm is the characteristic absorption of iodine and while absorption at 362nm and 290 nm indicated the formation of charge-transfer complex with acetonitrile^{128,129} which is a very good electron pair donor solvent. In THF, two absorption bands were observed. The iodine absorption band is at 446nm and the charge transfer complex at 365nm. In cyclohexane, only the absorption of iodine at 520nm was observed. This suggests that the solvent polarity is responsible in the formation of ground state complex with iodine. In polar solvents, the intensity of absorption bands of pyrene and pyrene labeled monodendrons was significantly increased with the successive addition of iodine. Figure 4-19 through Figure 4-24 show the absorption spectra of pyrene and 1-methoxypyrene in acetonitrile, THF and cyclohexane at different quencher concentrations. All these studies suggests that in acetonitrile and THF combined, dynamic and static quenching are present and the cause of static quenching might be the charge transfer interaction between quencher and fluorophore. These studies were not done in further detail so the exact nature of charge transfer-complex in polar solvents was not clearly established.

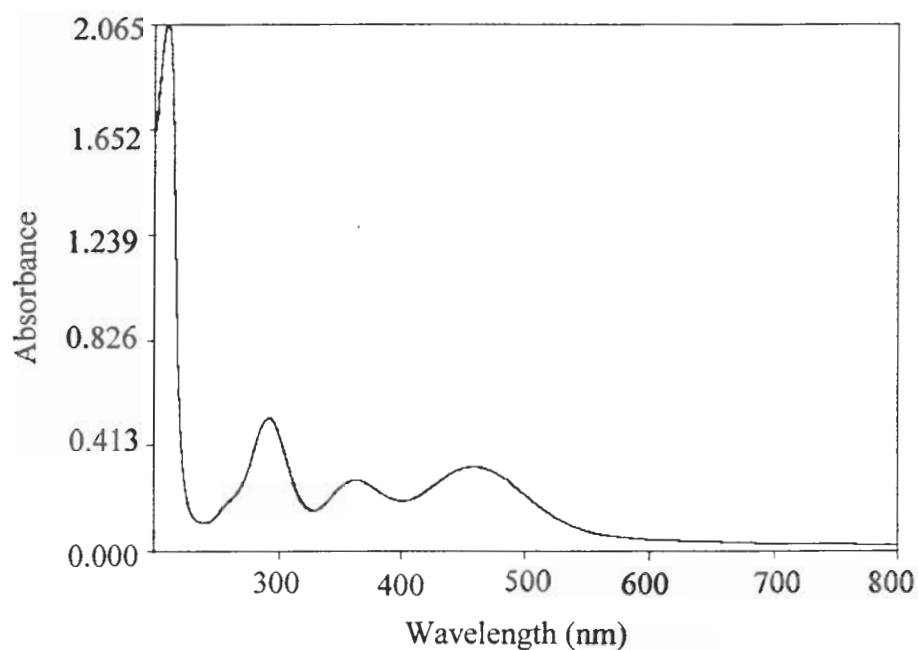


Figure 4-16. UV-Visible absorbance spectra of 0.735 mM iodine in ACN.

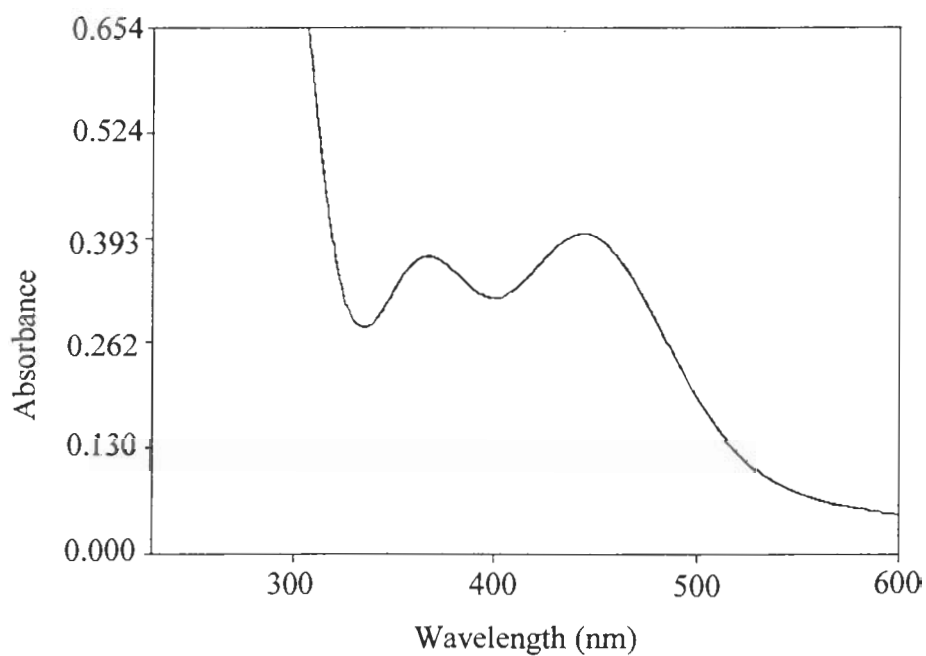


Figure 4-17. UV-Visible absorbance spectra of 0.735 mM iodine in THF.

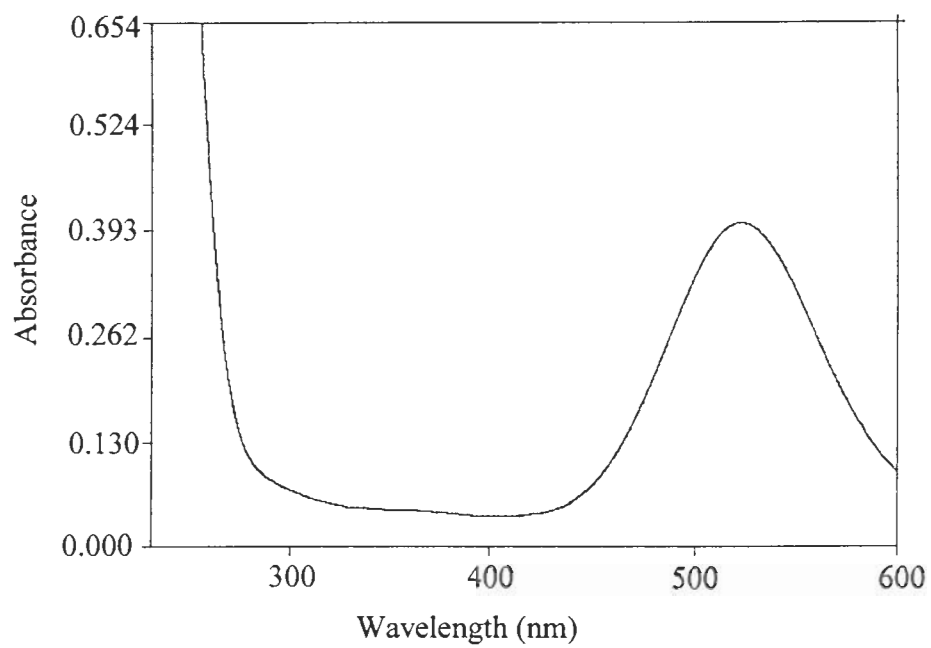


Figure 4-18. UV-Visible absorbance spectra of 0.56 mM iodine in CH.

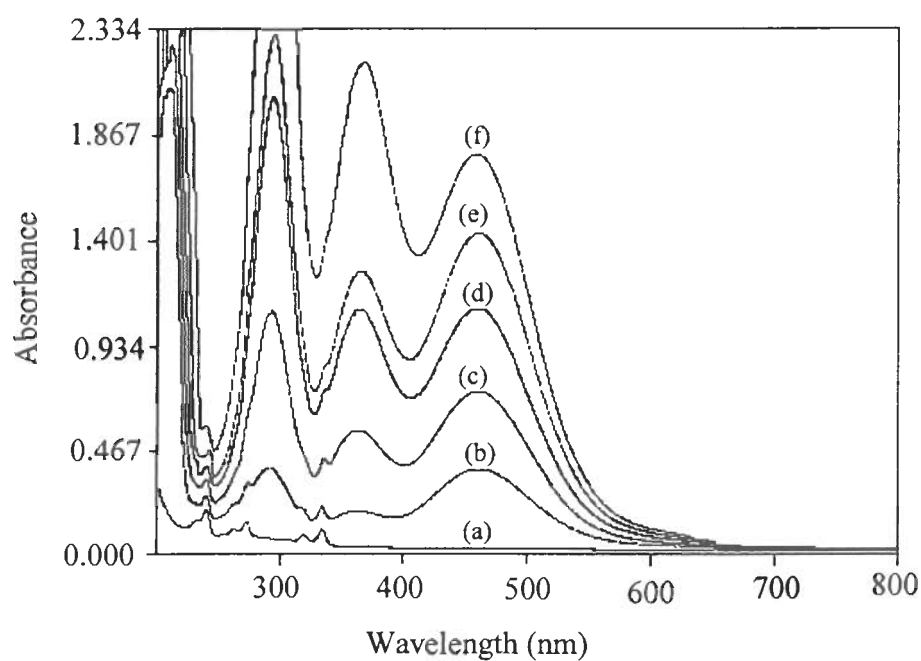


Figure 4-19. UV-Visible absorbance spectra of 1×10^{-6} M pyrene in ACN containing iodine: (a) 0 mM; (b) 0.735 mM; (c) 1.47 mM; (d) 2.21 mM; (e) 2.94 mM and (f) 3.67 mM.

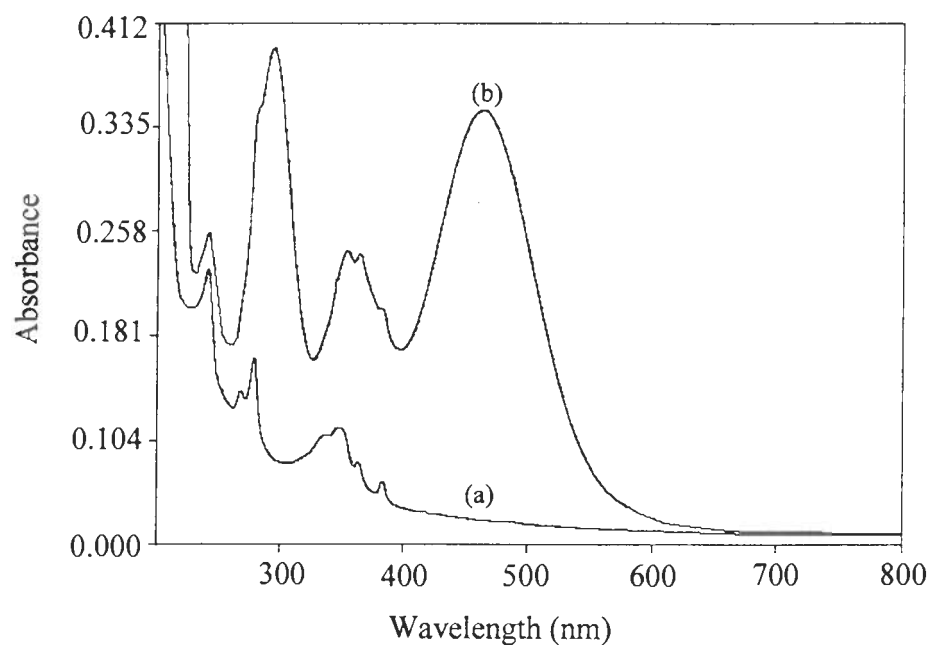


Figure 4-20. UV-Visible absorbance spectra of 1×10^{-6} M 1-methoxypyrene in ACN containing iodine: (a) 0 mM and (b) 0.735 mM.

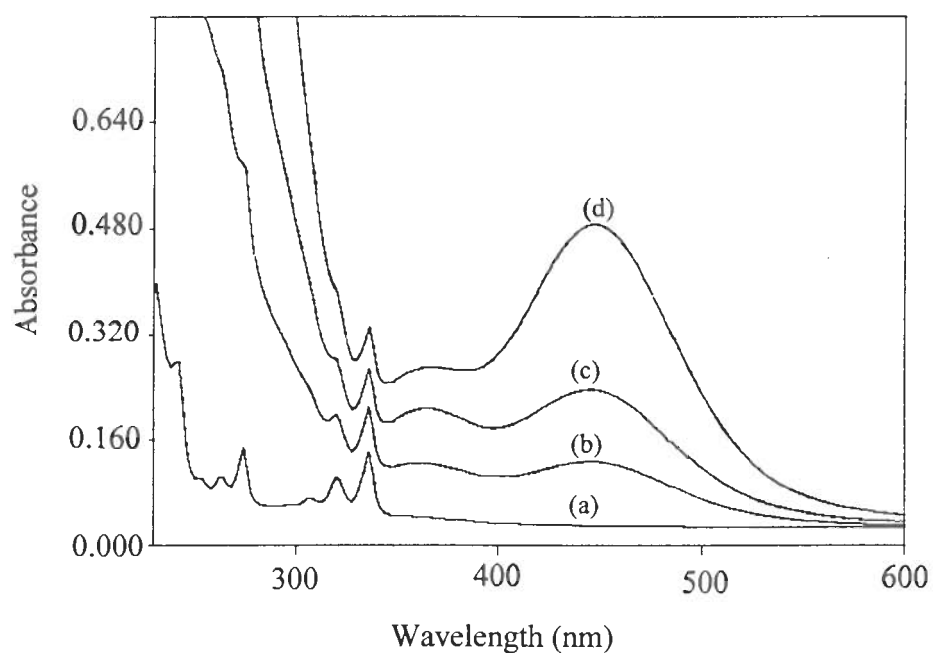


Figure 4-21. UV-Visible absorbance spectra of 1×10^{-6} M pyrene in THF containing iodine: (a) 0 mM; (b) 0.147 mM; (c) 0.294 mM and (d) 0.735 mM.

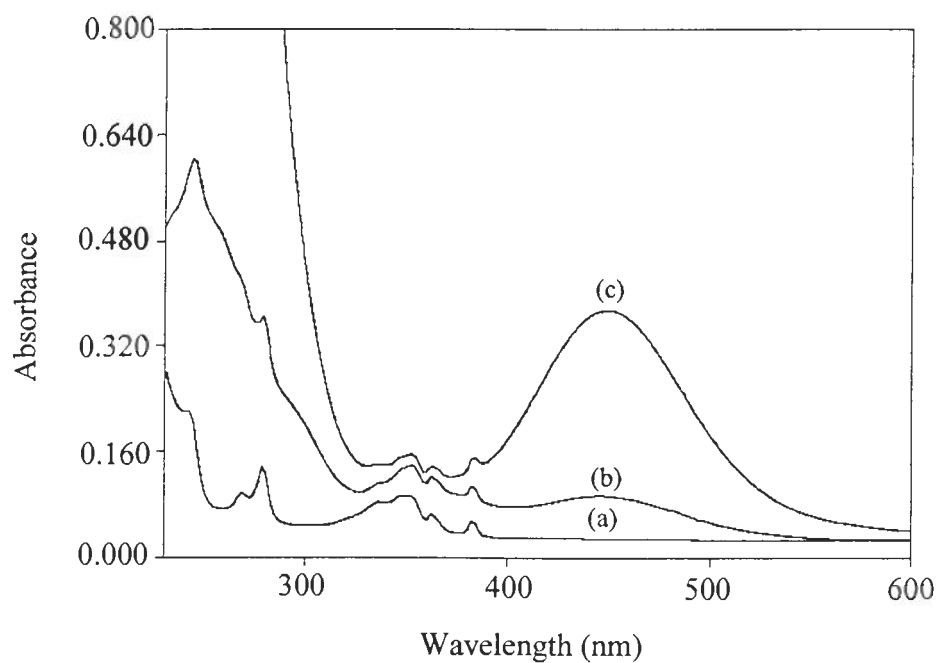


Figure 4-22. UV-Visible absorbance spectra of 1×10^{-6} M 1-methoxypyrene in THF containing iodine: (a) 0 mM; (b) 0.147 mM and (c) 0.735 mM.

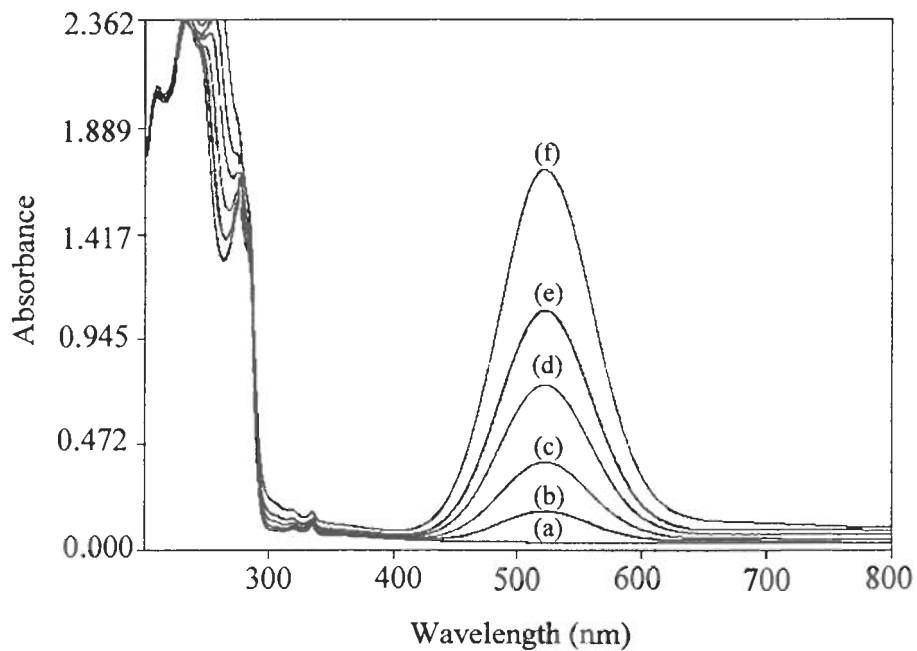


Figure 4-23. UV-Visible absorbance spectra of 1×10^{-7} M pyrene in CH containing iodine: (a) 0 mM; (b) 0.294 mM; (c) 0.735 mM; (d) 1.47 mM; (e) 2.206 mM and (f) 2.94 mM.

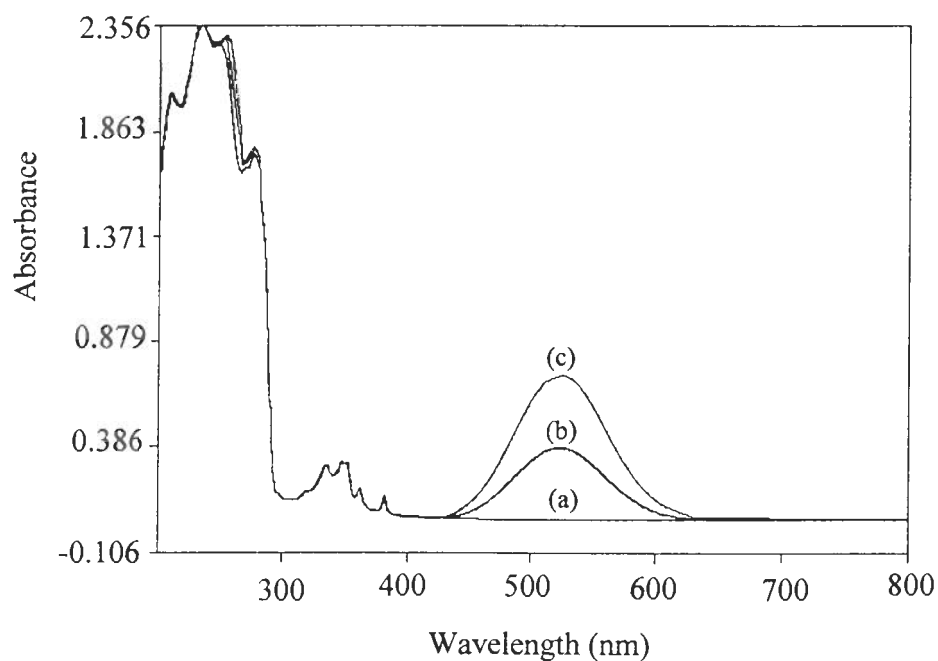


Figure 4-24. UV-Visible absorbance spectra of 1×10^{-6} M 1-methoxypyrene in CH containing iodine: (a) 0 mM; (b) 0.735 mM and (c) 1.47 mM.

II) Quenching of Excimer Fluorescence: The effect of quenchers on the intensity of excimer emission and the excimer lifetime was observed in 0.01 M pyrene and 0.05 M pyrene labeled poly(aryl ether) monodendrons solutions. Quenching of excimer fluorescence was determined by examining the fluorescence intensity and fluorescence intensity decay as a function of iodine concentration in acetonitrile, THF and cyclohexane. The emission spectra of excimer maintain their shape but displayed a decrease in intensity of monomer and excimer fluorescence with an increase in quencher concentration. This decrease in intensity is shown in Figures 4-25 and 4-26 for pyrene and 1-methoxypyrene in THF. Figure 4-27 shows the decrease in the ratio of excimer and monomer emission with the increase in quencher concentration.

The fluorescence intensity decays (λ) of pyrene and pyrene labeled monodendron excimers in acetonitrile, THF and cyclohexane were determined at different iodine concentrations. Figure 4-28 and Figure 4-29 shows the variation of the decay constant with the increase in quencher concentration for pyrene and 1-methoxypyrene. The excimer fluorescence quenching rate constants (k_{QD}) were determined from the Stern-Volmer plot and are reported in Table 4-4.

Quenching of excimer, like monomer quenching, decreased with a decrease in solvent polarity and an increase in the size of the monodendrons. When excimer quenching rate constants (k_{QD}) were compared with monomer quenching rate constants (k_{QM}), the results were interesting. Pyrene excimer has a significantly shorter lifetime than its monomer, and the excimer quenches faster than the monomer in all solvents. On

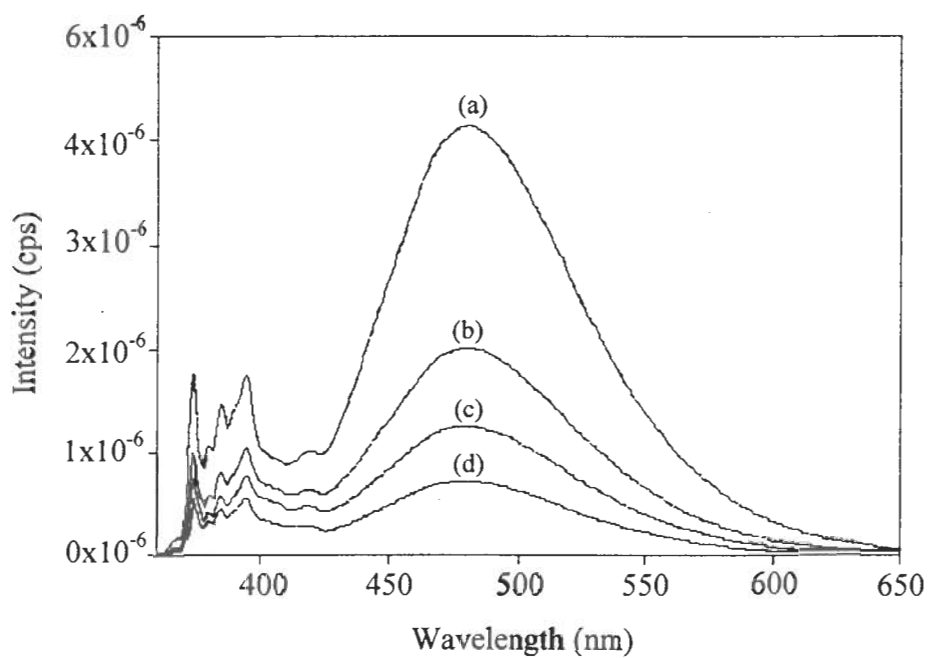


Figure 4-25. Emission spectra of 1×10^{-2} M pyrene in THF containing iodine: (a) 0.0 mM; (b) 0.29 mM; (c) 0.88 mM and (d) 2.20 mM.

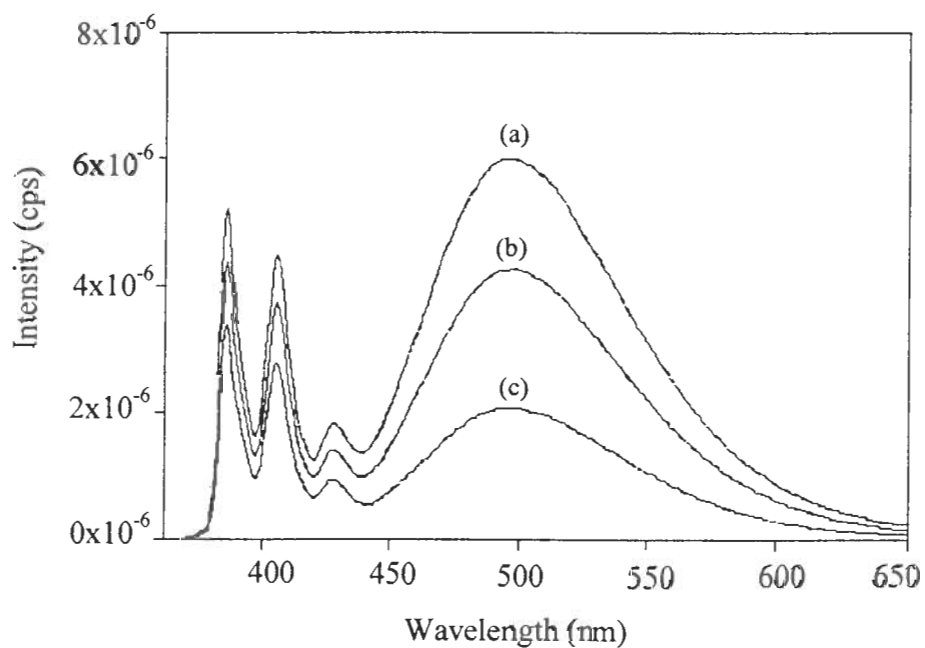


Figure 4-26. Emission spectra of 5×10^{-2} M 1-methoxypyrene in THF containing iodine: (a) 0.0 mM; (b) 0.29 mM; (c) 0.88 mM and (d) 2.20 mM.

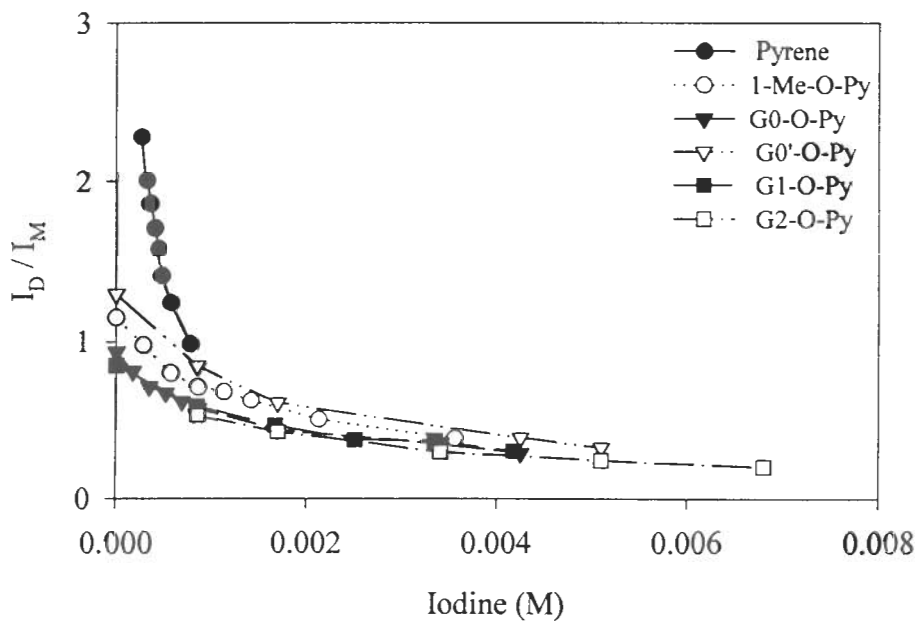


Figure 4-27. Change in the ratio of the intensity of excimer and monomer emission (I_D / I_M) with iodine concentration for pyrene (1×10^{-2} M) and pyrene labeled poly (aryl ether) monodendrons (5×10^{-2} M) in THF.

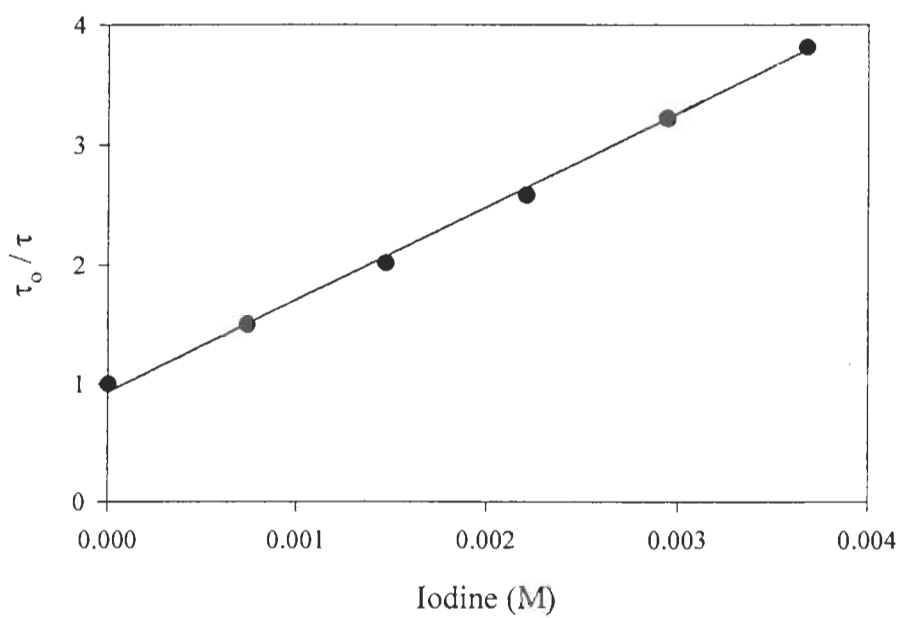


Figure 4-28. Stern-Volmer plot for 0.01 M pyrene excimer in THF containing iodine.

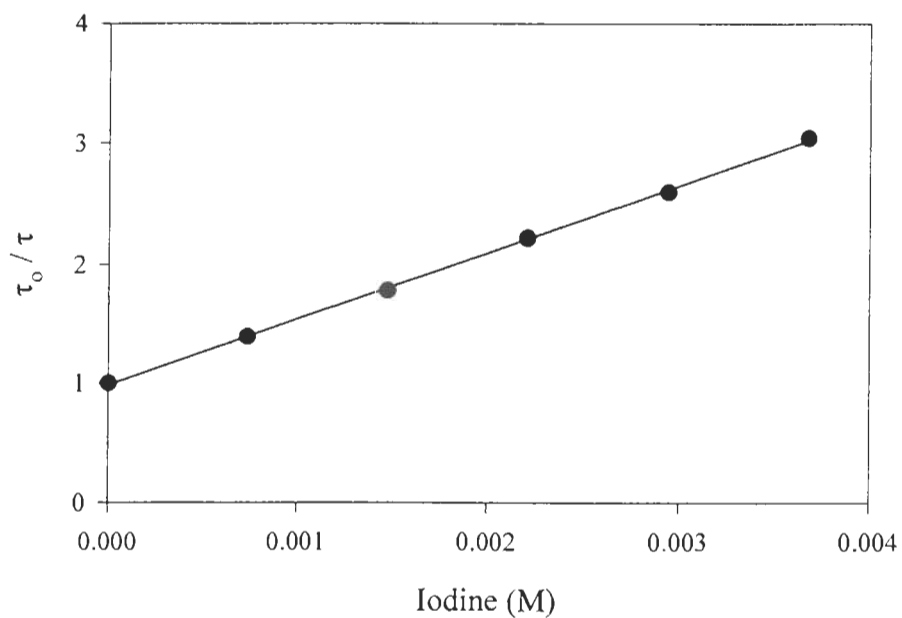


Figure 4-29. Stern-Volmer plot for 0.05 M 1-methoxypyrene excimer in THF containing iodine.

Table 4-4. Excimer fluorescence quenching rate constant (k_{QD}) for pyrene and pyrene labeled poly(aryl ether) monodendrons (**1-6**) in ACN, THF and CH for iodine quenching.

Compound	ACN $k_{QD} (M^{-1} s^{-1})$	THF $k_{QD} (M^{-1} s^{-1})$	CH $k_{QD} (M^{-1} s^{-1})$
Pyrene	2.16×10^{10}	1.26×10^{10}	1.22×10^{10}
1-Me-O-P (1)	1.95×10^{10}	1.23×10^{10}	1.21×10^{10}
G0-O-P (2)	1.74×10^{10}	1.06×10^{10}	1.08×10^{10}
G0'-O-P (3)	1.66×10^{10}	9.96×10^9	1.08×10^{10}
G1-O-P (4)	1.38×10^{10}	9.89×10^9	--- ^b
G2-O-P (5)	--- ^b	9.87×10^9	--- ^b
G3-O-P (6)	--- ^b	--- ^b	--- ^b

a. Concentration of iodine present in solution.

b. Compound was not soluble in appreciable amount to get the data.

the other hand, pyrene labeled monodendron monomers have a shorter lifetime than their excimers and have a faster quenching rate than their excimer. This difference is more obvious in acetonitrile, where pyrene labeled monodendron monomers have a significantly shorter lifetime than in cyclohexane and THF and have significantly higher quenching rates.

C. Oxygen Quenching

I) Quenching of Monomer Fluorescence: Molecular oxygen is known to be an efficient quencher of aromatic hydrocarbons. Quenching of fluorescence was observed for pyrene and pyrene labeled monodendrons in acetonitrile, THF and cyclohexane by saturating the sample by bubbling with air for 15 minutes. The lifetimes of air saturated samples of pyrene and pyrene labeled monodendrons were determined by measurement of their fluorescence intensity decay. The monomer quenching rate constants (k_{QM}) were determined from the Stern-Volmer equation by using the lifetime in the presence and absence of quencher along with the concentration of oxygen used. The concentrations of oxygen in air saturated solvents were taken from the literature.¹³⁰ The quenching rate constants are reported in Table 4-5.

From the results, it appears that like iodine quenching, quenching by oxygen changes with solvent viscosity. Quenching by oxygen is in order ACN > THF > CH. The decrease in the quenching rate constants with the increase in size of the monodendrons suggests that oxygen is blocked or shielded from the pyrene moiety and is less effective in quenching. This shielding might be a result of the folded dendrimer structures in solution or due to their slow diffusion in the solvent. Other published

Table 4-5. Monomer fluorescence quenching rate constants (k_{QM}) for pyrene and pyrene labeled poly(aryl ether) monodendrons (1-6) in ACN, THF and CH for oxygen quenching.

Compound	$[O_2]^a = 1.9 \text{ mM}$	$[O_2]^a = 1.5 \text{ mM}$	$[O_2]^a = 2.4 \text{ mM}$
	ACN $k_{QM} (M^{-1} s^{-1})$	THF $k_{QM} (M^{-1} s^{-1})$	CH $k_{QM} (M^{-1} s^{-1})$
Pyrene	4.15×10^{10}	2.87×10^{10}	2.80×10^{10}
1-Me-O-P (1)	4.03×10^{10}	2.72×10^{10}	2.68×10^{10}
G0-O-P (2)	3.95×10^{10}	2.67×10^{10}	2.59×10^{10}
G0'-O-P (3)	3.90×10^{10}	2.64×10^{10}	2.46×10^{10}
G1-O-P (4)	3.61×10^{10}	2.45×10^{10}	2.35×10^{10}
G2-O-P (5)	3.25×10^{10}	2.27×10^{10}	2.06×10^{10}
G3-O-P (6)	2.98×10^{10}	2.11×10^{10}	1.84×10^{10}

a. Concentration of oxygen¹³⁰ used in determining the quenching rate constants for air saturated solutions in ACN, THF and CH.

Table 4-6. Excimer fluorescence quenching rate constants (k_{QD}) for pyrene and pyrene labeled poly(aryl ether) monodendrons (1-6) solutions in ACN, THF and CH for oxygen quenching.

Compound	$[O_2]^a = 1.9 \text{ mM}$	$[O_2]^a = 1.5 \text{ mM}$	$[O_2]^a = 2.4 \text{ mM}$
	ACN $k_{QD} (M^{-1} s^{-1})$	THF $k_{QD} (M^{-1} s^{-1})$	CH $k_{QD} (M^{-1} s^{-1})$
Pyrene	3.40×10^{10}	2.86×10^{10}	2.35×10^{10}
1-Me-O-P (1)	3.33×10^{10}	2.84×10^{10}	2.31×10^{10}
G0-O-P (2)	3.28×10^{10}	2.81×10^{10}	2.33×10^{10}
G0'-O-P (3)	3.23×10^{10}	2.78×10^{10}	2.32×10^{10}
G1-O-P (4)	3.19×10^{10}	2.33×10^{10}	-- ^b
G2-O-P (5)	--- ^b	2.27×10^{10}	--- ^b

a. Concentration of oxygen used in determining the quenching rate constants for air saturated solutions in ACN, THF and CH. (Murov, S. L 1993).

b. Compound was not soluble enough to get the data.

studies show quenching by oxygen is a diffusion-controlled process in which every collision with the excited fluorophore is effective in quenching. This will be discussed later in detail while comparing the quenching efficiency of iodine and oxygen in different solvents.

II) Quenching of Excimer Fluorescence: Quenching of excimer fluorescence was determined from measurement of the fluorescence intensity decay of air saturated solutions of 0.01 M pyrene and 0.05 M pyrene labeled poly(aryl ether) monodendrons in acetonitrile, THF and cyclohexane. The excimer quenching rate constants (k_{QD}) were determined from Stern-Volmer analysis and are reported in Table 4-6.

The excimers have lower quenching rates (k_{QD}) than the monomers (k_{QM}), except for the pyrene labeled monodendrons in THF. The same decrease of the quenching rate is observed with increase in size of the monodendrons and change in polarity of the solvent as observed for monomer. The quenching by oxygen is in the order ACN > THF > CH and decreases with the increase in size of monodendrons (1-5).

D. Comparison of Iodine and Oxygen Quenching:

The quenching studies by iodine and oxygen have revealed that the quenching efficiency of both iodine and oxygen is affected by solvent polarity and size of the monodendrons. It increased with increases in solvent polarity and decreased with the increases in size of the monodendrons. Iodine quenching seems to be affected more by

the polarity of solvent. This is expected since I₂ quenching appears to have some charge transfer component.¹³¹⁻¹³³ Both iodine and oxygen are known to be efficient quenchers of many fluorophores.^{98,65}

Figures 4-30 and Figure 4-31 show the fluorescence decay (in logarithmic format) of dilute solutions of pyrene and 1-methoxypyrene in THF quenched by 1.515 mM iodine and 1.5 mM oxygen. Faster decay was observed for the air-saturated sample containing oxygen. In Figure 4-32 and 4-33 the fluorescence decay of concentrated solutions of pyrene and 1-methoxypyrene in THF is compared with the fluorescence decay quenched by iodine and oxygen. Oxygen has a greater quenching rate than iodine both in concentrated and dilute solutions of pyrene and pyrene labeled monodendrons in acetonitrile, THF and cyclohexane.

The quenching rates of iodine and oxygen decrease with increase in size of the monodendrons. This decrease in the quenching rate constant with the increase in size of monodendrons using iodine and oxygen as quencher indicates reduced permeability of quencher to the fluorophore. This difference was more significant for the iodine quenching. The iodine quenching includes a polar component in polar solvents that leads to increased rates and static quenching. The relative increase in k_{QM} (compared to cyclohexane) and the static component in polar solvents tends to decrease with increasing molecular weight. This suggests that the larger monodendrons are beginning to change the polarity of the solvent environment in the vicinity of pyrene.

Table 4-7 shows the observed diffusion coefficients (D_{py}) of the pyrene labeled monodendrons in acetonitrile and THF measured at room temperature by the pulsed-

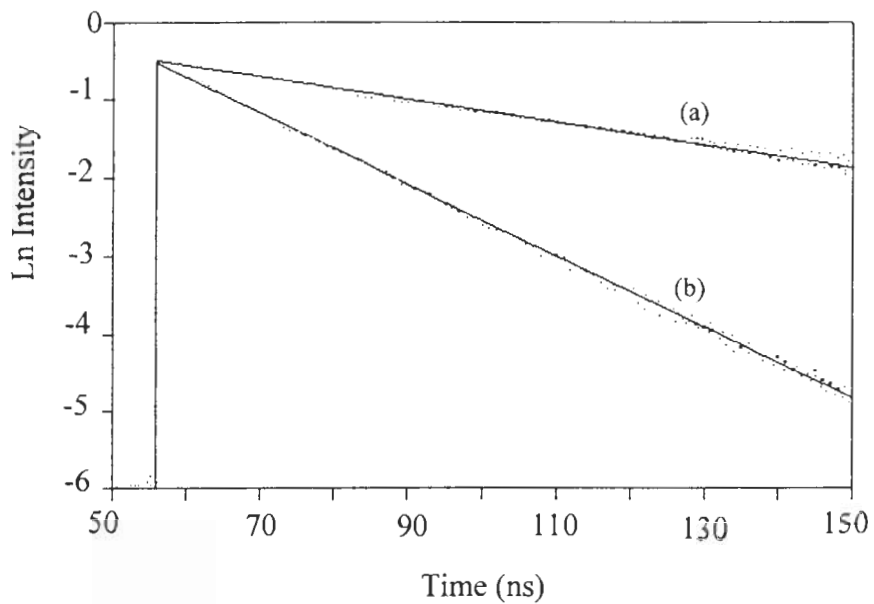


Figure 4-30. Fluorescence decay of 1×10^{-7} M pyrene in THF containing quencher: (a) Iodine = 1.515 mM and (b) oxygen = 1.5 mM.

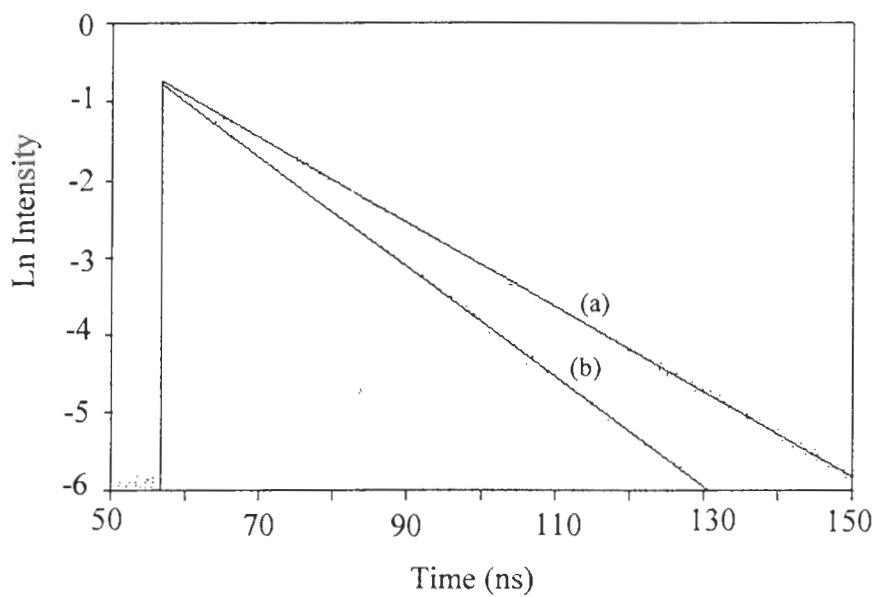


Figure 4-31. Fluorescence decay of 1×10^{-7} M 1-methoxypyrene in THF containing quencher: (a) Iodine = 1.515 mM and (b) oxygen = 1.5 mM.

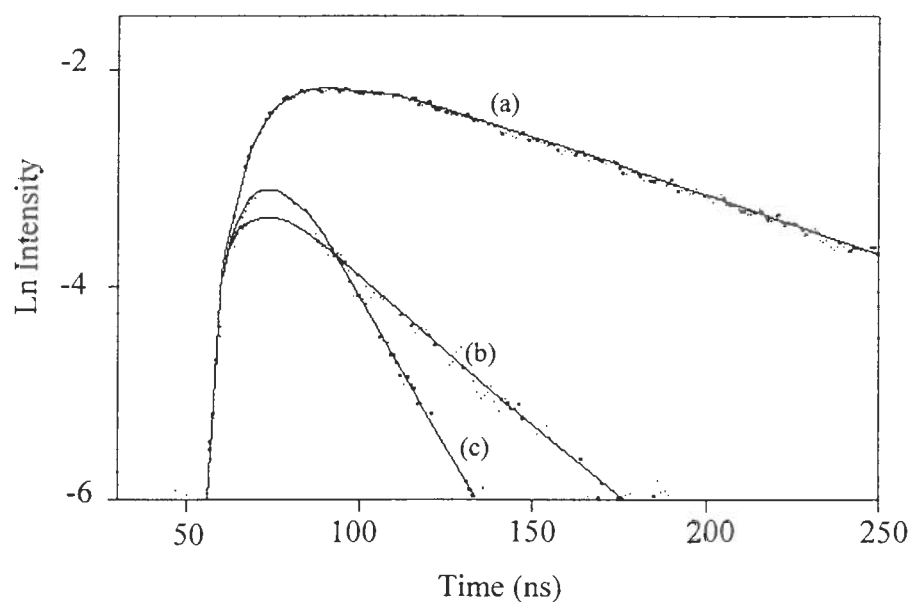


Figure 4-32. Fluorescence decay of 0.01 M pyrene in THF containing quencher: (a) no quencher; (b) Iodine = 1.515 mM and (c) oxygen = 1.5 mM.

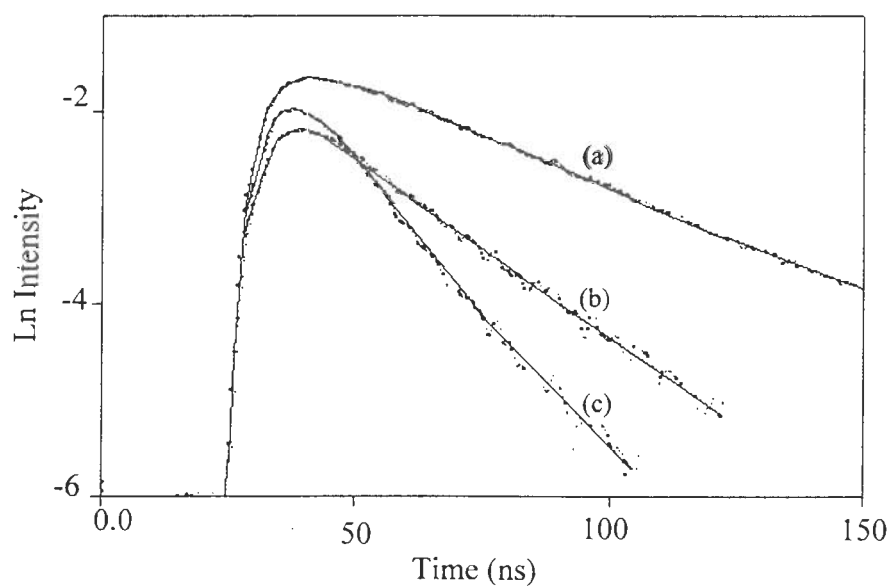


Figure 4-33. Fluorescence decay of 0.05 M 1-methoxypyrene in THF containing quencher: (a) no quencher; (b) Iodine = 1.515 mM and (c) oxygen = 1.5 mM.

field-gradient NMR (PFG NMR) technique. The diffusion of G3-O-Py is 2.0 times lower than for 1-methoxypyrene in acetonitrile and 1.7 times in THF. From the observed diffusion coefficient values, the radii (R) of pyrene labeled monodendrons were calculated using the Stokes-Einstein equation (1-24) and are given in Table 4-7 along with the radii calculated from the models. The observed radii in both acetonitrile and THF are significantly smaller than those predicted for the fully extended models (R_{calc}). The observed radii are not much different for pyrene labeled monodendrons (**1-6**) but there is a significant difference for G3-O-Py in acetonitrile and THF. THF is a better solvent as compared to acetonitrile. This points at a structural difference due to solvation so G3-O-Py is more extended in THF than in acetonitrile. Figure 4-34 and 4-35 show the plots of experimental radii (R_{exp}) versus molecular weight (MW) of pyrene labeled poly(aryl ether) monodendrons (**1-6**) in acetonitrile and THF respectively. The data seems to fit a power regression, with an exponent of 0.32 in acetonitrile and 0.58 in THF. The radii calculated for the fully extended models (R_{calc}), show an increase of 2.9 Å with the addition of a new generation from G0-O-Py to G3-O-Py, and the plot of calculated radii (R_{calc}) versus molecular weight (MW) seems to fit the logarithmic regression. This suggests that the monodendrons are not fully extended in solution and some back folding is present. Thus an apparent increase in density and reduced permeability with increasing generation number was observed.

Table 4-8 and 4-9 report the diffusion coefficients of quenchers (iodine and oxygen) and their relative viscosities in acetonitrile and THF respectively, calculated using the Smoluchowski equation¹⁰⁰ (1-23). The interaction radius (R_e) of the quenching event between iodine and pyrene was taken to be 5.9 Å⁹⁸ and for oxygen and pyrene was 4.48

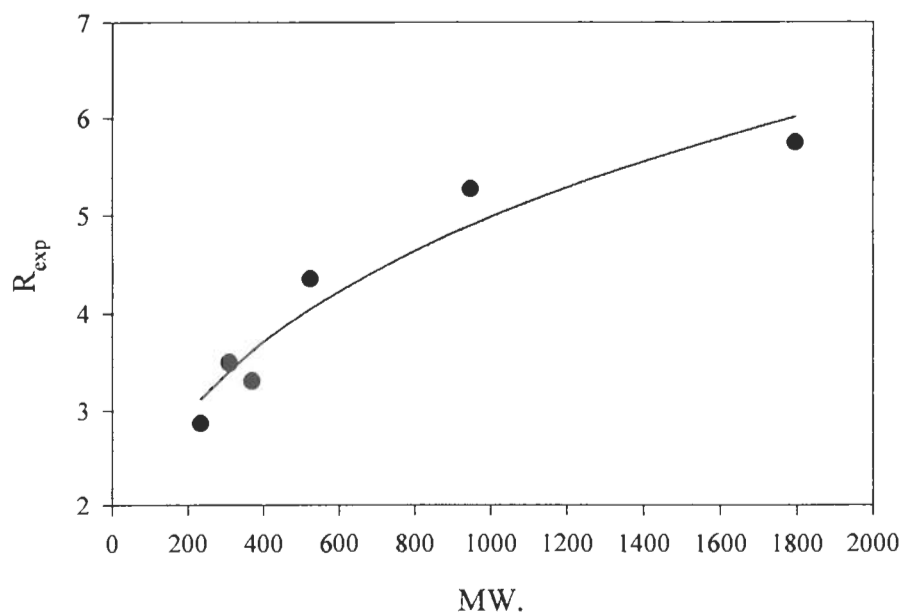


Figure 4-34. The power regression fit of R_{exp} vs MW. of pyrene labeled poly(aryl ether) monodendrons (1-6) in ACN.

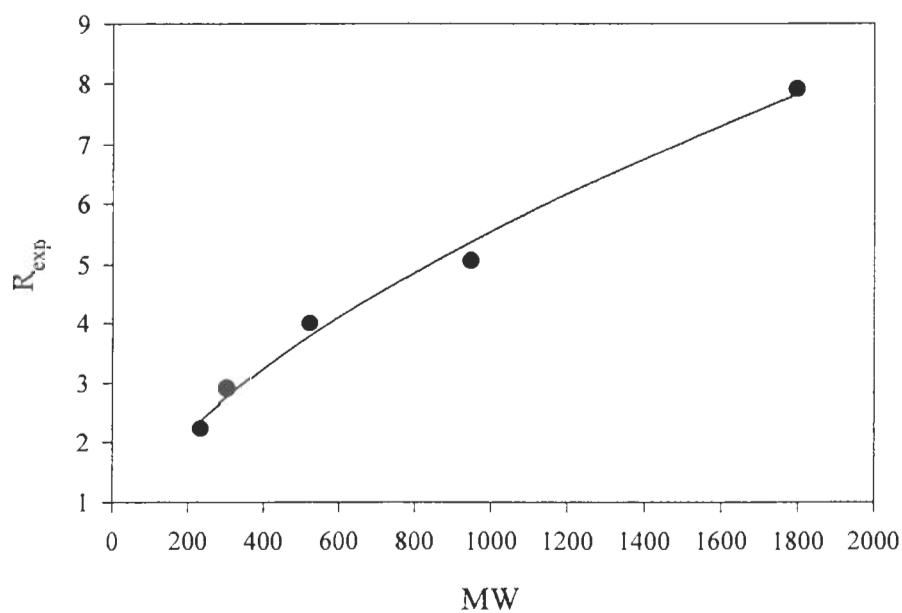


Figure 4-35. The power regression fit of R_{exp} vs MW of pyrene labeled poly(aryl ether) monodendrons (1-6) in THF.

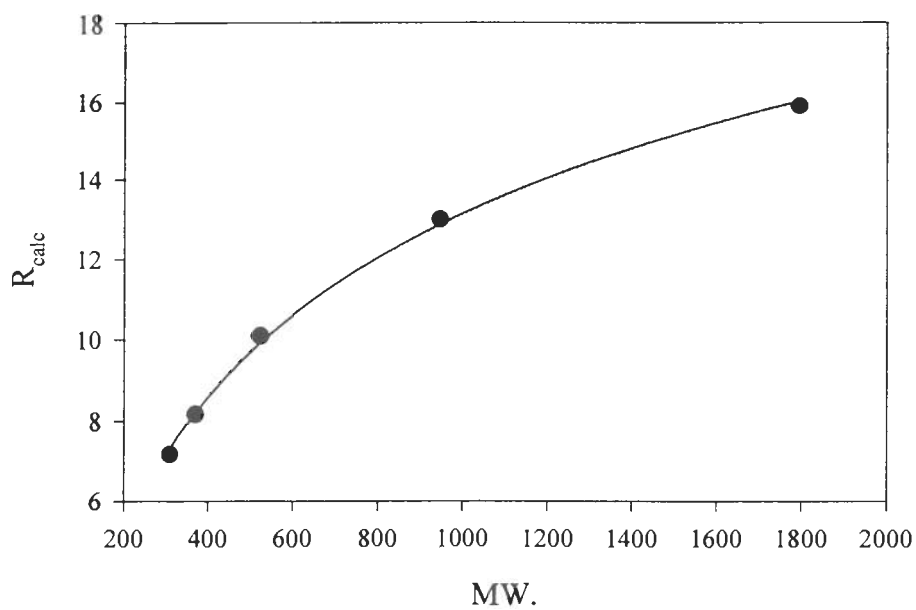


Figure 4-36 The logarithmic regression fit of R_{calc} vs MW. of pyrene labeled poly(aryl ether) monodendrons (1-6).

Å.⁶⁴ The diffusion coefficient of both quenchers decreased and the relative viscosities increased with an increase in the size of monodendrons in acetonitrile and THF. However, the relative viscosities for I₂ and O₂ in acetonitrile are significantly different than in THF. In THF the relative viscosities of I₂ and O₂ are almost identical. This suggests that for I₂ in acetonitrile, there is an electron transfer mechanism for the quenching and as the monodendrons increase in size the polarity of the local solvent environment decreases and this electron transfer mechanism becomes less favorable. In THF, the quenching rate constants for iodine quenching were significantly smaller than oxygen (Table 4-9). One probable reason for this difference might be the size of quencher. Quenching requires the actual collision of quencher with the fluorophore. Iodine is a big molecule and diffuses slowly. The smaller value of k_{QM} is a result of the smaller diffusion coefficient of iodine relative to oxygen (Table 4-9). Oxygen has a diffusion coefficient approximately three times greater than iodine. It diffuses faster and reaches the fluorophore with high probability of quenching at every collision. Quenching studies have revealed a significant decrease in quenching rate constant for the third generation monodendrons from the second generation, for each solvent studied. The decrease in k_{QM} with the increase in size of monodendrons illustrated the effects of steric protection upon quenching. If the monodendrons prevent contact between fluorophore and the quencher with significant back folding, then substantially decreased values of k_{QM} and k_{QD} are expected. Quenching is efficient in small size monodendrons indicating that they are more open and flexible than the large ones (G3-O-Py). This also suggests a significant change in the structure of higher generation monodendrons that reduces the access of quencher to the fluorophore.

Table 4-7. Diffusion coefficient (D_{Py}) of pyrene labeled monodendrons (1-6) and their radii in ACN and THF.

Compound	ACN		THF		R_{calc}^c (Å)
	D_{Py}^a (cm^2/sec)	R_{exp}^b (Å)	D_{Py}^a (cm^2/sec)	R_{exp}^b (Å)	
Pyrene	2.3×10^{-5}	2.87	1.7×10^{-5}	2.35	---
1-Me-O-P (1)	2.2×10^{-5}	2.87	1.7×10^{-5}	2.35	---
G0-O-P (2)	1.8×10^{-5}	3.51	1.3×10^{-5}	3.08	7.2
G0'-O-P (3)	1.9×10^{-5}	3.33	---	---	8.2
G1-O-P (4)	1.45×10^{-5}	4.36	0.95×10^{-5}	4.20	10.1
G2-O-P (5)	1.2×10^{-5}	5.27	0.75×10^{-5}	5.33	13.0
G3-O-P (6)	1.1×10^{-5}	5.75	0.48×10^{-5}	8.33	15.9

a. Calculated from the NMR data.

b. Calculated from Stokes-Einstein equation (1-24) using $\eta = 5.46 \times 10^{-4}$ Pa-sec for THF, $\eta = 3.45 \times 10^{-4}$ Pa-sec for ACN, $k_B = 1.381 \times 10^{-23}$ J/K, and $T = 25$ °C

c. Radii of fully extended structures, calculated from the models.¹³⁴

d. Calculations were not done.

Table 4-8. Diffusion coefficient of iodine (D_{I_2}) and oxygen (D_{O_2}) and relative viscosities (η_{rel}) for pyrene labeled monodendrons (1-6) in ACN.

Compound	Iodine		Oxygen	
	$D_{I_2}^a$ (cm ² /sec)	η_{rel}^b	$D_{O_2}^c$ (cm ² /sec)	η_{rel}^b
1-Me-O-P (1)	1.5×10^{-4}	1.0	9.69×10^{-5}	1.00
G0-O-P (2)	7.52×10^{-5}	1.99	9.75×10^{-5}	0.99
G0'-O-P (3)	5.85×10^{-5}	2.56	9.60×10^{-5}	1.01
G1-O-P (4)	5.02×10^{-5}	2.98	9.20×10^{-5}	1.05
G2-O-P (5)	4.93×10^{-5}	3.04	8.39×10^{-5}	1.15
G3-O-P(6)	3.42×10^{-5}	4.38	7.69×10^{-5}	1.26

- Diffusion coefficient of iodine calculated from Smoluchowski equation (1-23) using $Re = 5.9 \text{ \AA}$.⁹⁸
- Relative viscosity calculated from Stokes-Einstein equation (1-24).
- Diffusion coefficient of oxygen calculated from Smoluchowski equation (1-23) using $Re = 4.48 \text{ \AA}$.⁶⁴

Table 4-9. Diffusion coefficient of iodine (D_{I_2}) and oxygen (D_{O_2}) and relative viscosities (η_{rel}) for pyrene labeled monodendrons (1-6) in THF.

Compound	Iodine		Oxygen	
	$D_{I_2}^a$ (cm ² /sec)	η_{rel}^b	$D_{O_2}^c$ (cm ² /sec)	η_{rel}^b
1-Me-O-P (1)	2.18×10^{-5}	1.0	6.32×10^{-5}	1.0
G0-O-P (2)	1.95×10^{-5}	1.1	6.63×10^{-5}	0.96
G0'-O-P (3)	--- ^d	--- ^d	--- ^d	--- ^d
G1-O-P (4)	2.20×10^{-5}	1.0	6.24×10^{-5}	1.0
G2-O-P (5)	2.11×10^{-5}	1.03	5.96×10^{-5}	1.06
G3-O-P(6)	1.96×10^{-5}	1.11	5.76×10^{-5}	1.10

- Diffusion coefficient of iodine calculated from Smoluchowski equation (1-23) using $Re = 5.9 \text{ \AA}$.⁹⁸
- Relative viscosity calculated from Stokes-Einstein equation (1-24).
- Diffusion coefficient of oxygen calculated from Smoluchowski equation (1-23) using $Re = 4.48 \text{ \AA}$.⁶⁴
- Calculations were not done.

E. Molecular Modeling Studies

Molecular modeling was used as an aid in the interpretation of experimental results. Using Hyperchem (V5.0), structures of pyrene and pyrene labeled monodendrons were generated. These structures were geometry optimized (lowest energy and RMS gradient of 0.01 kcal / Å mol) using the MM⁺ force field and choosing Polak-Ribiere as the minimization algorithm. Geometry optimization calculates and displays a structure with a minimum energy and minimal atomic forces (gradient). Geometry optimized structures of pyrene and pyrene labeled monodendrons (1-6) are shown in Appendix B. From the structures, it is observed that with the increase in generation the size of monodendrons increases. Smaller monodendrons are extended, spatially localized and fully segregated. A significant change is observed in the structure of the third generation molecule (G3-O-Py). The structure of this molecule is less localized and is not fully segregated, instead, some backfolding is observed making the structure dense at the center of core. This might be the reason of decrease in diffusion coefficient of pyrene labeled monodendrons with the increase in size of monodendrons in acetonitrile and THF. (Table 4-7).

Molecular orbital calculations were performed to understand the difference between pyrene and 1-methoxypyrene in their photophysical properties. Both semiempirical and ab-initio (with minimal basis set) calculations were done to observe the effect of the lone pair of oxygen with the pyrene π -system in 1-methoxypyrene (Figure 4-36 and Figure 4-37). The results suggest very little oxygen character to the frontier orbital and do not explain the significant differences between the photophysical

properties of pyrene and 1-methoxypyrene. These are more likely the results of internal conversion resulting from coupling of the C-O stretch to the electronic transition (mentioned in detail in Chapter 3).

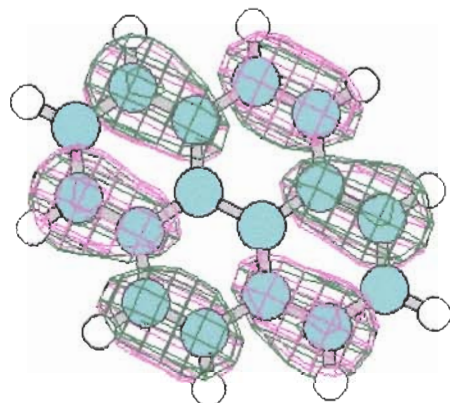


Figure 4-37. Highest Occupied Molecular Orbital (HOMO) of pyrene after semiempirical geometry optimization (using AM1).

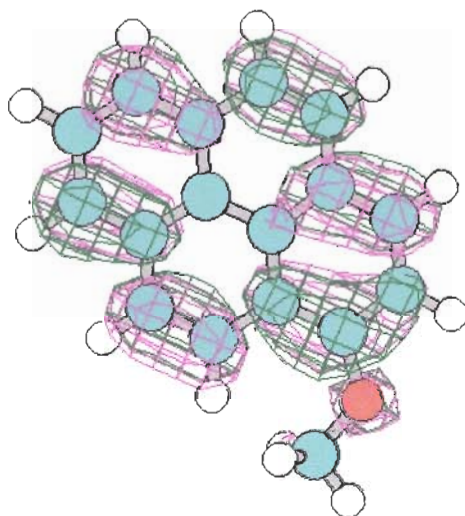


Figure 4-38. Highest Occupied Molecular Orbital (HOMO) of 1-methoxypyrene after semiempirical geometry optimization (using AM1).

CHAPTER 5
Conclusions

A. Conclusions

The photophysics of pyrene labeled poly(aryl ether) monodendrons were investigated by excimer formation and quenching of fluorescence to gain insight into the properties and the structures of the molecules in solution. The fluorescence studies indicate the presence of significant back folding in the higher generation monodendrons (G2-O-Py and G3-O-Py). This was supported by fluorescence quenching studies using iodine and oxygen as a quencher and also by molecular modeling studies using Hyperchem.

Fluorescence quenching involves the deactivation of the excited state by a quencher molecule. The object of this study was to determine the quenching rate constants of pyrene and pyrene labeled poly(aryl ether) monodendrons. Quenching studies were done to generate detailed data concerning the structure of pyrene labeled monodendrons in solution and the diffusion of quencher in the monodendrons.

Iodine quenching is known to be extremely sensitive to charge effects.¹⁰⁰ Oxygen is an uncharged molecule of very small dimension and also has the high probability of quenching at any collisions. It must be considered an ideal probe to obtain information about the internal structure of monodendrons

The rate constant associated with dynamic quenching and the equilibrium constant associated with static quenching were determined in acetonitrile, THF and cyclohexane. Results of these experiments provided information about the quenching behavior of pyrene labeled poly(aryl ether) monodendrons (1-6) in different solvents. The

absorption spectra in acetonitrile and THF consist of contributions due to complexed and uncomplexed iodine while cyclohexane has only uncomplexed iodine.

Fluorescence measurements and quenching studies provided information regarding differences among successive generations of pyrene labeled poly(aryl ether) monodendrons. Quenching experiments with iodine and oxygen indicated a generally decreasing trend in the quenching rate constant with increase in generation number. This decrease in rate can not be simply due to diffusion. This reflects that the monodendrons are not fully extended in solution and are shielding the excited fluorophore. Because of this back folding, the fraction of quencher accessible to the fluorophore decreases for higher generations. The amount of quenching observed is a function of dendrimer generation number and of solvent polarity and viscosity. The variation in quenching rate constant is consistent with the change in solvent polarity and increase in size of monodendrons.

Fluorescence quenching proved to be very effective tool in determining the permeability of the dendrimer structures. The experimentally measured diffusion coefficients for the pyrene labeled monodendrons in acetonitrile and THF when combined with their quenching rate constants gave more information about their structure in solution. They support the observation that the monodendrons are not fully extended. The quenching measurements by iodine and oxygen in cyclohexane have a similar trend of decreasing k_{QM} and k_{QD} with increasing generation. This behavior of monodendrons also suggests that the same shielding effect is occurring in cyclohexane, although a more detailed analysis cannot be performed. (The low solubility of pyrene labeled

monodendrons in cyclohexane has prevented determination of their diffusion coefficients by the NMR method).

The fluorescence and quenching studies have suggested a significantly folded structure of higher generation monodendrons. The quenching studies revealed that quenching is diffusion controlled for small size monodendrons with an extended structure and provides no barrier to quencher. A decrease in quenching efficiency with increasing monodendron size (especially in G2-O-Py and G3-O-Py) was observed that could not be explained by simple diffusion. This suggests that quenching rate constants are not purely diffusion controlled, but are reduced by shielding by the monodendrons which are folded back. This folding resulted in reduced size and increased density of monodendrons and reduced the permeability of quencher to the fluorophore.

All these studies lead to the considerable insight into the properties of dendrimers in solutions. The results obtained from the studies of dilute and concentrated solutions of pyrene labeled poly(aryl ether) monodendrons supports the newer treatment of dendrimers, where it is believed that the structure in solution falls between that of fully extended model of Gennes² and the extensively backfolded model of Muthukumar.¹² However, it would be of considerable interest to determine the diffusion coefficients and quenching rate constants in other solvents in order to understand the effect of solvent polarity in quenching efficiency and extent of back-folding.

CHAPTER 6
Experimental

A. General

All chemicals were purchased from Aldrich. Pyrene (99.55 %) obtained from Aldrich was recrystallized twice from ethanol. All synthesis was performed under an argon atmosphere. Analytical thin layer chromatography was performed using commercially coated silica plates (200-400 mesh, 60 Å). Melting points were determined on a Mel-Temp apparatus and are uncorrected. ¹H-NMR spectra were recorded at Johnson & Johnson Laboratories. Tetramethylsilane (TMS) was used as internal reference and data is given in δ units. The following abbreviations are used in the ¹H-NMR data: Ar' refers to the protons of the aromatic rings of the core pyrene molecule. Ar refers to protons on the aromatic ring and the subscript refers to the generation of the ring.

All photophysical measurements were performed using spectroscopic grade solvents at room temperature (25 °C). Spectroscopic grade acetonitrile (ACN), tetrahydrofuran (THF) and cyclohexane (CH) were obtained from Aldrich and used as received for photophysical studies. These solvents were kept under argon after use. Iodine was also used without any further purification for quenching studies. Absorption spectra were collected using a Hewlett-Packard HP 8452 photodiode array spectrophotometer. Emission spectra were acquired on Jobin-Yvon Spex Tau-2 (FLIT II) spectrofluorimeter consisting of a 450W Xenon lamp, a single grating excitation monochromator, a single grating emission monochromator and a T-box sampling module. The fluorescence signal was collected at right angle (for dilute solutions) and at front face angle (for

concentrated solutions). The photomultiplier tube used to detect the emission was a Hamamatsu R9928 red-sensitive photomultiplier tube with an absolute energy cut-off of 930nm. All emission spectra were corrected for detector response by an internal Rhodamine B quantum counter and correction files generated on site by the manufacturer.

B. Lifetime Measurements

Excited state lifetimes (τ) were determined by laser flash photolysis with the defocused 337 nm output of a pulsed Photochemical Research Associates model LN 100 nitrogen laser as the excitation source (nominal pulse width 300 ps). The luminescence decay after excitation was monitored with a Hamamatsu R928 photomultiplier tube mounted in an EME-Gencom Inc. model S photomultiplier housing. An Instruments SA Inc. model H10 monochromator with 2 nm slits (nominal band pass = 16 nm) was used to select the detection wavelength. The voltage vs time signal was acquired with a LeCroy model 9361 digital storage oscilloscope, with an internal 50 ohm terminator resistor used to convert current to voltage. The data obtained was stored on an MS-DOS formatted diskette and transferred to 80386 based personal computer. A program supplied by LeCroy (Wave386.Exe) was used to convert the binary files to ASCII. These files were then read into Sigma Plot, Version (4.0) for Windows and analyzed by semilog plot to determine the slope.

C. Sample Preparation

Dilute solutions of pyrene and pyrene labeled poly(aryl ether) monodendrons (1-6) were prepared from concentrated ones by successive dilutions. A 3.3-3.5 mL aliquot of the solution was pipetted into the quartz cuvette equipped with gas-tight septa and degassed by slow bubbling with zero grade argon for 15 minutes. The solutions were excited at 335 nm and fluorescence spectra were scanned from 360 to 600 nm. To measure lifetimes, the fluorescence decay curves were observed at 385 nm in dilute solutions and at 550 nm for concentrated solutions of pyrene labeled poly(aryl ether) monodendrons (540 nm for pyrene) to obtain the fluorescence decay of excimer only. For iodine quenching, iodine was added in 1 or 5 microliter aliquots from a concentrated solution (0.5 M in THF, 0.1 M in cyclohexane and acetonitrile) to a final iodine concentration of approximately 3.67 mM. Steady-state fluorescence and time resolved fluorescence intensity decay curves were measured for each iodine concentration. All oxygen quenching experiments were performed by bubbling the solutions in cuvettes with air for 15 minutes to ensure saturation. Steady-state fluorescence and time resolved fluorescence intensity decay curves were measured for air saturated solutions by using the above mentioned specifications for fluorescence measurements.

D. Synthesis

Synthesis of 1-Me-O-Py (1): A solution of 1-hydroxypyrene (1.00 g, 4.58 mmol), methyl iodide (2.85 mL, 46.0 mmol) and potassium carbonate (1.26 g, 12.71 mmol) in dry THF was refluxed under argon with stirring for 5 days until no 1-

hydroxypyrene was present by TLC (3:1 v:v hexanes: ethyl acetate). Once complete the reaction was cooled and solvent removed under reduced pressure. The residue was dissolved in water and methylene chloride and was extracted three times with methylene chloride. The combined organic layers were then washed with water and dried over anhydrous sodium sulfate. The solution was filtered and solvent removed under reduced pressure to yield yellow oil. The crude product was purified by column chromatography using 3:1 (v:v) hexanes: ethyl acetate as the solvent. The chromatography was easily followed with long wavelength UV. The first band contained the product. Removal of solvent gave 1-Me-O-Py (1) as yellow oil that solidified upon standing. This product was further purified by recrystallization from ethanol (2x) to give off-white shiny plate-like crystals (0.97 g, 91%), mp 74-76 °C.

¹H-NMR (CDCl₃): δ 4.15 (s, 3H, OCH₃), 7.45-7.55 (d, 1H, Ar'*H*), 7.85-8.20 (m, 7H, Ar'*H*) 8.41-8.44 (d, 1H, Ar'*H*)

Synthesis of G0-O-Py (2): A solution of 1-hydroxypyrene (1.00 g, 4.58 mmol), benzyl bromide (1.75 g, 6.87 mmol) and potassium carbonate (1.13 g, 11.45 mmol) in acetone was refluxed overnight under argon. The reaction was followed by thin layer chromatography while refluxing and was stopped when no starting material was present by TLC (3:1 v: v hexanes:ethyl acetate). The reaction was cooled and sodium hydroxide (0.36 g, 9.0 mmol) was added to convert the excess benzyl bromide to benzyl alcohol. The solvent was removed under reduced pressure and the residue dissolved in a mixture of water and methylene chloride. The solution was then extracted three times with methylene chloride. The collected organic layers were washed with 10% sodium

hydroxide and then with water and finally dried over anhydrous sodium sulfate. The solution was then filtered and the solvent removed under reduced pressure. The crude product was further purified by recrystallization from ethanol (2x) and was obtained as fluffy white crystals (1.31 g, 92%), mp 101-103 °C.

¹H-NMR (CDCl₃): δ 5.43 (s, 2H, ArCH₂O), 7.35-7.48 (m, 5H, ArH₀), 7.60-7.62 (d, 1H, Ar'H), 7.85-8.15 (m, 7H, Ar'H), 8.50-8.53 (d, 1H, Ar'H).

Synthesis of G0'-O-Py (3): This reaction was completed in two steps. The first step was the synthesis of 3,5-dimethoxy benzyl bromide. Carbon tetrabromide (7.39 g, 22.95 mmol) was added to a solution of 3,5-dimethoxy benzyl alcohol (3.00 g, 17.83 mmol) in THF. After it was dissolved, triphenylphosphine was added slowly while stirring at room temperature under argon. The reaction resulted in the formation of white precipitate with generation of heat. Stirring was continued for another one to two hours until no benzyl alcohol was present by TLC (3:1 v:v hexanes: ethyl acetate). When reaction was complete, the solution was filtered into an equal volume of water. The filtrate was collected and the solvent was removed under reduced pressure. The residue was dissolved in methylene chloride and water and was extracted three times with methylene chloride. The combined organic layers were then washed with water and dried over anhydrous sodium sulfate. The solution was filtered and the solvent removed under reduced pressure to yield an oily product that solidified at room temperature. This was purified by recrystallization twice from hot ethanol to yield white needle-like crystals of 3,5-dimethoxy benzyl bromide. The second step coupled 3,5-dimethoxy benzyl bromide to 1-hydroxypyrene. A solution of 1-hydroxypyrene (1.00 g, 4.58

mmol), benzyl bromide (1.38 g, 6.87 mmol) and potassium carbonate (1.1347 g, 11.45 mmol) was refluxed overnight under argon. The reaction was checked by TLC for completion. When complete, the reaction was cooled and sodium hydroxide (0.36 g, 9.0 mmol) was added to quench the excessive 3,5-dimethoxy benzyl alcohol and was let to stir for another half-hour at room temperature. The solvent was then removed under reduced pressure and the residue dissolved in water and methylene chloride. The solution was extracted three times with methylene chloride. The collected organic layers were washed with 10% sodium hydroxide and then with water. The washed organic layers were then dried over anhydrous sodium sulfate. The solution was filtered and the solvent removed under reduced pressure to give G0'-O-Py as brown colored oil that solidified upon standing. The product was further purified by recrystallization twice from an ethanol-acetone mixture. The product was obtained as shiny, light orange colored crystals (1.36 g, 80.6%), mp 108-109 °C.

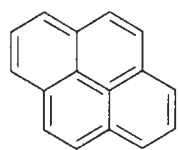
¹H-NMR (CDCl₃): δ 3.80 (s, 6H, OCH₃), 5.35 (s, 2H, ArCH₂), 6.46 (s, 1H, ArH₀), 6.75 (s, 2H, ArH₀) 7.58-7.60 (d, 1H, Ar'H) 7.88-8.15 (m, 7H, Ar'H) 8.52-8.54 (d, 1H, Ar'H)

Synthesis of G1-O-Py (4): This synthesis also required two steps. The first step involved the synthesis of 3,5-dibenzyloxy benzyl bromide from 3,5-dibenzaloxyl benzyl alcohol. 3,5-dibenzaloxyl benzyl alcohol (10.00 g, 30.0 mmol), carbon tetrabromide (12.43 g, 38.7 mmol) and triphenyl phosphine (10.16 g, 38.7 mmol) were dissolved in THF. The crude product was obtained by following the procedure described above and was purified by dissolving it in a minimal amount of 9:1 (v:v) toluene:petroleum ether mixture and running it through a short column of silica gel to remove the

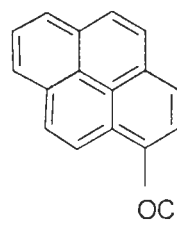
triphenylphosphine oxide. The volume was reduced under reduced pressure and the product was then precipitated into hexanes (10.38 g, 86.6%). In the second step, the 3,5-dibenzoyloxy benzyl bromide (10 g, 25.0 mmol) was refluxed along with 1-hydroxypyrene (4 g, 18.3 mmol) and potassium carbonate (4.717g, 47.6 mmol) in THF under argon. The reaction was followed by TLC (3:1 v:v hexanes: ethyl acetate). The reaction was completed by following the procedure above for G0'-O-Py and the product was obtained as an oil that solidified upon standing. It was further purified by recrystallization twice from an ethanol-acetone mixture (9.0 g, 75%) mp, 111-113 °C.

¹H-NMR (CDCl₃): δ 5.10 (s, 4H, ArCH₂O), 5.38 (2H, ArCH₂O), 6.65 (s, 1H, ArH₀), 6.85 (s, 2H, ArH₀) 7.26-7.48 (m, 10H, ArH₁), 7.52-7.54 (d, 1H, Ar'H), 7.88-8.18 (m, 7H, Ar'H), 8.49-8.51 (d, 1H, Ar'H).

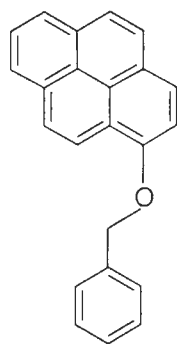
APPENDIX A
Structures



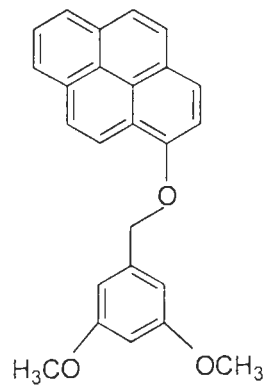
Pyrene



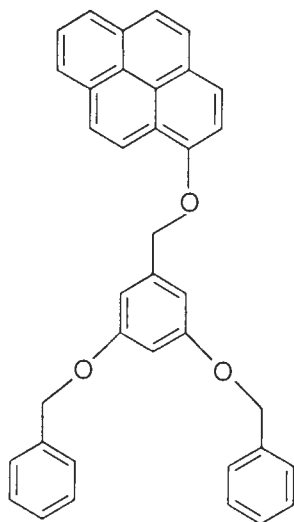
1-Me-O-Py (1)



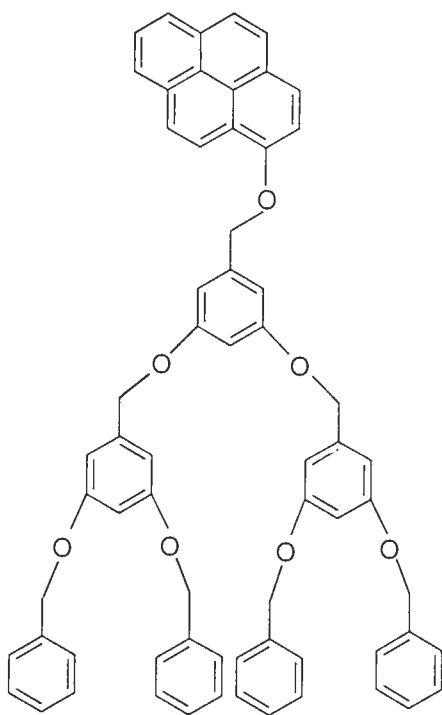
G0-O-Py (2)



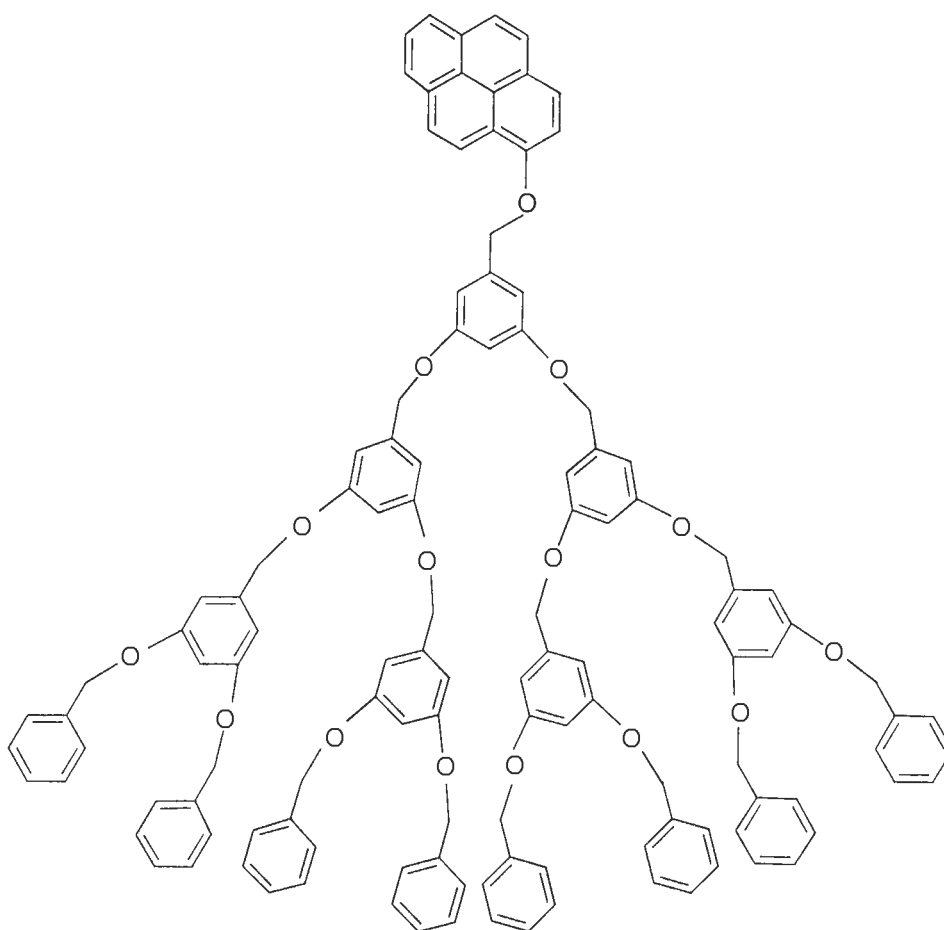
G0'-O-Py (3)



G1-O-Py (4)



G2-O-Py (5)

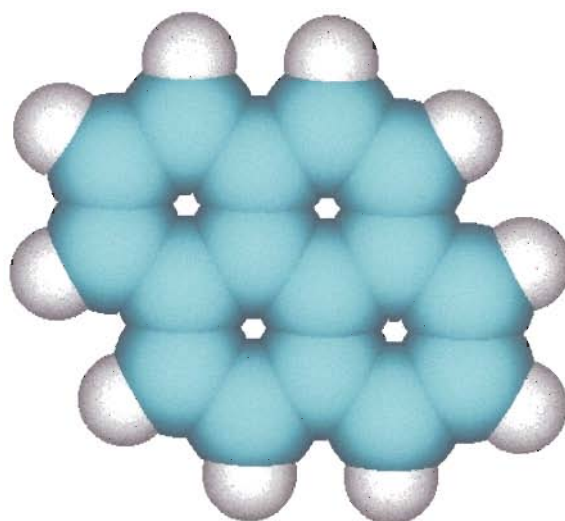


G3-O-Py (6)

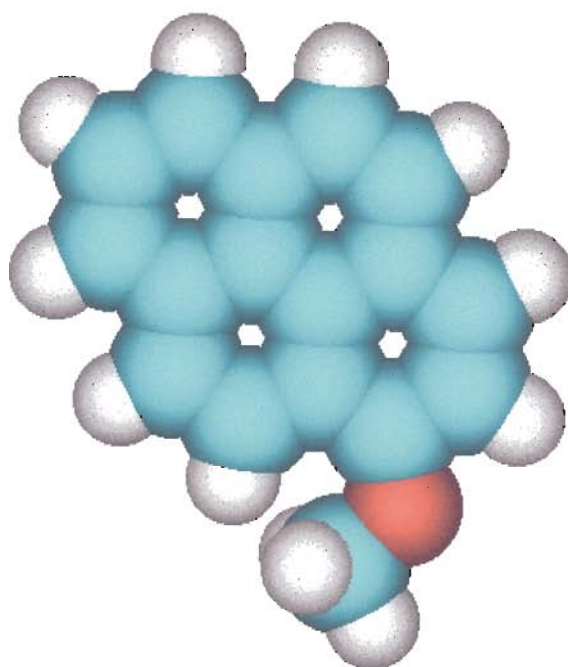
APPENDIX B

Geometry Optimized Structures

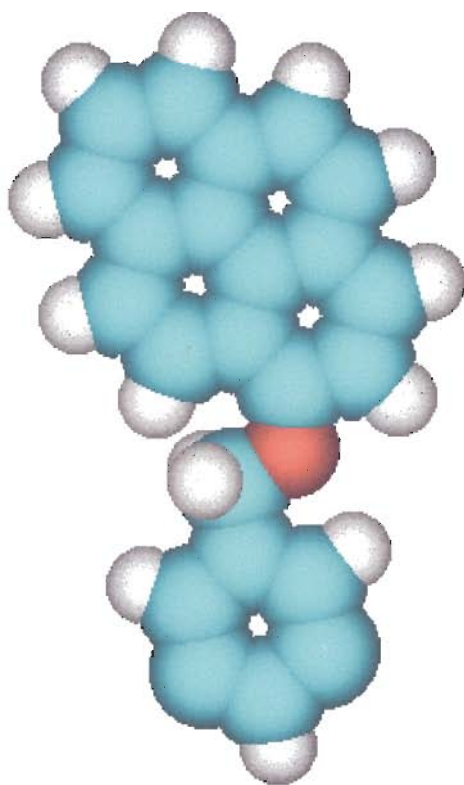
Pyrene



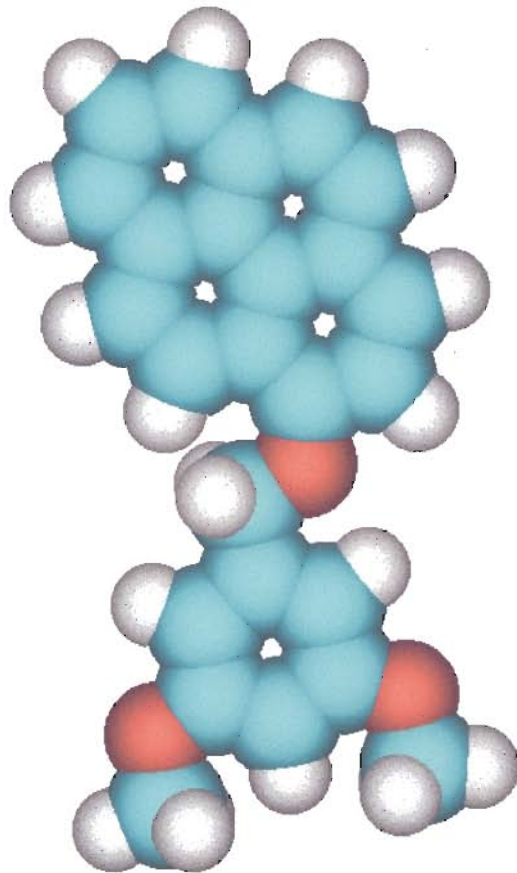
1-Methoxypyrene (1)



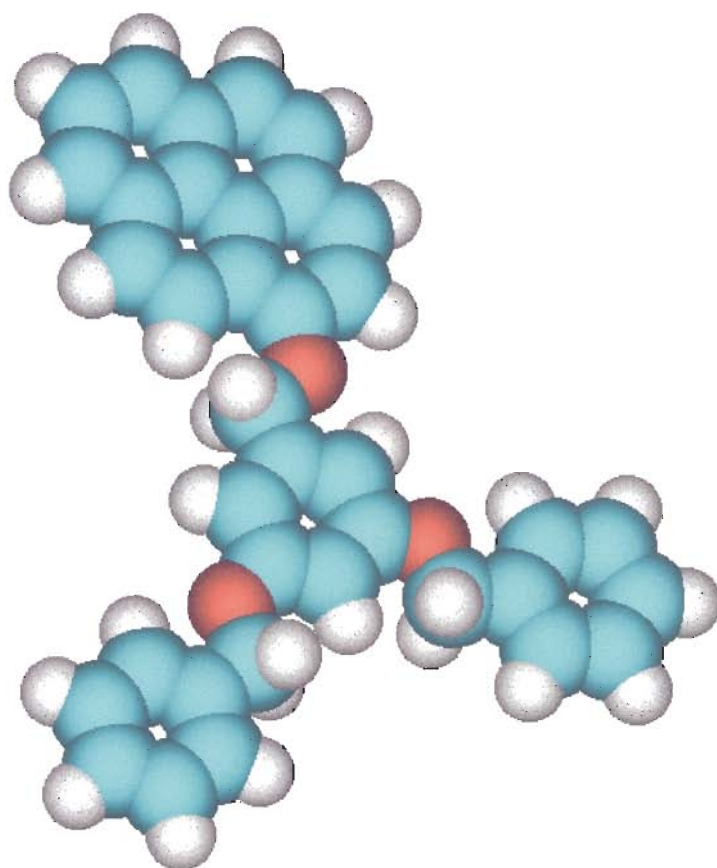
G0-O-Py (2)



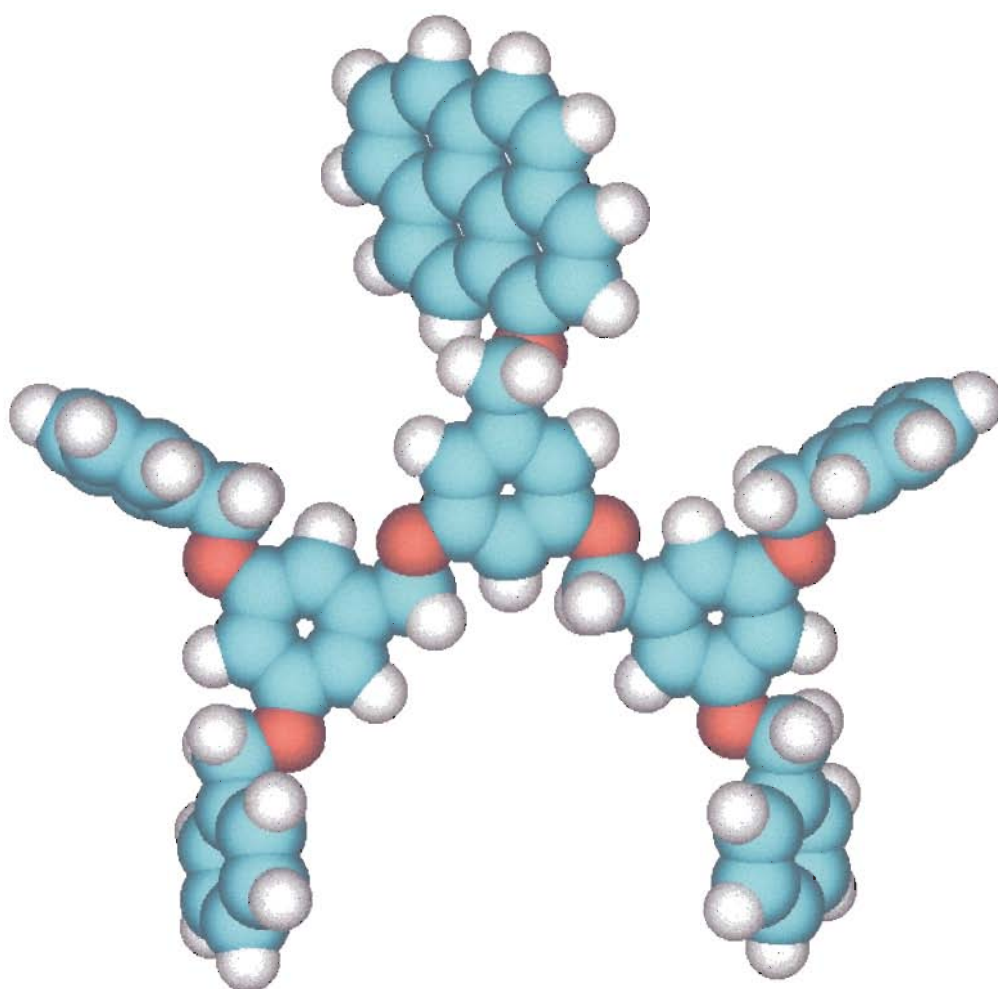
G0'-O-Py (3)



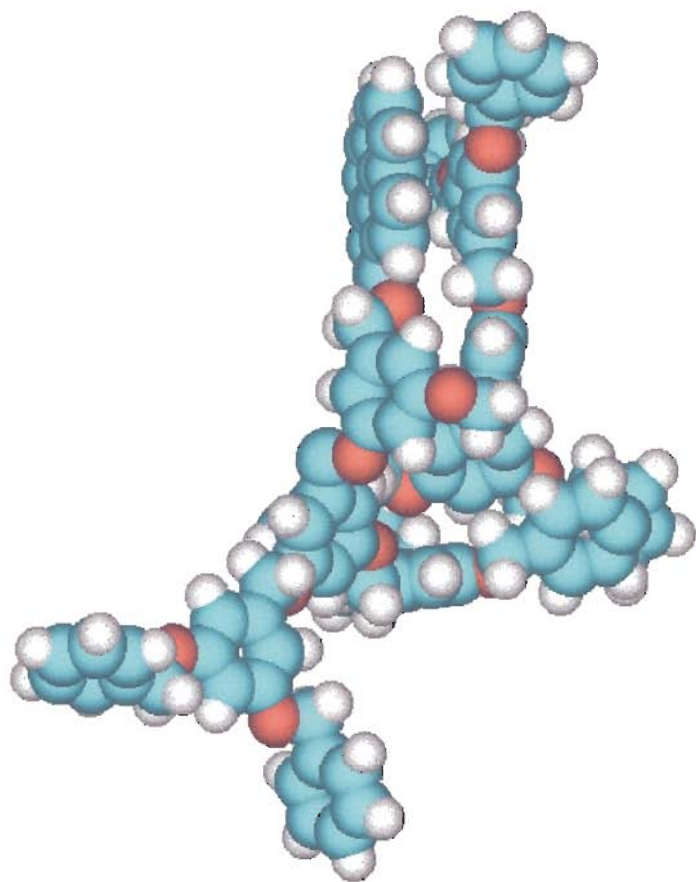
G1-O-Py (4)



G2-O-Py (5)



G3-O-Py (6)



REFERENCES

References:

1. a) Maciejewski, M.; *J. Macromol. Sci. Chem.* **1982**, *A17* (4), 689. b) Burchard, W.; Kajiwara, K.; Nerger, D. *J. Polym. Sci., Phys. Ed.* **1982**, *20*, 157. c) Alexander, S.; Orbach, R. *J. Phys. Lett.* **1982**, *43*, 625.
2. de Gennes, P. G.; Hervet, H. *J. Phys. Lett.*, **1983**, *44*, L-351.
3. a) Tomalia, D. A.; Baker, H.; Dewald, J.; Hall, M.; Kallos, G.; Martin, S.; Roeck, J.; Ryder, J.; Smith, P.; *Polym. J.* **1985**, *17*, 117. b) Tomalia, D. A.; Baker, H.; Dewald, J.; Hall, M.; Kallos, G.; Martin, S.; Roeck, J.; Ryder, J.; Smith, P. *Macromolecules* **1986**, *19*, 2466. c) Tomalia, D. A.; Hall, M.; Hedstrand, D. *J. Am. Chem. Soc.* **1987**, *109*, 1601. d) Tomalia, A.; Naylor, A. M.; Goddard III W. A. *Angew. Chem. Int. Ed. Engl.* **1990**, *29*, 138.
4. Denkewalter, R. G.; Kolc, J.; Lukasavage, W. J. *US Pat.* **1981**, 4 289 872.
5. Cai, C.; Chen, Z. Y. *Macromolecules* **1998**, *31*, 6393.
6. Fréchet, J. M. J.; Hawker, C. J.; Wooley, K. L. *Pure Appl. Chem.*, **1994**, *A31* (11), 1627.
7. a) Ardoin, N.; Astruc, D. *Bull. Soc. Chim. Fr.* **1995**, *132*, 875. b) Tomalia, D. A.; Dvornic, P. R. *Nature* **1994**, *372*, 617.
8. a) Hawker, C. J.; Wooley, K. L.; Fréchet, J. M. J. *J. Chem. Soc. Perkin Trans. 1* **1993**, 1287. b) Hawker, C. J.; Fréchet, J. M. J. *J. Am. Chem Soc.* **1990**, *112*, 7638. c) Hawker, C. J.; Fréchet, J. M. J. *J. Chem. Soc., Chem. Commun.* **1990**, 1010. d) Hawker, C. J.; Fréchet, J. M. *Polymer* **1992**, *33*, 1507.

9. a) Tomalia, D. A., Durst, H. D. *Top. Curr. Chem.* **1993**, *165*, 194. b) Tomalia, D. A.; Kaplan, D. A.; Kruper, W. J.; Cheng, R. C.; Tomlinson, I. A.; Fazio, M. J.; Hedstrand, D. M.; Wilson, L. R.; Jung, C. W.; Edwards, D. S. *US Pat.* **1994**, 5338532.
10. de Brabander-van den Berg, E. M. M.; Put, J. A. *Proc. Am. Chem. Soc., Polym. Mater. Sci. Eng.* **1995**, *73*, 79.
11. Wiener, E. C.; Brechbiel, M. W.; Brothers, H.; Magin, R. L.; Gansow, O. A.; Tomalia, D. A.; Lauterbur, P. C. *Magn. Res. Med.* **1994**, *31*, 1.
12. a) Lescanec, R. L.; Muthukumar, M. *Macromolecules* **1990**, *23*, 2280. b) Berlman, I. B. *Handbook of Fluorescence Spectra of Aromatic Molecules*, Academic Press: New York. 1965.
13. Jansen, J. F. G. A.; Peerlings, H. W. I.; de Brabander-van den Berg, E. M. M.; Meiger, E. W. *Angew. Chem. Int. Ed. Eng.* **1995**, *34*, 1206.
14. Hudson, S. D.; Jung, H. T. -T.; Perec, V.; Cho, W.-D.; Johansson G.; Ungar, G.; Balagurusamy, V. S. K. *Science* **1997**, *278*, 449.
15. Bosman, A. W.; Janssen, R. A. J.; Meijer, E. W. *Macromolecules* **1997**, *30*, 3606.
16. Prosa, T. J.; Bauer, B. J.; Amis, E. J.; Tomalia, D. A.; Scherrenberg, R. *J. Polym. Sci. B* **1997**, *35*, 2913.
17. Amis, E. J.; Topp, A.; Baur, B. J.; Tomalia, D. A. *Polym. Mater. Sci. Eng.* **1997**, *77*, 183.
18. Meltzer, A. D.; Tirrel, D. A.; Jones, A. A.; Inglefield, P. T.; Hedstrand, D. M.; Tomalia, D. A.; *Macromolecules* **1992**, *25*, 4541.
19. Wooley, K. L.; Klug, C. A.; Tasaki, K.; Schaefer, J. *J. Am. Chem. Soc.* **1997**, *119*, 53.

20. Mournay, T. H.; Turner, S. R.; Rubimstein, M.; Fréchet, J. M. J.; Hawker, C. J.; Wooley, K. L. *Macromolecules* **1992**, *25*, 2401.
21. Scherrenberg, R.; Coussens, B.; van Vilet, P.; Edouard, G.; Brackman, J.; de Brabander-van den Berg, E. M. M.; Mortensen, K. *Macromolecules* **1998**, *31*, 456.
22. Pedersen, C. J. *Angew. Chem. Int. Ed. Engl.* **1988**, *27*, 1021.
23. Suckling C. J. *J. Chem. Soc., Chem. Commun.* **1982**, 661-662.
24. a) Hyatt, J. A.; *J. Org. Chem.*, **1978**, *43*, 1808. b) Vögtle, F.; Weber, E. *Angew. Chem. Int. Ed. Engl.* **1974**, *13*, 814.
25. Murakami, Y.; Nakano, A.; Akiyoshi, K.; Fukuya, K. *J. Chem. Soc., Perkin Trans 1*, **1981**, 2800.
26. Hearshaw, M. A.; Moss, J. R. *J. Chem. Soc. Chem. Comm.* **1999**, *1*, 1.
27. a) Moors, R.; Vögtle, F.; *Chem. Ber.* **1993**, *126*, 2133 b) Wörner, C.; Mühlaupt, R.; *Angew. Chem. Int. Ed. Engl.* **1993**, *32*, 1306. c) de Brabander-van den Berg, E. M. M.; Meijer, E. W. *Angew. Chem. Int. Ed. Engl.* **1993**, *32*, 1308.
28. a) Newkome, G. R.; Yao, Z.; Baker, G. R.; Gupta, V. K. *J. Org. Chem.* **1985**, *50*, 2003. b) Newkome, G. R.; Yao, Z.; Baker, G. R.; Gupta, V. K.; Russo, P. S.; Saunders, M. J. *J. Am. Chem. Soc.* **1986**, *108*, 849.
29. Newkome, G. R.; Baker, G. R.; Aria, S.; Saunders, M. J.; Russo, P. S.; Theriot, K. J.; Morrefield, C. N.; Rodgers, L. E.; Miller, J. E.; Lieux, T. R.; Murray, M. E.; Phillips, B.; Pascal, L. *J. Am. Chem. Soc.* **1990**, *112*, 8458.
30. de Brabander-van den Berg, E. M. M.; Meijer, E. W. *Angew. Chem.* **1993**, *32*, 1308.
31. de Brabander-van den Berg, E. M. M.; Meijer, E. W. *Angew. Chem.* **1993**, *105*, 1370.
32. Roovers, J.; Toprowski, P. M.; Zhou, L. L. *Polym. Prepr.* **1992**, *33*, 182.

33. Fréchet, J. M. J.; Jiang, Y.; Hawker, C. J.; Philippides, A. E. *Proc. IUPAC Int. Symp. Macromol, Seoul* **1989**, 19.
34. Hawker, C. J.; Fréchet, J. M. J. *J. Am. Chem. Soc.* **1990**, *112*, 7638.
35. Jayaraman, M.; Fréchet, J. M. J. *J. Am. Chem. Soc.* **1998**, *120*, 12996.
36. Flory, P. J. *J. Am. Chem. Soc.* **1952**, *74*, 2718.
37. a) Hawker, C. J.; Fréchet, J. M. J. *J. Am. Chem. Soc.* **1991**, *113*, 4583. b) Turner, S. R.; Voit, B. I.; Mourey, T. H. *Macromolecules*, **1994**, *27*, 1611.
38. Wooley, K. L.; Fréchet, J. M. J. *Polymer* **1994**, *35*, 4489. (b) Wooley, K. L.; Hawker, C. J.; Fréchet, J. M. J. *Angew. Chem. Int. Ed. Engl.* **1994**, *33*, 82.
39. Zeng, F.; Zimmerman, S. C. *J. Am. Chem. Soc.* **1996**, *118*, 5326.
40. a) Achar, S.; Puddephatt, R. J. *J. Chem. Soc., Chem. Commun.* **1994**, 1895. b) Achar, S.; Puddephatt, R. J. *Organometallics* **1995**, *14*, 1681.
41. Campagna, S.; Denti, G.; Serroni, S.; Juris, A.; Venturi, M.; Ricevuto, V.; Balzani, V. *Chem. Eur. J.* **1995**, *1*, 211.
42. van Hest, J. C. M.; Delnoye, D. A. P.; Baars, M. W. P. L.; Elissen-Roman, C.; van Genderen, M. P. H.; Meijer, E. W. *Chem. Eur. J.* **1996**, *2*, 1616.
43. a) van Hest, J. C. M.; Delnoye, D. A. P.; Baars, M. W. P. L.; van Genderen, M. H. P.; Meijer, E. W. *Science*, **1995**, *268*, 1592. b) van Hest, J. C. M.; Baars, M. W. P. L.; Elissen-Roman, C.; van Genderen, M. P. H.; Meijer, E. W. *Macromolecules* **1995**, *28*, 6689.
44. a) Gitsov, I.; Fréchet, J. M. J. *J. Am. Chem. Soc.* **1996**, *118*, 3785. b) Gitsov, I.; Wooley, K. L.; Hawker, C. J.; Fréchet, J. M. J. *Polym. Prepr.* **1991**, *32*, 631.

45. Gitsov, I.; Ivanova, P. T.; Fréchet, J. M. J. *Macromol. Rapid Commun.* **1994**, *15*, 387.
46. Leduc, M. R.; Hawker, J. D.; Fréchet, J. M. J. *J. Am. Chem. Soc.* **1996**, *118*, 11111.
47. Leduc, M. R.; Hayes, W.; Fréchet, J. M. J. *J. Polym. Sci. A. Polym. Chem.* **1998**, *36*, 1.
48. Fréchet, J. M. J.; Gitsov, I. *Macromol Symp.* **1995**, *98*, 441.
49. Jansen, J. F. G. A.; de Brabander-van den Berg, E. M. M.; Meiger, E. W. *Science* **1994**, *265*, 1226.
50. Thomas, C. W.; Tor, Y. *Chirality* **1998**, *10*, 53.
51. Buhleier, E.; Wehner, W.; Vögtle, F. *Synthesis*, **1978**, 155.
52. Bhyrappa, P.; Young, J. K.; Moore, J. S.; Suslick, J. *J. Am. Chem. Soc.* **1996**, *118*, 5708.
53. Newkome, G. R.; Baker, G. R.; Saunders, M. J.; Russo, P. S.; Gupta, V. K.; Yao, Z.; Miller, J. E.; Bouillion, K. *J. Chem. Soc., Chem. Commun.* **1986**, 752.
54. Zanini, D.; Roy, R. *J. Org. Chem.* **1996**, *61*, 7348.
55. Mansfield, M. L.; Klushin, L. I. *Macromolecules* **1993**, *26*, 4262. b) Murat, M.; Grest, G. S. *Macromolecules* **1996**, *29*, 1278.
56. Steel, C.; Vögtle, F. *Angew. Chem. Int. Ed. Engl.* **1992**, *31*, 528.
57. Chessa, G.; Scrivanti, A.; Traldi, P. *Rapid. Comm. Mass. Spect.* **1998**, *12*, 1533.
58. Kriessel, J. W.; König, S.; Tilley, T. D. *J. Am. Chem. Soc.* **1998**, *120*, 12207.
59. a) Lehn, J. -M. *Acc. Chem. Res.* **1978**, *11*, 49. b) Lehn, J. -M. *Pure Appl. Chem.* **1978**, *50*, 871. c) Lehn, J. -M. *Science* **1985**, *227*, 849. d) Lehn, J. -M., *Angew. Chem. Int. Ed. Engl.* **1988**, *27*, 89.
60. Seyferth, D.; Son, Y.; Rheingold, A. L.; Ostrander, R. L. *Organometallics* **1994**, *13*, 2682.

61. a) Pekcan, O.; Egan, L. S.; Winnik, M. A. *Macromolecules* **1990**, *23*, 2210. b) Zhao, C. -L.; Winnik, M. A.; Riess, G.; Croucher M. D. *Langmuir* **1990**, *6*, 514.
62. Randy, S. F.; Gerhard, M.; Mario, G. *Macromolecules* **1997**, *30*, 5397.
63. a) Geiger, M. W.; Turro, N. J. *Photochem. Photobiol.* **1975**, *22*, 273. b) Gorman, A. A.; Lovering, G.; Rodgers, M. A. *J. Photochem. Photobiol.* **1976**, *23*, 399. c) Usui, Y.; Tsukada, M.; Nakamura, H. *Bull. Chem. Soc. Jpn.* **1978**, *51*, 379.
64. Vaughan, W. M.; Weber, G. *Biochemistry* **1970**, *9*, 464.
65. Lackowicz, J. R.; Weber, G. *Biochemistry* **1973**, *12*, 4161.
66. Brunner, A.; Minamitake, Y.; Gopferich, A. *Eur. J. Pharm. Bio.* **1998**, *45*, 265.
67. Caminati, G.; Turro, N. J.; Tomalia, D. A. *J. Am. Chem. Soc.* **1990**, *112*, 8515.
68. Turro, N. J.; Barton, J. K.; Tomalia, D. A. *Acc. Chem. Res.*, **1991**, *24*, 332.
69. a) Gopidas, K. R.; Lehenny, A. R.; Caminati, G.; Turro, N. J.; Tomalia, D.A. *J. Am. Chem. Soc.* **1991**, *113*, 7335. b) Gopidas, K. R.; Lehenny, A. R.; Turro, N. J.; Tomalia, D. A.; *J. Am. Chem. Soc.* **1991**, *113*, 7335.
70. Hawker, C. J.; Wooley, K. L.; Fréchet, J. M. J. *J. Am. Chem. Soc.* **1993**, *115*, 4375. b) Hawker, C. J.; Wooley, K. L.; Fréchet, J. M. J. *J. Chem Soc. Chem. Com.* **1994**, 925.
71. Hofstraat, J. W.; Veurink, J.; Verhoeven, J. W. *J. Fluoresce.* **1998**, *8*, 335.
72. Benjelloum, A.; Damas, C.; Lochon, P. *Macromol. Symp.* **1997**, *119*, 283.
73. Naylor, A. M.; Goddard III, W. A.; Kiefer, G. E.; Tomalia, D. A. *J. Am. Chem. Soc.*, **1989**, *111*, 2339.
74. Bircks, J. B. *Rep. Prog. Phys.* **1975**, *38*, 903.
75. Bircks, J. B.; Munro, I. H. *Prog. React. Kin.* **1967**, *4*, 239.

76. Zachariase, K.A.; Kozankiewicz, B.; Kuhnle, W. *Surfactants in Solution*, Mittal, K. L., Ed.; Plenum: New York, 1983.
77. Zachariase, K. A. *Fluorescent Techniques and Membrane Makers in cancer and Immunology*, Viallet, P., Ed.; Elsevier: Amsterdam, 1984.
78. Wang, F. W.; Lowry, R. E.; Grant, W. H. *Polymer* **1984**, *25*, 690.
79. Winnik, M. A. *Accounts of Chemical Research* **1985**, *106*, 1045.
80. Forster, T.; Kasper, K. *Phys. Chem*, N. F. **1954**, *1*, 275.
81. Birks, J. B. *Acta Phys. Polon.* **1964**, *26*, 367.
82. Forster, T.; Kasper, K. *Z. Electrochem.* **1955**, *59*, 976.
83. Williams, R. *J. Chem. Phys.* **1958**, *28*, 577.
84. Doller, E.; Forster, T. *Z. Phys. Chem. N. F.* **1962**, *34*, 132.
85. Birks, J. B.; Dyson, D. J.; Munro, H. I. *Proc. Roy. Soc. A.* **1963**, *275*, 575.
86. Birks, J. B. *Photophysics of Aromatic Molecules*, Wiley- Interscience: New York. 1970.
87. Duhamel, J.; Winnik, M. A. *J. Phys. Chem.* **1992**, *96*, 9805.
88. Rice. A. S. *Chemical Kinetics, Vol.25*, Bamford, C. H., Tipper, C. F.H., Compton, R. G., Eds.; Elsevier: New York, 1985.
89. Wilemski, G.; Fixman, M. *J. Chem. Phys.* **1985**, *83*, 1980.
90. Martinho, J. M. G.; Sienicki, K.; Blur, D.; Winnik, M. A. *J. Am. Chem. Soc.* **1988**, *110*, 773.
91. Berberan-Santos, M. N.; Martinho, J. M. G. *J. Chem. Phys.* **1991**, *95*, 1817.
92. Weixelbaumer, W. D.; Burabaumer, J.; Kauffman, H. F. *J. Chem. Phys.* **1985**, *83*, 1980.

93. Hui, M. H.; Ware, W. R. *J. Am. Chem. Soc.* **1976**, *98*, 4712.
94. Martinho, J. M. G.; Conte, J. C. *J. Chem. Soc., Faraday Trans. 2*, **1982**, *78*, 975.
95. Muentzer, J. S.; Deutsch, J. L. *J. Chem. Ed.* **1996**, *73*, 580.
96. Turro, N. J. *Modern Molecular Photochemistry*, Benjamin/Cummings Publishing Co., Inc. Menlo Park, California. 1978.
97. Zagrobelny, J.; Bells, T. A.; Bright, F. V.; *J. Am. Chem. Soc.* **1992**, *114*, 5249.
98. Martinho, J. M. G. *J. Phys. Chem* **1989**, *93*, 6687.
99. Stern, O.; Volmer, M. *Z. Phys.* **1919**, *20*, 183.
100. Lackowicz, J. R. *Principle of Fluorescence Spectroscopy*, Plenum Press: New York, 1986.
101. Perrin, F. *Ann. Phys.* **1929**, *12*, 169.
102. Wawilov, S. I. *Acta Phys. Pol.* **1936**, *5*, 417.
103. Szymanowsky, W.; *Z. Phys.* **1936**, *95*, 460.
104. Zeng, H; Durocher, G. *J. Luminesc.* **1995**, *63*, 75.
105. Nernnek, T. L.; Ware, W. R. *J. Chem. Phys.* **1975**, *62*, 477.
106. Eftink, M. R; Ghiron, C. A. *J. Phys. Chem.* **1976**, *80*, 486.
107. Riley, J. M; Ph.D. Dissertation, Seton Hall University, South Orange, NJ. 1998.
108. Moreno-Bondi, M. C.; Orellana, G.; Turro, N. J.; Tomalia, D.A. *Macromolecules* **1990**, *23*, 910.
109. Cao, T.; Yin, W.; Webber, S. E. *Macromolecules* **1994**, *23*, 2210.
110. Eckert, A. R.; Webber, S. E. *Macromolecules* **1994**, *27*, 745.
111. Kramar, M. C.; Welch, C. G.; Stegger, J. R.; McCormick, C. L. *Macromolecules* **1995**, *28*, 5248.

112. Branham, K. D.; Shafer, G. S.; Hoyle, C. E.; McCormick, C. L. *Macromolecules* **1995**, *28*, 6175.
113. Birks, J. B.; Christophorou, L. G. *Proc. Roy. Soc.* **1963**, *A274*, 552.
114. Birks, J. B.; Christophorou, L. G. *Proc. Roy. Soc.* **1964**, *A277*, 571.
115. Martinho, J. M. G.; Conte, J. C. *J. Chem. Soc., Faraday Trans. 2*, **1982**, *78*, 975.
116. Yusa, S.; Kamachi, M.; Morishima, Y. *Photochem. Photobio.* **1998**, *67*, 5119.
117. Murat, M.; Grest, S. G. *Macromolecules* **1996**, *29*, 1278.
118. Riley, J. M.; Chen, A.; Shapiro, M.; Murphy Jr, W. R.; Alkan, S.; Hanson, J. E. *J. Am. Chem. Soc.* (submitted for publication).
119. Eftink, M. R.; Ghiron, C. A. *Anal. Biochem.* **1981**, *114*, 199.
120. Hess, G. P.; Cash, D. J.; Aoshima, H. *Nature* **1979**, *282*, 329.
121. Frank, R. S.; Merkle, G.; Gauthier, M. *Macromolecules* **1997**, *30*, 5397.
122. Kautsky, H. *Trans. Faraday, Soc.* **1939**, *35*, 216.
123. Stryer, L. *Biochemistry* **1978**, *47*, 819.
124. Davidson, R. S.; Bonreau, R.; Jussot-Dubien, J.; Trethewey, K. R. *Chem. Phys. Lett.* **1980**, *74*, 318.
125. Harrocks, A. R.; Wikinson, F. *Proc. Roy. Soc. London* **1968**, *A 306*, 257
126. Bhowmik, B. B.; Zink, S. I. *Spectrochimica Acta* **1982**, *38A*, 877.
127. Juskowiak, B. *Spectrochimica Acta* **1993**, *49A*, 173.
128. Pullen, A.; Walker II, L. A.; Sension, R. J. *J. Chem. Phys.* **1995**, *103*, 7877.
129. Lyon, E. J.; Musie, G.; Reibenspies, H. J.; Darensbourg, M. Y. *Inorg. Chem.* **1998**, *37*, 6942.
130. Murov, S. L., Carmichael, I. Hug, G. L. *Handbook of Photochemistry* 2nd Ed. Marcel

Dekker, Inc.: New York, 1993.

131. Weller, A. *Pure. Appl. Chem.* 1982, 54, 1885.
132. Schroeder, J.; Wilkinson, F. *J. Chem. Soc. Faraday Trans. 2*, 1979, 75, 896.
133. Gorman, A. A.; Parekh, C. T.; Rodgers, M. A. J. *J. Photochem.* 1978, 9, 11.
134. Fully extended radii were measured from Drieding models, which gave an increment of 2.9 Å per generation. The baseline radius of 7.2 Å for G0-O-Py was estimated from the radius of pyrene and a benzyloxy group.